การเตรียมถ่านกัมมันต์ที่มีเหล็กออกไซด์ เพื่อกำจัดฟีนอล
ในฟลูอิดไซด์เบดแบบสามวัฏภาคขนาดนำร่อง

นายสุขุม เฉยศิริ

ศูนย์วิทยทรัพยากร
จุฬาลงกรณ์มหาวิทยาลัย

วิทยานิพนธ์นี้เป็นส่วนหนึ่งของการศึกษาตามหลักสูตรปริญญาวิศวกรรมศาสตรมหาบัณฑิต
สาขาวิชาวิศวกรรมเคมี ภาควิชาวิศวกรรมเคมี
คณะวิศวกรรมศาสตร์ จุฬาลงกรณ์มหาวิทยาลัย
ปีการศึกษา 2552

ลิขสิทธิ์ของจุฬาลงกรณ์มหาวิทยาลัย

PREPARATION OF ACTIVATED CARBONS DOPED WITH IRON OXIDE FOR REMOVING PHENOL WITHIN PILOT-SCALED THREE-PHASE FLUIDIZED BED

Mr. Sukhum Chaeysiri

ศูนย์วิทยทรัพยากร
จุฬาลงกรณ์มหาวิทยาลัย

A Thesis Submitted in Partial Fulfillment of the Requirements
for the Degree of Master of Engineering Program in Chemical Engineering
Department of Chemical Engineering
Faculty of Engineering
Chulalongkorn University
Academic Year 2009

Copyright of Chulalongkorn University

Thesis Title	PREPARATION OF ACTIVATED CARBONS DOPED WITH IRON OXIDE FOR REMOVING PHENOL WITHIN PILOT-SCALED THREE-PHASE FLUIDIZED BED
By	Sukhum Chaeysiri
Field of Study	Chemical Engineering
Thesis Advisor	Associate Professor Tawatchai Charinpanitkul, D.Eng.

Accepted by the Faculty of Engineering, Chulalongkorn University in Partial Fulfillment of the Requirements for the Master's Degree

.....Dean of the Faculty of Engineering
(Associate Professor Boonsom Lerdhirunwong, Dr.Ing.)

THESIS COMMITTEE

..... Chairman
(Associate Professor Muenduen Phisalaphong, Ph.D.)

..... Thesis Advisor
(Associate Professor Tawatchai Charinpanitkul, D.Eng.)

..... Examiner
(Apinan Soottitantawat, D.Eng.)

..... External Examiner
(Professor Wiwut Tanthapanichakoon, Ph.D.)

..... External Examiner
(Pratarn Wongsarivej, D.Eng.)

ศูนย์วิทยทรัพยากร
จุฬาลงกรณ์มหาวิทยาลัย

สุขุม เฉยศิริ : การเตรียมถ่านกัมมันต์ที่มีเหล็กออกไซด์ เพื่อกำจัดฟีนอลในฟลูอิดไดซ์เบดแบบสามวัฏภาคขนาดนำร่อง. (PREPARATION OF ACTIVATED CARBONS DOPED WITH IRON OXIDE FOR REMOVING PHENOL WITHIN PILOT-SCALED THREE-PHASE FLUIDIZED BED) อ. ที่ปรึกษาวิทยานิพนธ์หลัก: รศ. ดร. ธวัชชัย ชรินพาณิชกุล, 99 หน้า.

ถ่านกัมมันต์ที่มีเหล็กออกไซด์ถูกเตรียมขึ้นเพื่อการย่อยสลายตัวของสารละลายฟีนอลในเครื่องปฏิกรณ์แบบฟลูอิไดซ์เบดแบบสามวัฏภาค ในเครื่องปฏิกรณ์วัฏภาคแก๊สคือโอโซน วัฏภาคของเหลวคือสารละลายฟีนอล ส่วนวัฏภาคของแข็งคือเหล็กบนถ่านกัมมันต์ โดยถ่านกัมมันต์สองชนิดคือ AC-US และ AC-TH ที่รูพรุนมีขนาดเฉลี่ย 2.3 และ 1.7 นาโนเมตร มีพื้นที่ผิวจำเพาะ 1,060 และ 1,154 ตารางเมตรต่อกรัม ตามลำดับ จากการสังเกตุในข้อทดลอง AC-TH ถูกเลือกมาใช้ในทดลองที่ใหญ่ขึ้น โดยถ่านกัมมันต์ที่มีเหล็กอยู่ร้อยละ 5 โดยน้ำหนักของตัวรอบรับ การเตรียมได้โดยสองเทคนิคต่างกันสองวิธีคือ wet impregnation (IMA) หรือ incipient wetness impregnation (IMB) หลังจากนั้นจึงเผาที่ 500 องศาเซลเซียส ภายใต้ไนโตรเจนแก๊ส ได้ 5%CAT-TH-A-500 จากเทคนิค IMA และ 5%CAT-TH-B-500 จากเทคนิค IMB หากมีปริมาณเหล็กเป็นร้อยละ 10 โดยน้ำหนักของตัวรองรับได้ 10%CAT-TH-B-500 สำหรับปริมาณเหล็กเป็นร้อยละ 5 โดยน้ำหนักของตัวรองรับที่ใช้สภาวะในการเผาเป็น 200 องศาเซลเซียส ภายใต้อากาศได้ 5%CAT-TH-B-200 ถ่านกัมมันต์ทั้งหมดใช้ร่วมกับโอโซน ศึกษาประสิทธิภาพการการกำจัดฟีนอล และคาร์บอนอินทรีย์ (TOC) พบว่าประสิทธิภาพในการกำจัดฟีนอลในช่วงเวลา 60 นาทีเรียงลำดับได้ดังนี้ 5%CAT-TH-B-500 + O_3 (99%) = 5%CAT-TH-A-500 + O_3 (99%) > AC-TH + O_3 (98%) > 10%CAT-TH-B-500 + O_3 (97%) > 5%CAT-TH-B-200 + O_3 (90%) > only O_3 (67%) ในการกำจัดคาร์บอนอินทรีย์ในเวลา 360 นาทีเรียงลำดับได้ดังนี้ AC-TH + O_3 (92%) > 5%CAT-TH-B-200 + O_3 (81%) > 5%CAT-TH-A-500 + O_3 (71%) = 10%CAT-TH-B-500 + O_3 (71%) 5%CAT-TH-B-500 + O_3 (69%) > only O_3 (52%) ทดลองใช้ 5%CAT-TH-B-200 + O_3 อย่างไรก็ตาม AC-TH และ5%CAT-TH-B-200 มีความสามารถสูงสุดในการกำจัดคาร์บอนอินทรีย์ในเครื่องปฏิกรณ์แบบฟลูอิไดซ์เบดแบบสามวัฏภาคขนาดนำร่อง ย่อยสลายฟีนอลที่ความเข้มข้น 20 มิลลิกรัมต่อลิตร ปริมาตร 200 ลิตร โดยใช้ AC-TH + O_3 และ 5%CAT-TH-B-200 + O_3 พบว่า 5%CAT-TH-B-200 มีเสถียรภาพที่ดีในการใช้งาน แม้ใช้ซ้ำรวมสามครั้งเป็นเวลา 1,080 นาที จากการทดลองนี้แสดงให้เห็นว่าถ่านกัมมันต์มีอายุการใช้งานถึง 18 ชั่วโมง

ภาควิชา.....วิศกรรมเคมี.....ลายมือชื่อนิสิต.....สุขุม เฉยศิริ.....

สาขาวิชา.....วิศกรรมเคมี.....ลายมือชื่อ อ.ที่ปรึกษาวิทยานิพนธ์หลัก.....

ปีการศึกษา.....2552.....

4970813321 : MAJOR CHEMICAL ENGINEERING
KEYWORDS : PHENOL / THREE-PHASE FLUIDIZED BED / IRON OXIDE / ACTIVATED CARBON / OZONE

SUKHUM CHAEYSIRI : PREPARATION OF ACTIVATED CARBONS DOPED WITH IRON OXIDE FOR REMOVING PHENOL WITHIN PILOT-SCALED THREE-PHASE FLUIDIZED BED. ADVISOR : ASSOC. PROF. TAWATCHAI CHARINPANITKUL, D.Eng., 99 pp.

Activated carbons doped with iron oxide were prepared for decomposition of aqueous phenol in three-phase fluidized bed reactor. The gas, liquid and solid phases in the reactor were ozone, aqueous phenol and Fe/activated carbon, respectively. Two types of activated carbon (AC-US and AC-TH) with average pore diameter of 2.3 and 1.7 nm and specific surface area of 1,060 and 1,154 m^2/g, relatively were to use in this work. Based on laboratory-scaled investigation AC-TH was selected used in large-scaled experiments. 5 wt.% Fe on activated carbons were prepared by two techniques, namely wet impregnation (IMA) and incipient wetness impregnation (IMB). After impregnated and calcined at 500°C under nitrogen gas, 5%CAT-TH-A-500 could be prepared from IMA and 5%CAT-TH-B-500 form IMB. With 10 wt.% of Fe precursor, 10%CAT-TH-B-500 was prepared. With 5 wt.% of Fe precursor and calcined at 200°C under ambient air, 5%CAT-TH-B-200 was prepared. All activated carbons combined with ozone could provide detectable phenol and TOC removal efficiency. The sequence of phenol removal efficiency in a period of 60 minutes was as follows: 5%CAT-TH-B-500 + O_3 (99%) = 5%CAT-TH-A-500 + O_3 (99%) > AC-TH + O_3 (98%) > 10%CAT-TH-B-500 + O_3 (97%) > 5%CAT-TH-B-200 + O_3 (90%) > only O_3 (67%). The sequence of TOC removal efficiency at 360 min was as follows: AC-TH + O_3 (92%) > 5%CAT-TH-B-200 + O_3 (81%) > 5%CAT-TH-A-500 + O_3 (71%) = 10%CAT-TH-B-500 + O_3 (71%) > 5%CAT-TH-B-500 + O_3 (69%) > only O_3 (52%). However, AC-TH and 5%CAT-TH-B-200 could provide the hightest efficiency for TOC removal. In pilot-scaled three-phase fluidized bed reactor, the experiments were carried out using 200 L of 20 ppm aqueous phenol with AC-TH + O_3 and 5%CAT-TH-B-200 + O_3. It was found that 5%CAT-TH-B-200 exhibited with good stability even after repeated use in three consecutive runs (1,080 minutes) in pilot-scaled system. Usable lifetime of 18 hours could be verified from experiments using re-used activated carbon.

Department : Chemical Engineering Student's Signature Sukhum Chaeysiri
Field of Study : Chemical Engineering Advisor's Signature T. Charinpanitkul
Academic Year : 2009

ACKNOWLEDGEMENTS

The author would like to thank Assoc.Prof. Dr. Tawatchai Charinpanitkul, guidance throughout this study, deep discussion and constant encouragement throughout this project including the instructing for developing the self-learning. The author is very grateful to Prof. Wiwut Tanthapanichakoon, Dr. Apinan Soottitantawat and Dr. Pratarn Wongsarivej, who have contributed to make this thesis more understandable. Therefore I would like to give them my gratitude for their kindness.

Many thank for kind suggestions and useful help, in particular all catalysts and reactor used in this study, should be addressed from National Science and Technology Development Agency (NSTDA), National Nanotechnology Center (NANOTEC).

In addition, I would also grateful to thank to Assoc. Prof. Muenduen Phisalaphong, as the chairman. Many thank for kind suggestions and useful help, in particular in this study, should be addressed to Miss Pornsiri Tongprem and Miss. Pilasinee Limsuwan As well, the author thanks the teachers, research assistant, friends, brothers and sisters in Center of Excellence in Particle Technology, Chulalongkorn University

Last but not least, he also would like to dedicate this thesis to his parents who have always been the source of his support and encouragement.

ศูนย์วิทยทรัพยากร
จุฬาลงกรณ์มหาวิทยาลัย

CONTENTS

Page

ABSTRACT (THAI)……...…… iv
ABSTRACT (ENGLISH) …….……...…… v
ACKNOWLEDGEMENT…… vi
CONTENTS…….……. vii
LIST OF TABLE……...…… x
LIST OF FIGURES…….. xii
CHAPTER
I INTRODUCTION…… 1
1.1 Background……... 1
1.2 Objective…… 2
1.3 Scope…….. 2
1.4 Benefit of this research……...…….. 3
II FUNDAMENTALS AND LITERATURE REVIEW…….…… 4
2.1 Phenol…….. 4
2.2 Activated carbon……. 6
2.2.1 Advantage of activated carbon…… 6
2.2.2 Pores structure of activated carbon……. 7
2.2.3 Adsorption isotherm…… 8
2.3 Catalyst preparation……... 10
2.3.1 Incipient wetness impregnation…….. 11
2.3.2 Wet impregnation…… 12
2.3 Three-phase fluidized bed reactor……. 13
2.3.1 Applications of three-phase fluidized bed reactor…….. 13
2.3.2 Hydrodynamic relations for gas-liquid-solid fluidized bed reactor 13
2.3.3 Pressure drop and phase holdup……..... 17
2.3.3 Flow regime…… 20
2.4 Literature reviews……..... 21

III EXPERIMENTAL…….. 29
3.1 Chemicals…….. 29
3.2 Preparation of activated carbons doped with iron oxide……... 30
3.2.1 The commercial granular activated carbon pretreatment…… 31
3.2.2 The commercial granular activated carbon after pretreatment will be loaded with iron nitrate solution by each of two impregnation techniques…… 31
3.2.3 Activated carbon after impregnated with iron nitrate was calcined by two different conditions……. 31
3.3 Characterization of particle……... 32
3.3.1 Nitrogen physisorption (BET analyzer)…….. 32
3.3.2 Thermogravimetric Analyser (TGA analyzer)……... 32
3.3.3 The Scanning Electron Microscope (SEM) and Energy Dispersive Spectroscopy (EDS)……. 33
3.3.4 X-ray fluorescence spectroscopy (XRF)……. 34
3.3.5 X-ray diffraction (XRD)……. 34
3.4 Experimental system……. 35
3.4.1 Laboratory-scaled three phase fluidized bed reactor…….. 35
3.4.2 Pilot-scaled fluidized bed reactor…… 38
3.5 Analytical instrument……... 44
3.5.1 High performance liquid chromatography (HPLC)…… 44
3.5.2 Total organic carbon (TOC)……...….... 45
IV RESULTS AND DISCUSSION……. 46
4.1 Characteristics of activated carbon……... 46
4.1.1 Particle size distribution…….. 46
4.1.2 N_2 adsorption/desorption Isotherm……. 47
4.1.3 Pore size distribution…….. 48
4.1.4 Surface area of activated carbons…… 50
4.1.5 Attrition resistance of commercial activated carbon…….. 50
4.2 Effect of activated carbon…… 51
4.3 Characteristics of activated carbon doped iron oxide…….. 53
4.3.1 The thermal stability…… 53
4.3.2 Surface area of activated doped with iron oxide……. 56

4.3.3 Energy dispersive X-ray spectroscopy…… 57
4.3.4 Crystal structure on activated carbons…… 60
4.3.5 Production data…… 61
4.5 Effect of iron oxide on activated carbon for aqueous phenol removal…. 62
4.5 Aqueous phenol removal in a laboratory-scaled fluidized bed reactor…. 64
4.5.1 Phenol removal by different impregnation techniques of activated carbons…….. 65
4.5.2 Phenol removal by different Fe content in activated carbon…….. 68
4.5.3 Phenol removal by different calcination condition of activated carbons…….. 71
4.6 Aqueous phenol removal in a pilot-scaled fluidized bed reactor…….. 75
4.6.1 Ozonation combined with activated carbons in pilot-scaled…….. 75
4.6.2 Deactivation of activated carbon doped with iron oxide…… 78
V CONCLUSIONS AND RECOMMENDATIONS…….. 81
5.1 Conclusions…….. 81
5.2 Recommendations for future studies…… 82
REFERENCES…… 83
APPENDICES…….. 87
APPENDICES A…….. 88
APPENDICES B……..... 95
APPENDICES C…… 97
VITA…… 99

ศูนย์วิทยทรัพยากร
จุฬาลงกรณ์มหาวิทยาลัย

LIST OF TABLES

Page

Table 2.1 Physical and chemical properties of phenol……..……. 4

Table 2.2 Source materials that have been studied for the production of activated carbon…….… 6

Table 2.3 Types of catalyst impregnation…….……. 10

Table 2.4 Examples of applications of three-phase fluidized bed processing…... 13

Table 2.5 Kinetic constant, half-life and cost evaluation for all the processes….. 25

Table 3.1 The technical specification of granular activated carbon…….. 30

Table 3.2 Specification of the pilot scale fluidized bed reactor…….…… 40

Table 3.3 Technical data of ozone generator……. 42

Table 4.1 Particle size distribution of granular activated carbon…….....… 47

Table 4.2 The porous characteristics of virgin AC…… 50

Table 4.3 Properties of commercial activated carbon…… 51

Table 4.4 Code name of Fe/AC particles…… 53

Table 4.5 Weight loss of activated carbon at 500 °C under N_2 flow……. 54

Table 4.6 Weight loss of activated carbon at 200 °C under air flow……. 54

Table 4.7 Weight loss of 5 wt.% Fe on activated carbon at 500 °C under N_2 flow……. 54

Table 4.8 Weight loss of 5 wt.% Fe on activated carbon at 500 °C under air flow……. 54

Table 4.9 Weight loss of 5% Fe on activated carbon at 200 °C under air flow…. 55

Table 4.10 The porous characteristics of virgin AC supports and Fe/AC particles. 56

Table 4.11 Element compositions of different calcination condition of activated carbons doped with iron oxide……... 57

Table 4.12 Fe content in activated carbon …….. 59

Table 4.13 Information of Fe/AC prepared by different impregnation…… 61

Table 4.14 Information of Fe/AC calcined in two different conditions……... 61

Table 4.15 Experimental condition of a laboratory-scaled three-phase fluidized bed reactor…….. 62

Table 4.16 The characteristics of AC and Fe/AC particles…….. 62
Table 4.17 Experimental condition of a laboratory-scaled three-phase fluidized bed reactor…….. 64
Table 4.18 Phenol decomposition efficiency and TOC removal efficiency for AC-TH, 5%CAT-TH-A-500 and 5%CAT-TH-B-500……. 67
Table 4.19 Phenol decomposition efficiency and TOC removal efficiency for AC-TH, 5%CAT-TH-B-500 and 10%CAT-TH-B-500…… 70
Table 4.20 Phenol decomposition efficiency and TOC removal efficiency for AC-TH, 5%CAT-TH-B-500 and 5%CAT-TH-B-200……. 73
Table 4.21 Experimental condition of a pilot-scaled three-phase fluidized bed reactor…….. 75
Table 4.22 Phenol decomposition efficiency and TOC removal efficiency in pilot-scaled fluidized bed reactor…… 77
Table 4.23 Phenol decomposition efficiency and TOC removal efficiency for 5%CAT-TH-B-200 after repeated use in three consecutive runs.... 79
Table B.1 Hydrodynamics data of lab-scaled experiment…….. 95
Table B.2 Hydrodynamics data of pilot-scaled experiment…… 96
Table C.1 Pseudo first order rate constant for removal of aqueous phenol…… 98

ศูนย์วิทยทรัพยากร
จุฬาลงกรณ์มหาวิทยาลัย

LIST OF FIGURES

Page

Figure 2.1 Shapes of adsorption isotherm…… 8
Figure 2.2 Schematic representation of gas-liquid-solid fluidized bed for co-current upward gas-liquid-solid systems with liquid as the continuous phase…….. 14
Figure 2.3 Pressure drop and bed height and superficial velocity for a bed of solid…… 17
Figure 2.4 Route of catalytic oxidation of phenol in aqueous phase over a commercial copper catalyst……. 24
Figure 2.5 experimental flow sheet of three-phase fluidized bed…… 27
Figure 2.6 Pathway for photochemical decomposition of phenol…… 28
Figure 3.1 Automatic specific surface area/pore size distribution measurement (BELSORP mini, BEL Japan, Japan)…… 32
Figure 3.2 Thermogravimetric Analyzer (Pyris diamond, Perkin Elmer, USA)…. 33
Figure 3.3 Scanning Electron Microscopy (SEM) (S-3400N, Hitachi, Japan)…… 33
Figure 3.4 X-ray fluorescence spectroscopy (XRF) (Oxford, ED 2000)…… 34
Figure 3.5 X-ray diffraction (XRD) (Rigaku, TTRAX III)……. 34
Figure 3.6 The laboratory scale fluidized bed reactor……. 36
Figure 3.7 Schematic diagram of the laboratory scale fluidized bed reactor…….. 36
Figure 3.8 The top part of laboratory scale fluidized bed reactor…… 37
Figure 3.9 The middle part of laboratory scale fluidized bed reactor……. 37
Figure 3.10 The lower part of laboratory scale fluidized bed reactor…… 38
Figure 3.11 Schematic flow diagram of the pilot scale fluidized bed reactor…… 39
Figure 3.12 Design configurations of three phase fluidized bed reactor in the pilot scale system……. 40
Figure 3.13 Fluidized bed columns…… 41
Figure 3.14 Wire mesh and steel flange…… 41
Figure 3.15 Ozone generator (OZ-754, Ozzon, Thailand)…… 43

Figure 3.16 Swagelok stainless steel, check valve and air distributor…….. 43
Figure 3.17 The picture of HPLC (column class VP, Shimadzu)……. 44
Figure 3.18 The picture of TOC analyzer (TOC-VCPH, Shimadzu)……..... 45
Figure 4.1 N_2 adsorption/desorption isotherm on AC-US and AC-TH……... 47
Figure 4.2 Micropore size distribution of AC-US and AC-TH…… 49
Figure 4.3 Mesopore size distribution of AC-US and AC-TH……..... 49
Figure 4.4 Phenol concentrations as a function of time for Ozone, AC-TH + Air and AC-TH + Ozone…… 52
Figure 4.5 TOCs as a function of time for Ozone, AC-TH + Air and AC-TH + Ozone…… 52
Figure 4.6 SEM of (a) AC-TH, (b) 5%CAT-TH-B-200 and (c) 5%CAT-TH-B-500…… 58
Figure 4.7 XRD of AC and Fe/AC…….. 60
Figure 4.8 Phenol concentrations as a function of time for ozonation combined with AC-TH and Fe/AC…… 63
Figure 4.9 TOCs as a function of time for ozonation combined with AC and Fe/AC…… 63
Figure 4.10 Phenol concentrations as a function of time for ozonation combined with AC-TH, 5%CAT-TH-A-500 or 5%CAT-TH-B-500……. 65
Figure 4.11 TOCs as a function of time for ozonation combined with AC-TH, 5%CAT-TH-A-500 and 5%CAT-TH-B-500…… 66
Figure 4.12 Phenol concentrations as a function of time for ozonation combined with AC-TH, 5%CAT-TH-B-500 and 10%CAT-TH-B-500……. 69
Figure 4.13 TOCs as a function of time for ozonation combined with AC-TH, 5%CAT-TH-B-500 and 10%CAT-TH-B-500……. 69
Figure 4.14 Phenol concentrations as a function of time for ozonation combined with AC-TH, 5%CAT-TH-B-500 and 5%CAT-TH-B-200…… 71
Figure 4.15 TOCs as a function of time for for ozonation combined with AC-TH, 5%CAT-TH-B-500 and 5%CAT-TH-B-200…… 72
Figure 4.16 Phenol concentrations as a function of time for oxidation with only ozone and ozone combined with solid particle in pilot-scaled…... 76

Figure 4.17 TOCs as a function of time for oxidation with only ozone and ozone combined with solid particle in pilot-scaled….. 76
Figure 4.18 Phenol concentrations as a function of time for oxidation with 5%CAT-TH-B-200 after repeated use in three consecutive runs…….. 78
Figure 4.19 TOCs as a function of time for oxidation with 5%CAT-TH-B-200 after repeated use in three consecutive runs…….. 79
Figure C.1 Phenol removal rates…….. 97

ศูนย์วิทยทรัพยากร
จุฬาลงกรณ์มหาวิทยาลัย

CHAPTER I

INTRODUCTION

1.1 Background

Water is essential for life because it is used in industrial process, household consumption and application for daily life, such as washing, farming. Wastewater is emitted from many sources, for example, wastewater drainage from processes and community etc. It becomes one of the greatest problems in various countries, because it has exerted environmental and health threats to the society.

Phenol is one of the most harmful aromatic hydrocarbon compounds existing in wastewater. The component of phenol in wastewater has been emitted from various chemical industries such as wood preservative, resin, pesticide, textile, paper and dye industrial. It can damage the skin and other tissues of the human and animals. When digested, phenol-containing liquids could also lead to liver damages, dark urine, irregular heartbeats, muscle tremors and loss of spatial coordination, among others **[1]**. There are essential requirements of efficient treatment system, which could meet legally regulated standard and economic constraints.

Phenol in wastewater can be decomposed by many methods, such as conventional energy-intensive combustion. Furthermore, phenol can be decomposed by wet air oxidation using metallic catalysts and oxidizing agents **[2,3]**. Though decomposition of phenolic compounds by ozonation have been investigated **[4,5]**, there is still room for improvement. Therefore, ozonation combined with metallic catalysts process is proposed as a proper choice for wastewater treatment process because of its various advantages such as non-toxicity and insolubility. A three-phase fluidized bed reactor where fluidized particles are moving inside the reactor has been recognized as a promising method for wastewater treatment. It is a novel reactor for ozonation process. It allows an intimate contact between phases and present many advantages concerning hydrodynamic and mass transfer phenomena.

An aqueous phenol solution is decomposed by the fluidized particles and oxidation reaction in reactor **[5]**.

Activated carbon (AC) is widely used as adsorptive material to remove numerous organic compounds from wastewater because of its large specific surface area, highly porous structure and low cost **[6]**. Metal supported on AC is a promising alternative because of the synergy of huge number of active sites and the concentration of the adsorbed species on the internal surface area. Therefore, the high efficiency of wastewater treatment is extremely importance. In this research using a pilot-scaled of three-phase fluidized bed reactor for decomposing the phenolic compounds in wastewater treatment process which Fe on activated carbon (Fe/AC) as solid metallic on activated carbon and ozone as gas oxidizing agent under ambient conditions in order to provide a new alternative mean to tackle this problem.

1.2 Objective of the research

The prime objective of this thesis is to study a method to prepare activated carbon doped with Fe for removing aqueous phenol in a three-phase fluidized bed. The performance of phenol removal using activated carbon doped with Fe under different condition would be experimentally examined.

1.3 Scope of experiment and analyses in this research

1.3.1 Set up a laboratory-scaled and pilot-scaled wastewater treatment system

- Reactor: Three-phase fluidized bed reactor
- Solid particle: Fe on commercial activated carbons or virgin commercial activated carbon
- Oxidizing agent (Oxidant): Ozone (O_3)
- Oxidizing target: Aqueous phenol

1.3.2 Preparation of activated carbon doped with iron oxide

- Range of Fe content is 5 - 10 wt. %
- Techniques of preparation are wet impregnation and incipient wetness impregnation
- Calcination conditions are 500 °C under nitrogen gas or 200 °C under ambient air condition

1.3.4 Test activated carbons by decomposition of phenol in laboratory-scaled

- Solid particle loading per column of 5 g
- Initial phenol concentration of 10 ppm
- Solution flow rate of 1 L/min
- Gas flow rate of 2 L/min

1.3.5 Test activated carbons decomposition of phenol in pilot-scaled

- Solid particle loading per column of 1.3 kg
- Initial phenol concentration of 20 ppm
- Solution flow rate of 8 L/min
- Gas flow rate of 5 L/min

1.3.6 Analyze the decomposition of phenol and intermediate product.

- HPLC (High performance liquid chromatography, Shimadzu column class VP)
- TOC (Total organic carbon analyzer, Shimadzu TOC-VCPH)

1.3.7 Analyze the characteristic of catalyst.

- BET (BELSORP mini, BEL Japan)
- SEM&EDS (S-3400N, Hitachi)
- TGA (Pyris diamond, Perkin Elmer)
- XRD (Rigaku, TTRAX III)
- XRF (Oxford, ED 2000)

1.4 Benefit of this research

The expected benefit to be obtained from this research is an understanding in an alternative wastewater treatment system using Fe/AC and ozone within a three-phase fluidized bed reactor. Knowledge of this work should be adaptable for high level treatment of actual wastewater from industrial estate.

CHAPTER II

FUNDAMENTALS AND LITERATURE REVIEW

2.1 Phenol

Phenol is the simplest aromatic alcohol which could be characterized by a hydroxyl group (-OH) attached to a benzene ring. The term phenol is not only phenol itself but also for a class of aromatic compounds possessing a hydroxyl group attached to a benzene ring or a complex ring system.

Table 2.1 Physical and chemical properties of phenol

Phenol	
Chemical formula	C_6H_5OH
Chemical structure	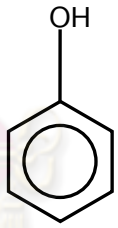
Other names	Carbolic acid Benzenol Phenylic acid Hydroxybenzene Phenic acid
Molecular weight (g mol^{-1})	94.11
Boiling point (°C)	181.7
Melting point (°C)	40.5
Solubility in water at 20 °C (g/l)	83

Some phenols interface with the endocrine system and disrupt the function of hormones. They have antiseptic property and are used in formulating disinfectants, deodorizers, and pesticides. **Table 2.1** summarizes the important properties of phenol. Phenol in water solution is sometimes called carbolic acid. Phenol differs from aliphatic alcohols which hydroxyl group is bonded to a saturated carbon atom. Due to the tendency of pi-orbital overlap between carbon and oxygen, phenol can lose easily the hydrogen cation (H^+) from the hydroxyl group, resulting in higher acidity than aliphatic alcohols (but weaker acidity than carboxylic acids). The intermediate state losing H^+ ion from the hydroxyl group in a phenol is called phenoxide anion $C_6H_5O^-$. It reacts with strong bases to from salts called phenolate. Pure phenol is a colorless-to-white crystalline solid. It is moderately soluble in water and is soluble in ethanol and ether. Phenols form stronger hydrogen bonds than aliphatic alcohols. Phenols are more soluble in water than alcohols and have higher boiling points. Many phenols have a sharp, spicy odour, but phenol smells blend and sweetish. It is highly toxic and caustic **[7].**

Phenol exists naturally and is manufactured in large quantity. It is in many industrial processes. It is found in nature in some foods, in human and animals wastes, and in decomposing organic material. It is produced by the body and excreted independent of external exposure or intake. It is used primarily as an intermediate in the production of phenolic resins. The main source of phenolic wastewater is the industries such as petrochemicals, coal gasification, pesticide manufacture, and electroplating and metallurgical operations.

The acceptable phenolic compound concentration to be treated in central wastewater treatment process must be controlled at the industrial effluent standard (1.0 mg/l). This means that any particular plant (located in the industrial estates) which discharges phenolic and related compounds greater than the Industrial Estate Authority of Thailand (IEAT) acceptable limits (1.0 mg/l for phenolic compounds) must have their own effective wastewater treatment unit before transferring the wastes to the central treatment process.

2.2 Activated carbon [8]

Activated carbon is a processed carbon material with a highly developed porous structure and a large internal specific surface area. It consists, principally of carbon (87 to 97 %) but also contains such elements as hydrogen, oxygen, sulphur and nitrogen, as well as, various compounds either originating from the raw material used in its production or generated during its manufacture. Activated carbon has the ability to adsorb various substances both from the gas and liquid phase by collecting them on the surface of its pores.

2.2.1 Advantage of activated carbon

Activated carbon is widely used as adsorbent of waste gases and vapor e.g. for remaining CS_2 from air, of solvents for their recovery, of contaminants of aqueous solution, e.g. the purification of sugar syrup, in the treatment of portable water and waste water, in air conditioning devices, in vacuum technology, e.g. in sorption pumps, in adsorption of toxins from systemic fluids, etc. Activated carbon is also finding increasing application as catalyst supports as well as materials for electrodes in chemical sources of electricity. Compared with other commercial adsorbents, activated carbon has a broad spectrum of adsorptive activity, excellent physical and chemical stability, and ease of production from carbonaceous waste or useless material.

Almost any carbonaceous raw material can be used for the manufactured of activated carbon. However, the principle properties of manufactured activated carbon depend on the type and properties of the raw material used.

Table 2.2 Source materials that have been studied for the production of activated carbon

Bagasse	Corncobs	Lignin	Saw dust
Bones	Distillery waste	Peat	Petroleum coke
Coal	Flue dust	Polymer scrap	Wood
Coconut shells	Fruit pits	Rubber waste	etc.

2.2.2 Pores structure of activated carbon

The formation of the crystalline structure of activated carbon begins early during the carbonization process of the starting material. During the process of activation the spaces between the elementary crystallites, become cleared of various carbonaceous compounds and disorganized carbon, and carbon is also remove partially from the layers of the elementary crystallites. The resulting voids are called pores. A suitable methods and condition of production process cause a layer number of pores to be formed so that the total surface area of their walls. I.e. the internal surface of the activated carbon is very large so this, cause large adsorption capacity. Activated carbon usually has several groups of pores, each group having a certain range of values of the effective diameter.

Generally pores can be classified into three group: macropores, mesopores and micropores.

Macropores are those having effective diameter > 50 nm and their volumes are not entries filled with adsorbate via the mechanism of capillary condensation. The values of their surface area are negligibly small when compared with the surface area of the remaining type of pore. Consequently macropores are not important in the process of adsorption as they merely act as transport arteries rendering the internal parts of the carbon grains accessible to the molecules of the adsorbate.

Mesopores, also known as transitional pores, have effective diameter falling in the range of 2-5 nm. The process of filling their volume with adsorbate takes place via the mechanism of capillary condensation. For average activated carbon, the volumes of mesopores lie between the limits 0.02-0.2 cm^3/g. The peak of the distribution curve of their pore volume versus their radius is mostly in the range of 4-20 nm. For adsorption in liquid phase, activated carbon should have pores size larger than 3 nm in diameter, which falls in the range of mesopores. Besides their significant contribution to adsorption, mesopores also perform as the main transport arteries for the adsorbate.

Micropores have small sizes comparable with those of adsorbed molecules. Their effective diameters are usually smaller than 2 nm, and average pore volumes of activated carbons usually fall in the range of 0.15-0.5 cm^3/g. In general, the surface area of microporous activated carbon lies between 1,00-1,000 m^2/g. The energy of adsorption in micropores is substantially greater than that for adsorption in mesopores or at the nonpores surface. In micropores, adsorption proceeds via the mechanism of volume filling.

2.2.3 Adsorption isotherm

The adsorption isotherm provides essential information about the porosity in solids and there are significant variations in isotherm shape. According to IUPAC classification, the shapes of adsorption isotherm are shown in **Figure 2.1**.

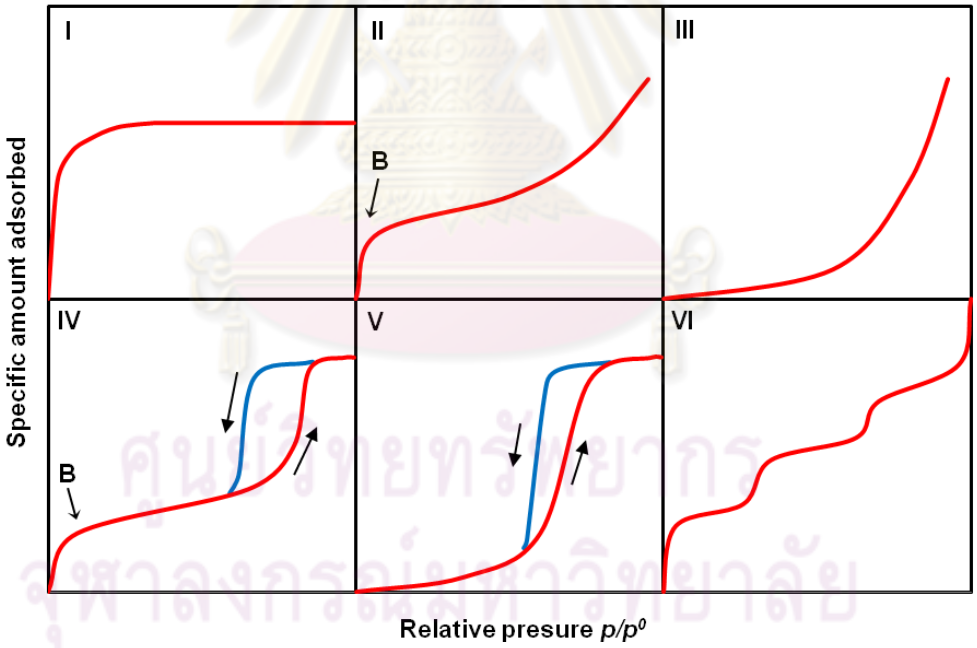

Figure 2.1 Shapes of adsorption isotherm

Type I isotherm is concave to the relative pressure (p/p^0) axis. It rises sharply at low relative pressures and reaches a plateau: the amount adsorbed by the unit mass of solid approaches a limiting value as $p/p^0 \rightarrow 1$. The narrow range of relative pressure necessary to attain the plateau is an indication of a limited range of pore size and the

appearance of a nearly horizontal plateau indicates a very small external surface area. The limiting adsorption is dependent on the available micropore volume.

Type II isotherm is concave to the p/p^0 axis, then almost linear and finally convex to the p/p^0 axis. It indicates the formation of an adsorbed layer whose thickness increases progressively with increasing relative pressure until $p/p^0 \rightarrow 1$. If the knee of the isotherm is sharp, the uptake at Point B is usually considered to represent the completion of the monomolecular layer and the beginning of the formation of the multimolecular layer.

In Type III, the isotherm is convex to the p/p^0 axis over the complete range and therefore has no Point B. This feature is indicative of weak adsorbent-adsorbate interactions.

Type IV isotherm, whose initial region is closely related to the Type II isotherm, tends to level off at high relative pressures. It exhibits a hysteresis loop, the lower branch of which represents measurements obtained by progressive addition of gas of adsorbent, and the upper branch by progressive withdrawal. The hysteresis loop is usually associated with the filling and emptying of the mesopores by capillary condensation.

Type V isotherm is initially con vex to the p/p^0 axis and also levels off at high relative pressures. As in the case of the Type III isotherm, this is indicative of weak adsorbent-adsorbate interactions. A Type V isotherm exhibits a hysteresis loop which is associated with the mechanism of pore filling and emptying.

Eventually, Type VI isotherm, or stepped isotherm, is associated with layer-by-layer adsorption on a highly uniform surface such as graphite. The sharpness of the steps is dependent on the system and the temperature.

2.3 Catalyst preparation [9]

Preparation of heterogeneous catalyst can be carried out through numerous routes. The following underlying steps are common to all procedures for heterogeneous catalysis. The support may be either a metal oxide, crystalline or amorphous. The impregnating solution may be either aqueous or organic. The dominant driving force for pore filling is capillary pressure (i.e., fluid mechanical), thus rendering the quality of impregnation insensitive to surface interactions between support and surface precursor that might otherwise limit the overall loading by other methods (e.g., equilibrium adsorption). Based on its simplicity, impregnation method represents the most widely cited synthesis method for supported metal oxides.

Impregnation entails wetting a solid support material (typically of high surface area) with a liquid solution containing the dissolved surface oxide precursor. Subclassification of impregnation methods depends upon the relationship between impregnating liquid volume (V_{imp}) and support pore volume (V_p): Capillary, dry or incipient wetness impregnation (IWI) is often used to describe the process when $V_{imp} \approx V_p$ whereas wet impregnation (WI), equilibrium adsorption, diffusional or ion exchange is preferred when $V_{imp} > V_p$.

Table 2.3 Types of catalyst impregnation

Methods:	Incipient wetness impregnation	Wet impregnation
Distinguishing characteristics:	Use sufficient metal solution to fill pore volume of catalyst support; adjust metal concentration for desired weight loading	Amount of solution in excess of pore volume of support; precursors that interact weakly with support are washed/filtered away
Advantages:	Simplest to employ; no filtering; metal content is fixed	Mixing is improved
Disadvantages:	Strong precursor-support interaction is not guaranteed	Filtering required; metal loading must be measured; metal wasted if it does not strongly interact with support

The types of impregnations can be classified as in **Table 2.3**. The first, incipient wetness impregnation is procedurally the simplest. The thick paste formed from contacting the support with just the amount of liquid needed to fill the pore volume contains a precise metal loading and does not need to be filtered. The drawbacks from this method arise when metal precursors do not interact strongly with the support surface. Metal complexes that remain in solution can migrate significantly during drying.

Impregnations can be considered wet whenever an amount of solution in excess of the support pore volume is employed. Wet impregnation is as simple as contacting the solution for a certain lime and then recovering the solid by filtration. The amount of metal retained by the solid must be determined by analysis either the solid or liquid. The extent of metal retained by the support is a function of the precursor-support interaction, which may be chemical or physical (electrostatic) in nature. As WI is defined here, no attention is paid to controlling the impregnation conditions to optimize the interaction.

2.3.1 Incipient wetness impregnation

IWI is notoriously deficient at achieving uniform surface coverage. Multiple resistances exist to achieving uniform coverage that may lead to undesirable distribution profiles (crusting) of the surface oxide. For example, rising hydraulic pressure at blocked pore ends prevents complete wetting of the surface as pore-filling liquid compresses trapped gas; even after the gas eventually dissolves, different residence times of wetting and adsorption can lead to concentration profiles. Another resistance is the narrowing of pore necks at their entrance created by (1) crystallization of active precursor due to premature solvent evaporation or (2) unfavorable charge balancing between support and surface precursors such as most metal oxides on SiO_2. It is even conceivable that a sample intended to possess submonolayer surface coverage may, in fact, possess crystalline regions of locally high concentration (i.e., above monolayer coverage), whereas areas of respectively low concentration remain noncrystalline (submonolayer coverage).

2.3.2 Wet impregnation

Impregnation methods that immerse a solid support into an excess of solution ($V_{imp} > V_p$) of dissolved surface oxide precursor for long periods of time are frequently called *equilibrium adsorption*, *wet impregnation* or *ion exchange*. In contrast to IW impregnation, the dominant driving forces for these methods are the concentration gradient and electrostatic interactions. Almost all supports are oxides that bear a net positive or negative electrical surface charge, which attracts oppositely charged ions in aqueous solution. The charge of these amphoteric oxides is a function of aqueous solution pH and is dictated by the oxide's point-of-zero charge (pzc). For pH > pzc, terminal hydroxyls on the support deprotonate, leaving the surface with a net negative charge that attracts cationic species. For pH < pzc, the hydroxyls protonate and favor anionic adsorption. For a given oxide support, adjusting the difference between pzc and solution pH allows control of the surface oxide loading.

Wet impregnation is generally thought to yield better dispersion of surface metal oxide overlayers than IWI, although this is difficult to measure for metal oxides. By way of comparison, chemisorption reveals much better atomic dispersion of the active species for supported metal catalysts made via WI versus IWI. Nonetheless, despite uniform distribution of active precursor species throughout the support interior, WI does not necessarily provide uniform distribution between interior and exterior regions of the support. Recovery of the solid support from solution leads to surface evaporation of residual solvent, which preferentially deposits noninteracung precursor species on the support's exterior shell, thereby enriching the precursor outer surface concentration. A final wash step should be employed to remove this physisorbed (i.e., weakly bound) active species, but precise control of the wash pH is required to avoid inadvertently expelling the electrostatically bound species. Another disadvantage of WI is that the final loading of active species is rarely known a *priori* and requires subsequent elemental analysis.

2.3 Three-phase fluidized bed reactor [10]

The expression of three-phase fluidization was used to describe fluidization of solid particles by two fluids. A gas and a liquid were the fluidizing media used in the applications.

2.3.1 Applications of three-phase fluidized bed reactor

Studies of three-phase fluidization had been of interest and their numerous applications existed in various industrial processes, which varied in size from bench to commercial scale. In such system, the individual phases could be reactants, products, catalysts, or inert. Some examples of three-phase fluidization applications were shown in **Table 2.4**.

Table 2.4 Examples of applications of three-phase fluidized bed processing.

Physical processing	Chemical processing	Biochemical processing
Drying of calcium carbonate and polyvinylchloride	Production of zinc hydrosulfite	Aerobic biological waste treatment
Dust collection	Methanol fermentation	Production of animal cells
Crystallization	Electrode	Enzyme immobilization
Sand filter cleaning	Coal liquefaction	Ethanol fermentation
Drying of granular material	Coal gasification	Antibiotic production
Lactose granulation	Fuel gas desulfurization	Conversing of sucrose to glucose by plant cells

2.3.2 Hydrodynamic relations for gas-liquid-solid fluidized bed reactor **[11]**

As mentioned previously, the gas-liquid-solid fluidization was an operation, in which the solid particles layer, fluidized by gas and liquid and then behaved like a fluid. In general, the state of the particle motion in the fluidized bed operation by the upward flow of the fluid could be subdivided into three basic operating regimes: the fixed bed regime, the expanded bed regime, and the transport regime.

The fixed bed regime existed when the drag force on the particle induced by the flow of a gas-liquid mixture was smaller than the effective weight of the particle layer. With an increase in gas and/or liquid velocity, the drag force counterbalances the effective weight of the particles then the bed would achieve the state of minimum fluidization and marked the onset of the expanded bed regime. With a further increase in gas and/or liquid velocity beyond the minimum fluidization velocity, the solid bed would change to the expanded bed regime until the gas or liquid velocity reached the terminal velocity of the particles in the medium (U_t'). At the gas or liquid velocity above U_t', operation would be considered as the transport regime.

Hydrodynamic behavior of three-phase fluidized bed reflected, the complex interactions between the individual phases. The most prominent interaction occurred between the rising gas bubbles and the surrounding liquid-solid mixture. Three distinct regions above the gas-liquid distributor were identifiable based on the prevailing physical phenomena: the distributor region, the bulk fluidized bed region, and the free board region. A schematic diagram was shown in **Figure 2.2**.

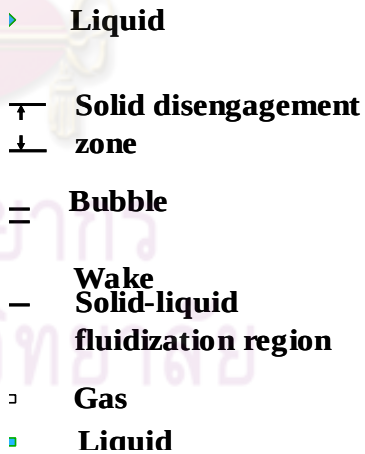

Figure 2.2 Schematic representation of gas-liquid-solid fluidized bed for co-current upward gas-liquid-solid systems with liquid as the continuous phase **[10]**

The distributor region referred to the region immediately above the gas-liquid distributor where gas spouts might occur. It included the region from initial bubble formation to the establishment of the final bubble shape. The hydrodynamic behavior in the distributor region inherently depended on the gas-liquid distributor design and the physical properties of the liquid-solid medium.

The bulk fluidized bed region included the main portion of the fluidized bed. The hydrodynamic behavior in the bulk fluidized bed region varied drastically over large ranges of operating conditions. However, for a given operating condition, there was a minimum axial transport property variation in the region.

Drastically different from the previous regions, the freeboard region mainly contained entrained particles from the bulk fluidized bed region. Particle entrainment led to a solids hold up profile above the fluidized bed surface that decreased axially in a manner similar to that in a gas-solid fluidized bed. Generally, the demarcation between the freeboard region and the bulk fluidized bed region was much more distinct for large/heavy particles than for small/light particles.

Some general models of gas-liquid-solid fluidized-bed reactors for the gas phase reactant *A* for a single solid catalyzed reaction *A* to products are represented in this section. Starting with information about the particle size, density of each phase and viscosity of liquid, the provided hydrodynamic relations may be used to determine bed characteristics such as the minimum fluidization velocity, particle terminal settling velocity, and so on. The equations in this section (2-1 to 2-6) are referred from.

Minimum fluidization velocity, U_{mf}

Minimum fluidization velocity was the velocity of fluid, which the solid particles moved apart and few vibrate. The equation for minimum fluidization velocity for gas-liquid-solid fluidized bed reactor was

$$U_{mf} = U_{mf,LS}[1 - 376U_G^{0.327}\mu_L^{0.227}d_p^{0.213}(\rho_S - \rho_L)^{-0.423}] \quad (2\text{-}1)$$

$$U_{mf,LS} = \frac{\mu_L(\sqrt{1135.69 + 0.0408Ar} - 33.7)}{d_p\rho_L} \quad (2\text{-}2)$$

$$Ar = \frac{\rho_L(\rho_S - \rho_L)gd_p^3}{\mu_L^2} \quad (2\text{-}3)$$

where U_{mf} = minimum fluidization velocity (m/s)

$U_{mf,LS}$ = minimum fluidization liquid velocity (m/s)

Ar = Archimedes number (-)

U_G = gas velocity (m/s)

μ_L = liquid viscosity (m/s)

d_p = diameter of particle (m)

ρ_S = density of solid (kg/m^3)

ρ_L = density of liquid (kg/m^3)

Terminal velocity, U_t

Terminal velocity of a single particle could be considered with an assumption that the particle moving through a fluid under the action of an external force. If the external force was the acceleration of gravity, *g*, which was constant. Also, the drag force always became larger with an increasing in velocity. The particle quickly reached a constant velocity, which was the maximum attainable under the circumstances, and which was called the terminal velocity. The equation for the terminal velocity was

$$U_t = \frac{gd_p^2(\rho_S - \rho_L)}{18\mu_L} \qquad K < 2.6 \quad (2\text{-}4)$$

$$U_t = 1.75\sqrt{\frac{gd_p(\rho_S - \rho_L)}{\rho_G}} \qquad K > 60 \quad (2\text{-}5)$$

$$K = d_p \left(\frac{g\rho_L(\rho_S - \rho_L)}{\mu_L^2} \right)^{1/3} \qquad (2\text{-}6)$$

2.3.3 Pressure drop and phase holdup **[12]**

When consider a fluidized bed column, which was partly filled with a fine granular material as shown schematically in **Figure 2.3**. The column was opened at the top and had a porous plate at the bottom to support the bed and to distribute the flow uniformly over the entire cross section. Fluid was admitted below the distributor plate at a low flow rate and passes upward through the bed without causing any particle motion. If the particles were quite small, flow in the channels between the particles would be laminar and the pressure drop across the bed would be proportional to the superficial velocity. As the fluid velocity was gradually increased, the pressure drop increased, but the particles did not move and the bed height remained the same. At a certain velocity, the pressure drop across the bed counterbalances the force of gravity on the particles or the weight of the bed, and any further increase in velocity caused the particles to move. This was point A on the graph. Sometimes the bed expanded slightly with the grains still in contact, since just a slight increased in porosity, **ε** could offset an increase of several percent in superficial constant and keep pressure drop, ΔP constant. With a further increase in velocity, the particles became separated enough to move above in the bed, and true fluidization begins (point B).

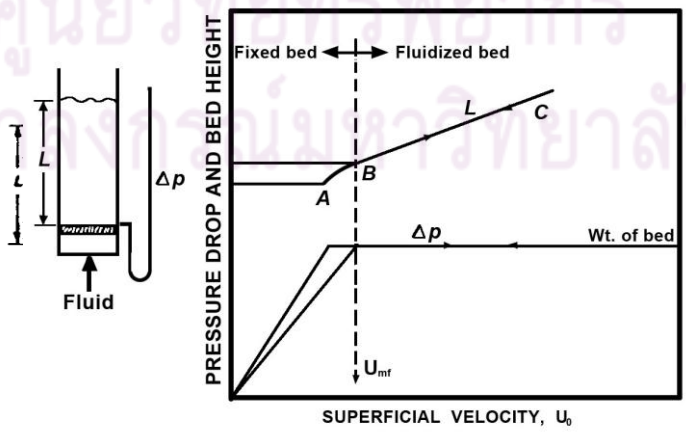

Figure 2.3 Pressure drop and bed height and superficial velocity for a bed of solid

Once the bed was fluidized, the pressure drop across the bed became constant, but the bed height continues to increase with increasing flow. The bed could be operated at quite high velocities with very little or no loss of solids, since the superficial velocity needed to support a bed of particle was much less than the terminal velocity for individual particles.

If the flow rate to the fluidized bed was gradually reduced, the pressure drop remained constant, and the bed height decreased, following the line BC that was observed for increasing velocities. However, the final bed height might be greater than the initial value for the fixed bed, since solids dumped in a column tended to pack more tightly than solids slowly settling from a fluidized bed state. The pressure drop at low velocities was then less than in the original fixed bed. On starting up again, the pressure drop offset the weight of the bed at point B, and this point, rather than point A, should be considered to give the minimum fluidization velocity, U_{mf} To measure U_{mf}, the bed should be fluidized vigorously, allowed to settle with the fluid turn off, and the flow rate increased gradually until the bed starts to expand. More reproducible value of U_{mf} could sometimes be obtained from the intersection of the graphs of pressure drop in the fixed bed and the fluidized bed.

The pressure drop through the bed was strongly related to the individual phase holdup in the bed. The phase holdup was defined as the fraction of the solids, liquid or gas phase to volume of the column. In the fluidized bed section with low solids entrainment rates, the solid holdup, ε_s, could be expressed as

$$\varepsilon_s = \frac{W}{\rho_s SH} \tag{2-7}$$

However, behavior of gas holdup in the freeboard region strongly depended on the flow regimes and hence, on both particle and liquid properties. Gas holdup in three-phase fluidized beds could be lower than that in a corresponding bubble column because the particles promoted bubble coalescence, however it could also be higher than that in a corresponding bubble column when the particles helped break up gas bubble in some certain operating ranges. Furthermore, gas holdup was important for

determining residence time of the gas in liquid. Kato et al. had proposed that the gas holdup in a system of gas-liquid-solid fluidization could be approximated by the following equation;

$$\varepsilon_g = \frac{0.3W^{1.3}}{(1+1.1W^{1.15})} \tag{2-8}$$

when the parameter W was defined as

$$W = \left(\frac{gD_c^2\rho_L}{\sigma}\right)^{0.196}\left(\frac{gD_c^2}{\mu_L^2}\right)^{0.035}\left(\frac{U_G}{\sqrt{gD_c}}\right) \tag{2-9}$$

The following relationship held among individual holdups:

$$\varepsilon_G + \varepsilon_L + \varepsilon_S = 1 \tag{2-10}$$

Under the steady state condition, the total axial pressure gradient (static pressure gradient) at any cross section in the column represented the total weight of the bed consisting of the three phases per volume as given by

$$g\frac{-dP}{dZ} = (\varepsilon_G\rho_G + \varepsilon_L\rho_L + \varepsilon_S\rho_S)d \tag{2-11}$$

where $\varepsilon_G, \varepsilon_L, \varepsilon_S$ = gas, liquid, and solid holdup (-), respectively

$\rho_G\rho_L\rho_S$ = gas, liquid, and solid density (kg/m^3), respectively

W = weight of solid particle in the bed (kg)

S = cross-section area of empty column (m)

H = effective height of bed expansion (m)

g = gravitational acceleration (m/s^2)

$\frac{dP}{dZ}$ = static pressure gradient.

D_c = column diameter (m)

σ = surface tension (mN/m)

μ_L = kinematic liquid viscosity (m^2/s)

U_G = gas velocity (m/s)

The frictional drag on the wall of the column and the acceleration of the gas and liquid flows could be neglected. In equation (2-11), the term $\varepsilon_G \rho_G$ in the right hand side was usually negligibly small compared to the other terms. The evaluation of individual phase holdups based on the pressure gradient method, ε_S could be directly obtained from equation (2-7) with the height of bed expansion measured experimentally while ε_G could be directly calculated from equation (2-8). Finally, ε_L could be calculated from equation (2-10) and (2-11) simultaneously with the experimentally measured static pressure gradient.

2.3.4 Flow regime

Three flow regimes could be identified based on the bubble flow behavior in three-phase fluidized bed: the coalesced bubble, the dispersed bubble, and the slugging regimes. In the coalesced bubble regime, bubbles tended to coalesce and both the bubble size and velocity became large and shown a wide distribution. Coalesced bubbles rose near the column near the column center with high velocity and stirred the bed violently. The coalesced bubble regime predominated at low liquid and high gas velocities. In the dispersed bubble regime, no bubble coalescence occurred and the bubbles were of uniform, small size. The dispersed bubble regime predominated at high liquid velocities and at low and intermediate gas velocities. In a small diameter column (e.g., D_c < 15 cm), the gas bubble could easily grew to the size of the column diameter at high gas flow rates creating “slug” bubbles which occupied nearly the whole cross section. In columns of large diameter, however, slugging might not occur. The flow regimes varied significantly with the column diameter. Particle properties also profoundly affected the prevailing flow regime at given gas and liquid velocities and terminal velocity of the fluidized particles affected the liquid velocity of transition from the coalesced to the dispersed bubble regime

2.4 Literature reviews

Wu et al. **[13]** studied oxidation of aqueous phenol by ozone and peroxidase. Aqueous phenol was ozonated for the first time at pH over 12. Results obtained under conditions favoring rapid generation of radicals completely eliminated the possibility deduced from the absorption theory that the indirect radical reaction might be one of the reaction pathways. Meanwhile, it was found in this study that the apparent first-order rate constant of phenol ozonation decreased logarithmically with increasing initial phenol concentration. On the other hand, despite the phenomenological resemblance between the two oxidation processes (the removal of aqueous phenol by ozone and horseradish peroxidase (HRP)), the mechanisms of the two processes were proved to be quite different. Results of this study also indicate that the integration of ozone and HRP did not improve the efficiency of phenol removal.

Santos et al. **[14]** has investigated catalytic wet oxidation of phenol as model pollutant by using three commercial active carbons as catalysts. Experiments were carried out in a fixed bed reactor, at 160 °C of temperature and 16 bar of oxygen pressure. All the AC tested showed high catalytic activity in both phenol conversion and mineralization. Small amounts of intermediates were found in phenol oxidation being the main compounds detected hydroquinone, p-benzoquinone, p-hydroxybenzoic acid, catechol and short chain acids C_2–C_4, mainly maleic, acetic and formic acids. Only small amounts of oxalic acid were found in the liquid phase. These SCA were the most refractory compounds to catalytic oxidation

Dong et al. **[15]** studied a stable microporous material, de-aluminated Y zeolite has been used for the first time as an ozonation catalyst and showed remarkable activity for the removal of phenol and chemical oxygen demand (COD) in aqueous solution. The Y zeolite exhibited excellent repetitive-use performance even after continuous operation for 10 cycles. The ozone decomposition rate, influence of hydroxyl radical scavenger and influence of reaction temperature were investigated. The de-aluminated Y zeolite has beensuccessfully used as an ozonation catalyst for the degradation of phenol. Y zeolite exhibited high catalytic activity and nonexpendable performance for the ozonation degradation of phenol and the removal

rate of COD, owing to the stable framework structure of de-aluminated Y zeolite. By investigating the ozone decomposition rate, influence of hydroxyl radical scavenger and influence of reaction temperature, it was shown that the Y zeolite could accelerate the transformation from ozone molecules to hydroxyl radicals, which is essential for a catalyst. Due to the interaction between ozone and Y zeolite, the decomposition of ozone and the generation of hydroxyl radicals were accelerated, and the degradation of phenol and the removal of COD were enhanced. As a catalyst, the de-aluminated Y zeolite has supplied a feasible and environmental friendly choice for the catalytic ozonation of phenol in wastewater.

Pintar et al. **[16]** studied of the catalytic liquid-phase oxidation of aqueous phenol solution, a proprietary catalyst comprising copper (7.4 wt.%), zinc (9.0 wt.%) and cobalt (3.2 wt.%) oxides was used. The oxides were supported by a steam-treated cement that was designed for reactions in aqueous solutions. Aqueous-phase deep oxidation at comparatively low temperatures and pressures made possible by the use of heterogeneous catalysts is a promising technique for the destruction of organic water pollutants. Catalytic liquid-phase oxidation of aqueous phenol solutions was investigated in an isothermal trickle-bed reactor at T = 403-423 K and oxygen partial pressure of 7 bar. The results obtained in the presence of a catalyst composed of supported copper, zinc and cobalt oxides show that during the reaction course only small amounts of aromatic and aliphatic hydrocarbons are accumulated in the liquid phase, thus resulting to a constant pH value of the aqueous solution along the axial reactor coordinate. In the off-gas, no carbon monoxide was detected at any operating conditions. Process simulation using one-dimensional axial dispersion and plug-flow models demonstrates that efficiency of the catalyst bed for phenol removal is influenced by the mass-transfer rate of oxygen from the gas phase to the bulk liquid phase, and by resistance due to a surface reaction step. It is believed that partial wetting of catalyst particles in a trickle-bed reactor increases phenol conversion to intermediates and CO_2 as the main reaction product, through the formation of a larger number of active sites on the catalyst surface.

Santos et al. **[17]** were present route of catalytic oxidation of phenol in aqueous phase over a commercial copper catalyst. The chemical composition was: 67-

77% copper oxide, 20-30% copper chromite, 1-3% synthetic graphite. A reaction pathway of phenol oxidation under intermediate temperature and pressure has been proposed. Temperatures employed were 140 and 160 °C and catalyst concentration ranged from 4 to 1550 g/l of liquid phase. To achieve this wide interval of catalyst concentration values, two experimental set-ups were employed: a basket stirred tank reactor, with the liquid phase in batch, and an integral fixed-bed reactor with co-current up-flow of gas and liquid phases. The main intermediates detected in the phenol oxidation were ring compounds (hydroquinone, catechol, benzoquinone), which break to yield CO_2 and short chain acids, mainly maleic, formic, acetic and oxalic acids, and also traces of malonic, succinic and fumaric acids. Oxalic acid was also found to form a complex with the copper which oxidizes to CO_2. The only non-oxidizable intermediate under the conditions sets was acetic acid. In order to propose a phenol oxidation pathway, several runs were carried out where the main intermediates detected in the phenol oxidation were fed to the FBR under different temperatures and catalyst loadings. It was found that catechol oxidation does not yield either benzoquinone or maleic acid but oxalic acid which finally mineralized to CO_2. However, benzoquinone and maleic acid are products clearly detected in the hydroquinone oxidation. Oxidation reactions of phenol and those intermediates studied take place not only on the solid surface but also in the liquid phase.

ศูนย์วิทยทรัพยากร
จุฬาลงกรณ์มหาวิทยาลัย

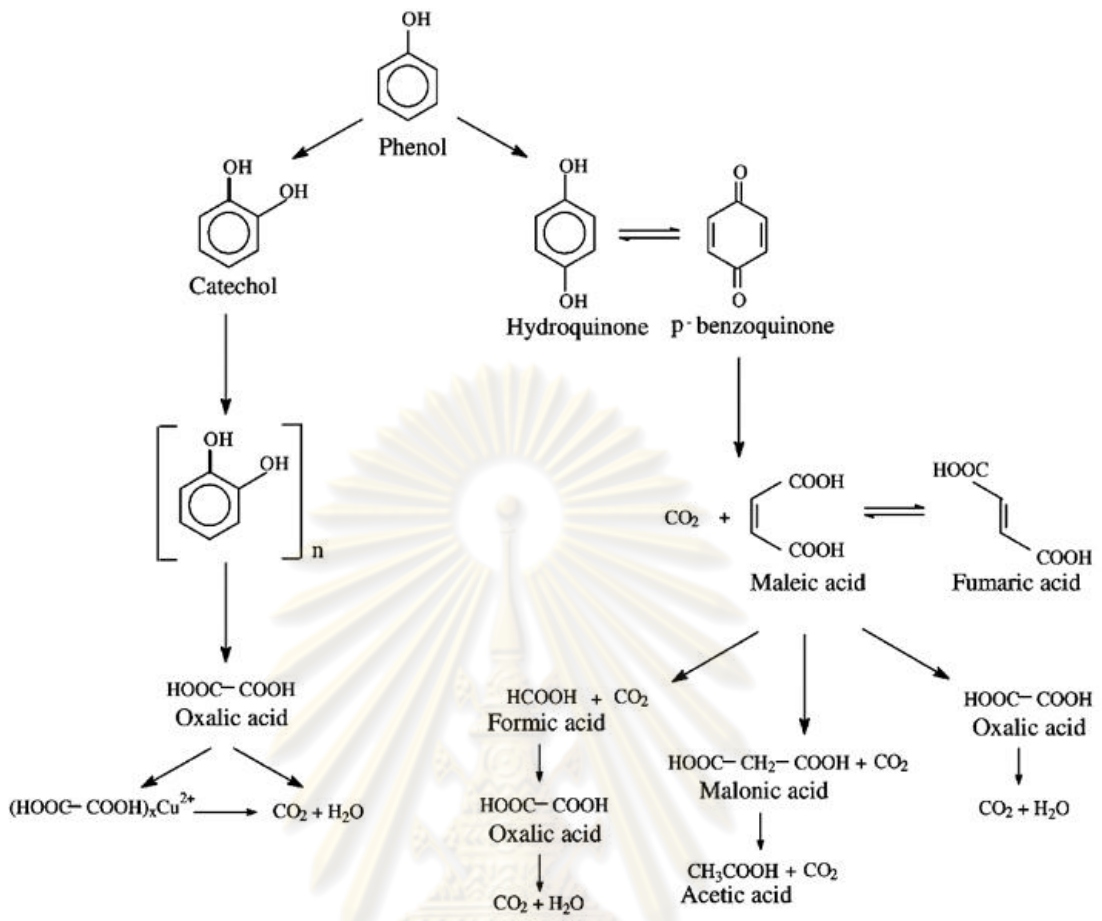

Figure 2.4 Route of catalytic oxidation of phenol in aqueous phase over a commercial copper catalyst

Esplugas et al. **[18]** investigate of comparison of different advanced oxidation processes for phenol degradation. Advanced oxidation processes (O_3, O_3/H_2O_2, UV, UV/O_3, UV/H_2O_2, O_3/UV/H_2O_2, Fe^{2+}/H_2O_2 and photocatalysis) for degradation of phenol in aqueous solution have been studied in earlier works. In this paper, a comparison of these techniques is undertaken: pH influence, kinetic constants, stoichiometric coefficient and optimum oxidant/pollutant ratio. Different advanced oxidation processes have been studied and compared (with a view to the decrease in the pollutant concentration, the pseudo-first order kinetic constant and cost estimation) for the degradation of phenol in aqueous solution. It has been found that none of the ozone combinations (O_3/H_2O_2, O_3/UV and O_3/UV/H_2O_2) improved the degradation rate of the ozone process, resulting even in an slightly inhibitory effect. With regard to the UV processes (UV, UV/H_2O_2 and photocatalysis), the degradation rate with the UV/H_2O_2 process was almost five times higher than photocatalysis and

UV alone, as evidenced by the kinetic constant values. Fenton's reagent showed the fastest degradation rate, 40 times higher than UV process and photocatalysis and five times higher than ozonation. Of the tested processes, Fenton reagent was found to the fastest one for phenol degradation. However, degradation rate and the lower costs obtained with ozonation makes it the most appealing choice for phenol degradation. In the ozone combinations, the best results were achieved with single ozonation. As for the UV processes, UV/H_2O_2 showed the highest degradation rate. **Figure 2.5** shown as kinetic constant, half-life and cost evaluation for all the processes.

Table 2.5 Kinetic constant, half-life and cost evaluation for all the processes

Process	k (h^{-1})	$t_{1/2}$ (h)	Costs/kg ($)	$t_{3/4}$ (h)	Costs/kg ($)
UV	0.528	1.31	172.2	3.33	293.1
O_3/H_2O_2	2.13	0.325	2.71	0.63	2.93
O_3/UV	3.14	0.221	9.28	0.417	11.7
O_3/UV/H_2O_2	4.17	0.166	7.12	0.333	9.51
O_3	4.42	0.157	0.81	0.317	1.09
UV/H_2O_2	6.26	0.111	13.1	0.383	28.7
Fenton	22.2	0.0312	3.92	0.067	2.61

Quintanilla et al. **[19]** studied phenol oxidation by a sequential catalytic wet peroxide oxidation (CWPO) – catalytic wet air oxidation (CWAO) treatment with a Fe/activated carbon catalyst (Fe/AC). CWPO of phenol with a homemade Fe/AC catalyst has been studied in a stainless steel fixed-bed reactor at different operating conditions (T = 23-100 °C, P_T = 1-8 atm, W = 0-2.5 g, and τ = 20-320 g_{CAT} h/g_{Phenol}). The results show that, thanks to the incorporation of Fe on the activated carbon, phenol conversion improved dramatically, reaching a 90% at 65 °C, 2 atm, and 40 g_{CAT} h/g_{Phenol}. However, TOC conversion values remain fairly low, (around 5% at 40 g_{CAT} h/g_{Phenol}), and no improvement was obtained with the inclusion of Fe. The presence of Fe seems to promote the nondesirable coupling reactions that take place in CWPO of phenol due to the condensation of the ring intermediates (the primary

phenol oxidation products). CWPO proceeds at higher initial rates than CWAO but most of the intermediates produced are refractory to further oxidation. These refractory compounds are condensation products from ring intermediates and short chain acids, which remain even after complete disappearance of hydrogen peroxide. On the opposite, CWAO at mild conditions (100 °C and 8 atm) leads to the oxidation of most of the intermediates, including the condensation products detected at short space-times values. The final products are only acetic and formic acids. A sequential treatment consisting of CWPO at ambient conditions followed by CWAO at mild conditions (100 °C and 8 atm), both using a homemade Fe/AC catalyst. A CWPO–CWAO sequential treatment has been successfully performed by using a fixed-bed and trickle-bed reactor in series, allows to obtain phenol conversions up to 90% at short space-times (20 g_{CAT} h/g_{Phenol}) from a starting phenol concentration of 1 g/L. This sequential treatment reduces TOC as much as the CWAO process does, leading to a complete oxidation of ring intermediates, and avoiding the presence of condensation by-products in the reactor effluent when appropriate space-times are used.

Allia et al. **[20]** investigated biological treatment of water contaminated by hydrocarbons in three-phase gas-liquid-solid fluidized bed. Biological treatment has been carried out in two different systems: aerated closed and three-phase fluidized bed reactors for hydrocarbons removal from refinery wastewaters. For the two systems, hydrodynamic study allowed the determination of operating conditions before treatment experiments. Then, in a second time, biological treatments have been conducted in the same operating conditions. The obtained results showed that in the three-phase fluidized bed we can degrade hydrocarbons more rapidly than in a closed aerated bioreactor. Among the different appropriate techniques available to create efficient contacts between phases, the three-phase fluidization gas-liquid-solid where carrier particles are moving inside the reactor seems very interesting. It allows an intimate contact between phases and present many advantages concerning hydrodynamic and mass transfer phenomena. It was depended on operating conditions and the bubble flow behavior. It could display different flow regimes. In these systems called bioreactors the solid particles covered with a biofilm are fluidized by two ascending flows of air and contaminated water. With favorable operating

conditions, from a hydrodynamic and mass transfer point of view, the pollutant can be biologically degraded up to 90%.

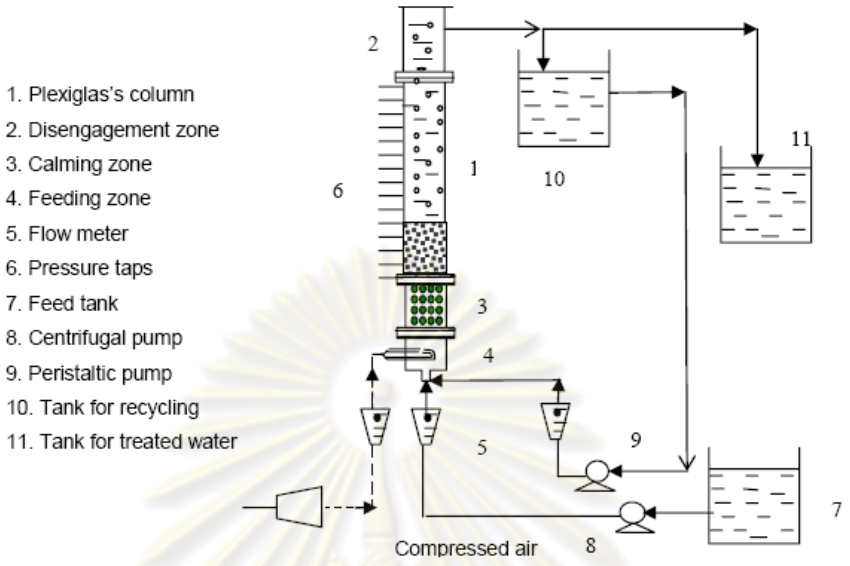

Figure 2.5 experimental flow sheet of three-phase fluidized bed

Kanki et al. **[11]** studied about water purification in a fluidized bed photocatalytic reactor using TiO_2-coated ceramic particles.TiO_2-coated mm-size spherical ceramic particles which are very stable for dynamical impact and whose specific density is very near to unity were developed and applied to a fluidized bed reactor for water purification. Two types of test-scale fluidized bed photocatalytic reactors were prepared: the reactor *a* which holds the ultra violet light source (254 nm) inside it and the reactor *b* which holds the light source (365 nm) outside it. The latter one is supposed to be operated under solar light. Phenol and bisphenol A were selected for target contaminants and the decomposition experiments by fluidized bed photocatalytic reactor were conducted. It was shown with the reactor a that aqueous phenol and bisphenol A with 10 mg/dm^3 in 2 L water can be decomposed rapidly in about 200 min and TOC originated from their byproducts can eventually be mineralized in short time in 300 min. It was also shown through the decomposition experiment using the reactor *b* that water purification under solar light can be possible, though the decomposability is less effective: it took about 20 h to mineralize

the aqueous contaminants with10 mg/dm^3 in 1 L water. Phenol is therefore, thought to be photochemically oxidized through the intermediate path as shown in **Figure 2.6**.

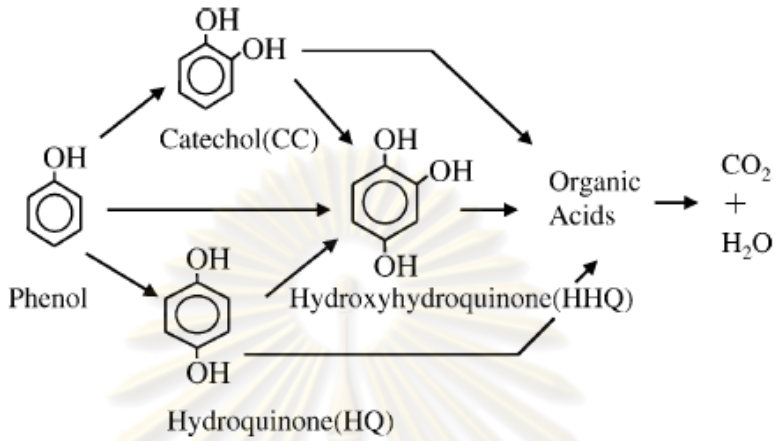

Figure 2.6 Pathway for photochemical decomposition of phenol

ศูนย์วิทยทรัพยากร
จุฬาลงกรณ์มหาวิทยาลัย

CHAPTER III

EXPERIMENTAL

The three-phase fluidized bed reactor was used to investigate aqueous phenol wastewater treatment. The metal oxide was loaded onto the surface of activated carbon. The efficiency of wastewater treatment was developed by enhancing with ozone. The chemicals, preparation of activated carbons doped with iron oxide and characterization of particle are shown in sections **3.1, 3.2** and **3.3**, respectively. In section **3.4** and **3.5,** the experimental system and the analytical instrument were explained, respectively.

3.1 Chemicals

Iron precursor for impregnate on catalytic support was prepared from:

- Iron (III) nitrate nonahydrate, $Fe(NO_3)_3 \cdot 9H_2O$, available from Asia Pacific Specialty Chemical, 98.0%

Phenol solution for testing the reaction and preparing HPLC standard were prepared from:

- Phenol, C_6H_6O, available from Fisher Scientific, 99.98%

In addition, the chemicals which used to be the HPLC mobile phase were as follows:

- Acetonitrile, CH_3CN, available from Fisher Scientific, 99.99%
- Methanol, CH_3OH, available from Fisher Scientific, 99.99%

Finally, the chemicals which used to be standard solution of TOC were as follows:

- Potassium hydrogen phathalate, $C_6H_4(COOK)(COOH)$, available from Nacalai Tesque
- Sodium hydrogen carbonate, $NaHCO_3$, available from Nacalai Tesque
- Sodium carbonate, Na_2CO_3, available from Nacalai Tesque

3.2 Preparation of activated carbons doped with iron oxide

The Fe/AC, an iron on commercial granular activated carbon, is employed for investigating the phenol removal efficiency and the possibility of the fluidized bed reactor for application on wastewater treatment. Meanwhile the Fe/AC, homemade 5 wt.% iron (Fe) by support weight, were prepared by using Iron (III) nitrate nonahydrate ($Fe(NO_3)_3 \cdot 9H_2O$) from Asia Pacific Specialty Chemical Co., Ltd.. The microporous activated carbon that supplied from Calgon Co., Ltd. in USA (AC-US) and Carbokarn Co., Ltd. in Thailand (AC-TH) was used to be the support. The main characteristics of the activated carbons that used in the present investigations were presented in **Table 3.1.**

Table 3.1 The technical specification of granular activated carbon

Physical Properties	Specification	
	AC-US (Calgon Co., Ltd.)	AC-TH (Carbokarn Co., Ltd.)
Particle size distribution:	0.60-2.36 mm	0.42-1.70 mm
+ 12 mesh (1.70 mm)		MAX. 5%
12×40 mesh (1.70 – 0.42 mm)		MIN. 90%
- 40 mesh (0.42 mm)		MAX. 5%
Apparent density (g/cc)		MIN. 0.49
Moisture (%) (As packed)	MAX. 2	MAX. 8
Ash (%) (As packed)	MAX. 10	MAX. 3.5
pH		9 – 11
Surface area (m^2/g)	MIN. 950	MIN. 1150
Iodine number (mg/g)	MAX. 900	MAX. 1100
Carbon tetrachloride adsorption (%)		MIN. 55
Hardness number (%)	MIN. 95	MIN. 98

The activated carbons doped with iron oxide were prepared by loading Fe precursor over on the surface of granular activated carbon. It was prepared by impregnation techniques. The activated carbon pretreatment and activated carbons doped with iron oxide preparation were shown as follows:

3.2.1 The commercial granular activated carbon pretreatment

(1) Activated carbon was sieved out in the size range below of 0.42 mm particle diameter (40 mesh).

(2) The classified activated carbon was heated and held at 200 °C for 4 hrs to eliminate its impurities.

3.2.2 The commercial granular activated carbon after pretreatment was loaded with iron (III) nitrate solution by each of two impregnation techniques

a) *IMA technique:*

Wet impregnation (10 ml metal solution/g activated carbon)

(1) Impregnate iron (III) nitrate solution onto the activated carbon under stirring and refluxing.

(2) The sample was dried and stirred under vacuum at constant temperature 60 °C.

(3) Heat up the activated carbon in the oven overnight at 100 °C.

b) *IMB technique:*

Incipient wetness impregnation (0.5 ml metal solution/g activated carbon)

(1) Impregnate iron (III) nitrate solution onto the activated carbon under stirring at 80 °C.

(2) Heat up the activated carbon in the oven overnight at 100 °C.

3.2.3 Activated carbon after impregnated with iron nitrate was calcined by two different conditions

a) *500 °C nitrogen gas condition*:

Calcinate at 500 °C under nitrogen gas flow for 5 hrs.

b) *200 °C ambient air condition*:

Calcinate at 200 °C under ambient air for 5 hrs.

3.3 Characterization of particle

Characteristics of AC and Fe/AC were analyzed by BET analyzer, TGA analyzer, XRF, XRD, SEM and EDS**.**

3.3.1 Nitrogen physisorption (BET analyzer)

The specific surface areas and porosities of activated carbons and catalysts were determined from N_2 adsorption-desorption isotherms measured at 77 K using an automated adsorption apparatus (BELSORP mini, BEL Japan, Japan). The samples were degassed under vacuum at 473 K for 2 hrs prior to measurement. The specific surface areas were calculated by the BET method. The pore distribution was calculated according to the MP-plot method. Automatic specific surface area/pore size distribution measurement was shown in **Figure 3.1**.

Figure 3.1 Automatic specific surface area/pore size distribution measurment (BELSORP mini, BEL Japan, Japan)

3.3.2 Thermogravimetric Analyzer (TGA analyzer)

Thermal analysis measurements were performed in flowing N_2 atmosphere using Pyris diamond (Perkin Elmer). TGA analyses were conducted in the original activated carbon and metal impregnated samples. All of samples were studied by TGA using a heating rate of 10°C/min to quantify the amount of weight loss. The

temperature ranging of analysis was 30-500 °C, holding time was 5 hours at 500 °C and N_2 gas flow rate was 50 mL/min.

Figure 3.2 Thermogravimetric Analyzer (Pyris diamond, Perkin Elmer, USA)

3.3.3 The Scanning Electron Microscope (SEM) and Energy Dispersive Spectroscopy (EDS)

Figure 3.3 Scanning Electron Microscopy (SEM) (S-3400N, Hitachi, Japan)

The activated carbon and Fe coating on the surface of activated carbon were observed using SEM images. SEM specimens were prepared by directly placing a small piece of activated carbon or catalysts onto a stub. The stub was covered with a carbon tape. The specimens were loaded into a sample chamber, and observations were immediately started using image catcher scanner for taking the photos at 20 kV. A photo of the Scanning Electron Microscopy (SEM) machine was shown in **Figure 3.3.**

3.3.4 X-ray fluorescence spectroscopy (XRF)

Energy dispersive X-ray fluorescence spectrometry is a form of atomic spectroscopy ideal for the rapid, simple measurement of elements in a range of materials. The XRF method is widely used to measure the elemental composition of materials. Since this method is fast and non-destructive to the sample, it is the method of choice for field applications and industrial production for control of materials. XRF spectrometer could determine how much Fe content is present in catalyst. The samples were analyzed by XRF (Oxford, ED 2000) as shown in **Figure 3.4**.

Figure 3.4 X-ray fluorescence spectroscopy (XRF) (ED 2000, Oxford, England)

3.3.5 X-ray diffraction (XRD)

X-ray diffraction is of course of paramount importance in determining the structures of crystals. The application of XRD to nanocrystalline solids, powders, single-crystal thin films or multilayers may be less spectacular. In this experiment, The samples were analyzed by XRD (Rigaku, TTRAX III) as shown in **Figure 3.5**, to find their crystalline phase. The samples were spread on the glass slide and then set in the equipment which provide X-ray beam for the analysis.

Figure 3.5 X-ray diffraction (XRD) (TTRAX III, Rigaku, USA)

3.4 Experimental system

The experimental system consists of laboratory-scaled three-phase fluidized bed reactor and pilot-scaled three phase fluidized bed reactor, respectively.

3.4.1 Laboratory-scaled three phase fluidized bed reactor

Laboratory-scaled consists of 6 liters acrylic tank, water and air pumps, control and bypass valves, water and air flow meters, fluidized bed reactor, pressure gauge and ozone generator. The figure and schematic diagram of equipment were shown in **Figure 3.6 and 3.7**, respectively. The fluidized bed reactor was made from transparent acrylics that allowed observing the phenomena occurring inside. It has effective volume of 272 mL. The reactor was composed of 3 parts: lower, middle and top part, as shown in **Figure 3.8-3.10**. The lower part consists of air, water and drainage channel. The middle part was cylindrical in shape with 40 mm outside diameter and 300 mm height. The top part composed of water recycle pipe and air exhaust channel. These three components were connected with acrylic flange. Wastewater containing phenol was pumped to the bottom of fluidized bed reactor. By opening and shutting off a few valves with the monitoring from water flow meter, the water flow rate could be constantly controlled in the range of 1 L/min. The wastewater flowed through the reactor and returned to the feed tank. The ozone generator model OZ-6501T was used to generate ozone from atmosphere at concentration 300 mg/hr and constant flow rate of 2 L/min. The 6 liters of 10 ppm phenol was tested with a Fe on activated carbon concentration of $0.83 g_{CAT}/L_{phenol}$.

Figure 3.6 The laboratory-scaled fluidized bed reactor

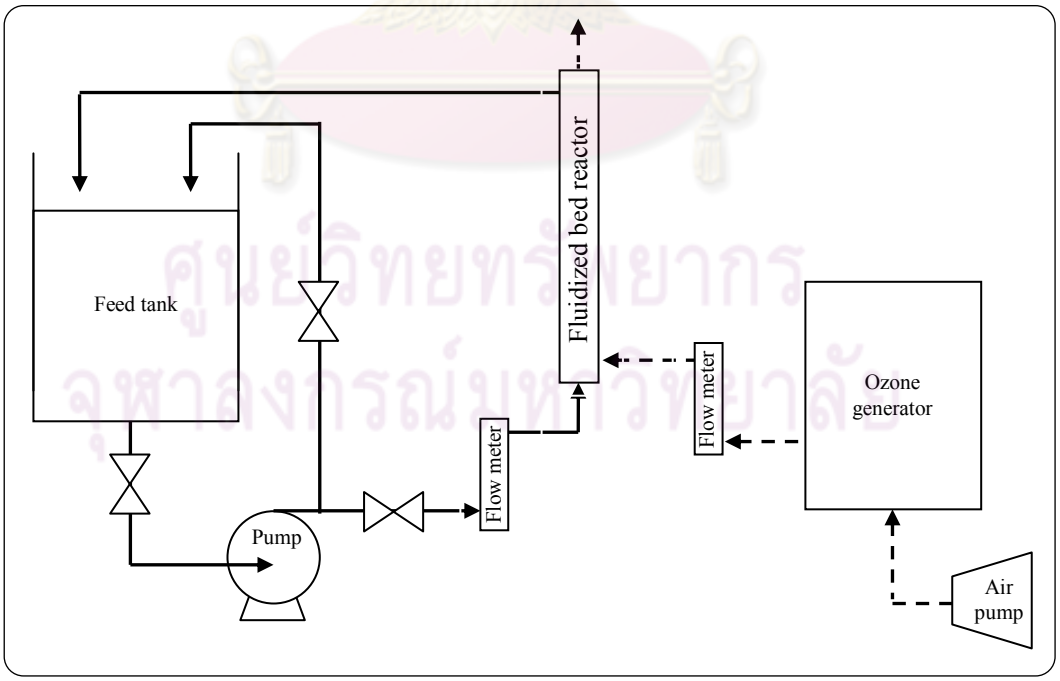

Figure 3.7 Schematic diagram of the laboratory-scaled fluidized bed reactor

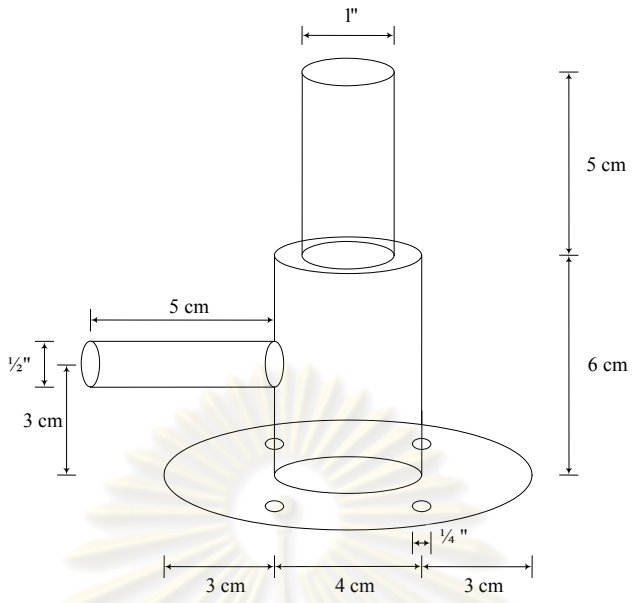

Figure 3.8 The top part of laboratory-scaled fluidized bed reactor

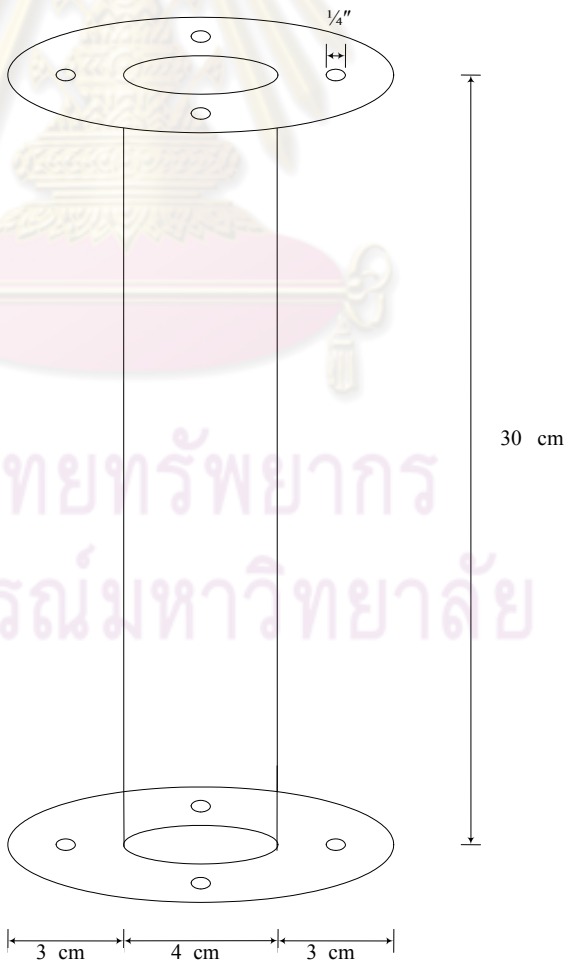

Figure 3.9 The middle part of laboratory-scaled fluidized bed reactor

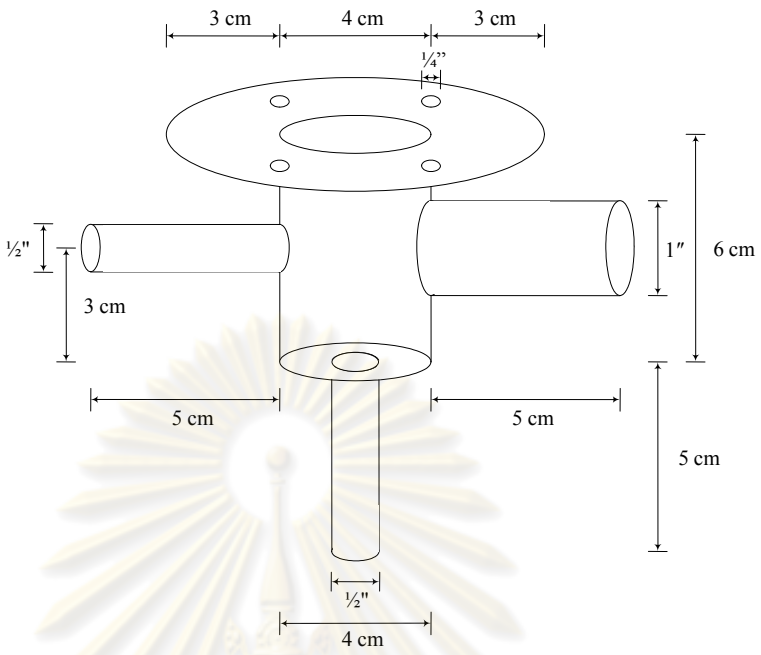

Figure 3.10 The lower part of laboratory-scaled fluidized bed reactor

3.4.2 Pilot-scaled fluidized bed reactor

In pilot-scaled, the reactor was constructed, modified and set up in series. (see the schematic diagram of equipment in **Figure 3.11**. This system consisted of a reactor column (V1), two wastewater preparation tanks (T1, T2), a treated tank (T3) and two chemical resistant pumps with the same specifications. For the water stream, there were liquid flow meters to measure the inlet wastewater flow rate of each column. Two wastewater preparation tanks were set because one of them will be used for preparing the wastewater while the other was used during the operation. The evaporated water in the system should be negligible so the make-up water was not necessary in this system. For the gas stream, ambient air was employed for producing ozone. Gas flow rate was gas lines into column. Before entering column, the gas flow meters were used for fine adjusting the flow rate. The ozone was passed through the ceramic distributor to reduce size of gas bubbles in the column, leading to an increased contact area of the reactants. The check valves were also set below in each column for preventing the damage of gas flow meters due to the water inside column flowing backward into the ozone flow meters.

The experiments in pilot-scaled system were carried out with co-current upward flow as through in laboratory-scaled system. However, instead of passing through just one reactor, the liquid had flown through five reactors in series. The entire liquid from last reactor was re-circulated into the preparation tank until finish.

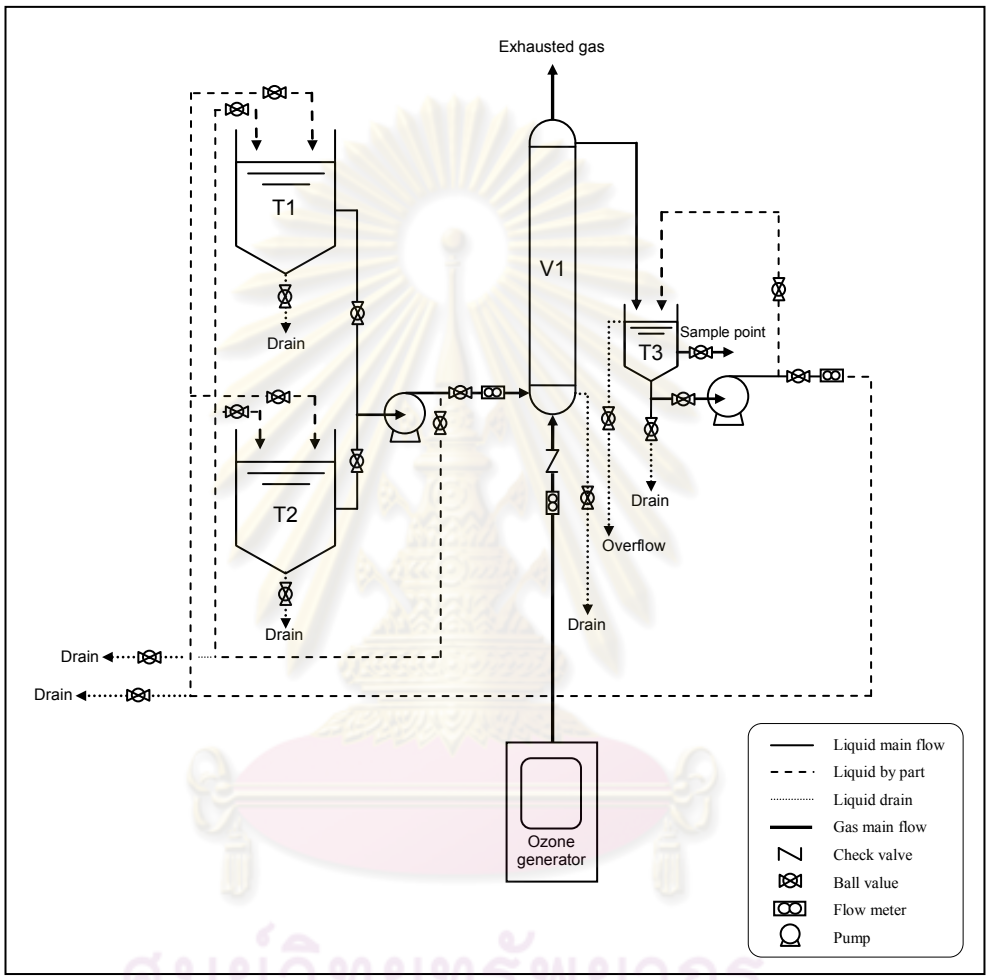

Figure 3.11 Schematic flow diagram of the pilot-scaled fluidized bed reactor

ศูนย์วิทยทรัพยากร
จุฬาลงกรณ์มหาวิทยาลัย

Fluidized bed column

The specification of pilot-scaled three-phase fluidized bed reactor was shown in **Table 3.2**. These reactors were made from transparent acrylic. The shape of the top of reactor was carefully designed to be a conical shape in order to reduce the dead volume above the liquid surface as much as possible. At the bottom of the column, three pipes were built for many purposes: water draining, gas inlet, and water inlet, respectively (see **Figure 3.12-3.14**).

Table 3.2 Specification of the pilot-scaled fluidized bed reactor

Effective volume of each reactor	50 L
Outer diameter of each reactor	0.2 m (I.D. = 0.19 m)
Height of each reactor	Approx. 2 m (effective height 1.6 m)
H/D ratio (height of water/ diameter of reactor)	8
Amount of solid particle in column	1300 g per each reactor

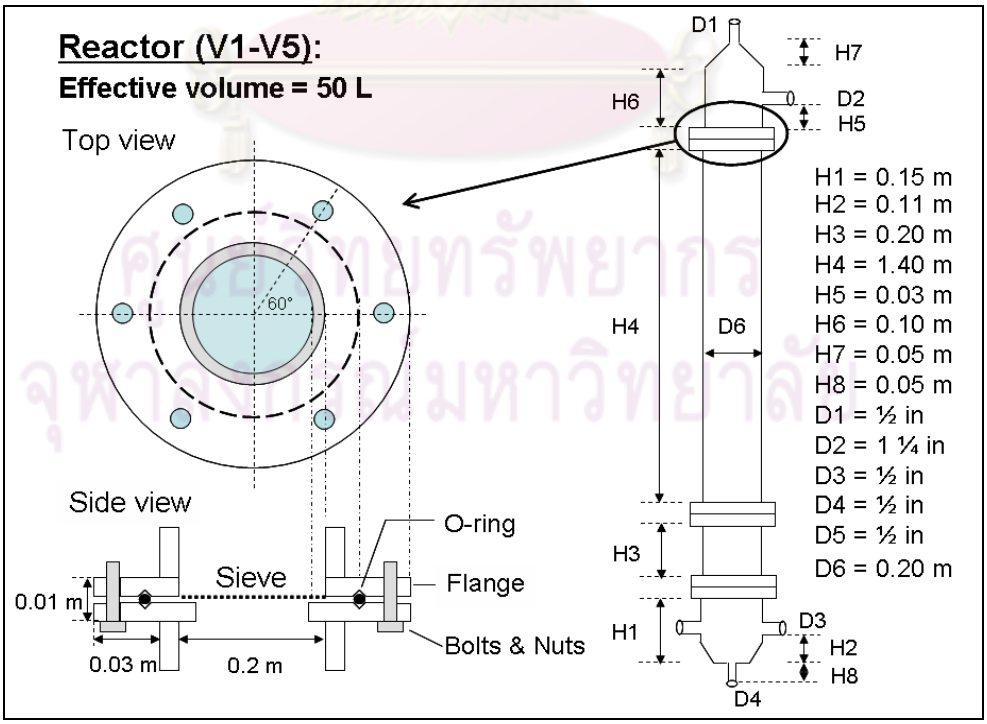

Figure 3.12 Design configurations of three phase fluidized bed reactor in the pilot-scaled system

Figure 3.13 Fluidized bed columns

Figure 3.14 Wire mesh and steel flange

Ozone generator

Ozone was generated by an ozone generator shown in **Figure 3.15**. **Table 3.3** shows the technical data of ozone generator model OZ-7540, Ozzon. The selection of material to convey ozone was very important because ozone is extremely corrosive. Due to the excellent characteristic of stainless steel, Swagelok stainless was selected as shown in **Figure 3.16**. The air ball valve was added to cut of the flow in the emergency case.

Table 3.3 Technical data of ozone generator

Model	OZ-7540
Ozone capacity (max)	40 g/hr
Air flow rate (max)	40 L/min
Operating function	Manual / Auto
Power consumption	2.2 kW
Ozone concentration	3 % by weight from dry air
Power supply	380 VAC, 50 Hz
Type of generating mechanism	High frequency Corona discharge
Type of cooling system	Cooled water
Type of electrode	Stainless steel 316 L with glass tube
Type of ozone tube	Teflon tube
Type of fitting	Stainless steel 316
Type of cabinet	Steel with epoxy paint
Ozone unit dimension (W×H×D)	600×1700×500 mm.
Chiller dimension (W×H×D)	530×700×530 mm.
Weight	310 kg

Figure 3.15 Ozone generator (OZ-754, Ozzon, Thailand)

Figure 3.16 Swagelok stainless steel, check valve and air distributor

3.5 Analytical instrument

The concentration of phenol was analyzed by High Performance Liquid Chromatography (HPLC) and total organic carbon was analyzed by Total Organic Carbon (TOC).

3.5.1 High performance liquid chromatography (HPLC)

The concentration of phenol was measured by HPLC (Shimadzu column class VP). It can be used for indicating the compounds and the number of the compounds in the sample as well. The results from the samples taking place in sequent of time were exhibited in graph presentation. Peak area of each compound that occurred at the individual resident time was brought for calculating the concentration. The mixture of 4 mM aqueous sulfuric and acetonitrile (4:1, v/v) was used to be the mobile phase of 1.0 mL/min. The column Phenomenex C18 was operated at 31.5 °C. The wavelength of UV-vis detector was 254 nm. **Figure 3.17** shows the picture of this equipment.

Figure 3.17 The picture of HPLC (column class VP, Shimadzu)

3.5.2 Total organic carbon (TOC)

The concentration of TOC was measured by TOC analyzer (Shimadzu TOC-VCPH). It could be used for indicating the total mineralization of phenol. The picture of TOC analyzer was shown in **Figure 3.18.**

Figure 3.18 The picture of TOC analyzer (TOC-VCPH, Shimadzu)

ศูนย์วิทยทรัพยากร
จุฬาลงกรณ์มหาวิทยาลัย

CHAPTER IV

RESULTS AND DISCUSSION

Before employing activated carbon doped with iron oxide decompose aqueous phenol by incorporating ozone gas as oxidizing agent characterization of virgin activated carbon and activated carbon doped with iron oxide was carried out. Based on comparison of then characteristics (size distribution, pore sized distribution and specific surface area), potential activated carbon doped with iron oxide were intended in a three-phase fluidized bed for examining their performance on phenol decomposition without employing ozone.

4.1 Characteristics of activated carbon

Commercial granular activated carbons employed in this work were supplied by Calgon Co., Ltd. form the United State of America (AC-US) and Calgon Co., Ltd. from Thailand (AC-TH). AC-US was made from coal and AC-TH was made from coconut shell.

4.1.1 Particle size distribution

Two types of commercial granular activated carbon which AC-US made from coal and AC-TH made from coconut shell were subject to particle size distribution analysis using sieves shaker. Before the impregnation, the activated carbon with the size range below of 0.42 mm was classified by a sieve. If the particle size is smaller than mesh screen reactor, the particles will move through the screen and flow upward with fluid stream at the top of reactor. Therefore, the solid particle for this process must be larger than 0.42 mm diameter size. The particle size distribution of commercial granular activated carbon shows in **Table 4.1**. The most range of particle size was 1.19 to 2.00 mm in diameter**.** The greatest percentage of particle by weight for AC-US and AC-TH were 82 and 67%, respectively.

Table 4.1 Particle size distribution of granular activated carbon

Particle size (mm)	Weight (%)	
	AC-US	AC-TH
0.42-0.60	-	3
0.60-0.84	-	9
0.84-1.19	-	21
1.19-2.00	82	67
2.00-2.38	18	-

In the other hand, attrition resistance for solid particle is an important factor in use to three-phase fluidized bed reactor. Attrition could be occurred by loss of particle size smaller than 0.42 mm due to the breakage by impact or collision of particles.

4.1.2 N_2 adsorption/desorption Isotherm

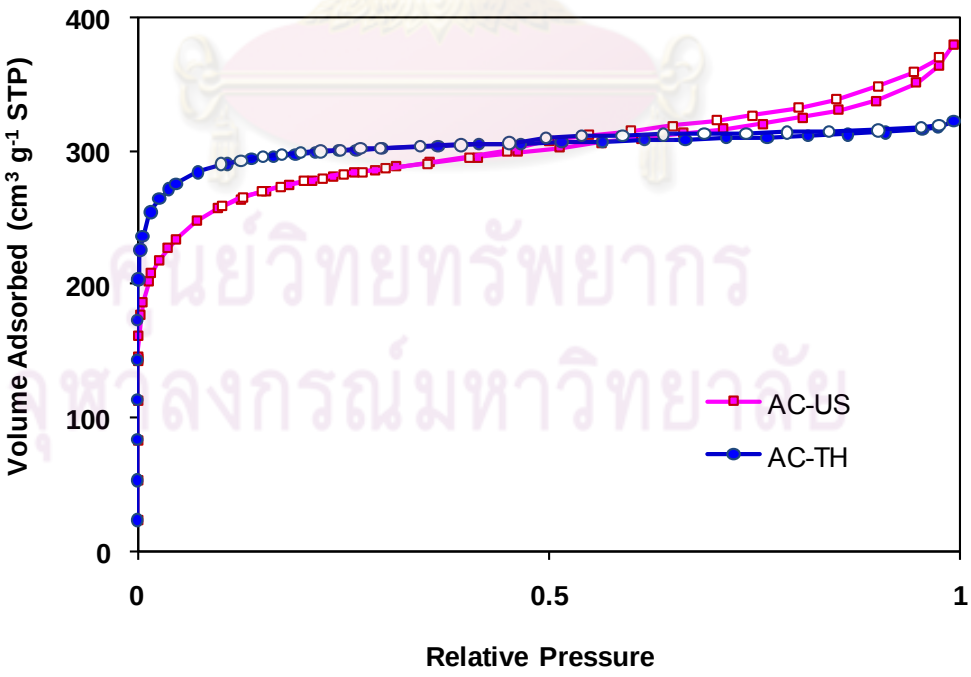

Figure 4.1 N_2 adsorption/desorption isotherm on AC-US and AC-TH

N_2 adsorption/desorption isotherms obtained at 77 K shown in **Figure 4.1**. Two different nitrogen adsorption/desorption isotherm types of commercial granulated activated carbons were AC-US and AC-TH. Based on the shape of isotherm by International Union of Pure and Applied Chemistry (IUPAC) classification, both ACs exhibit Type I isotherm which indicated a huge quantity of microporous structure. Obviously, a slight hysteresis loop was noticed in the isotherms, suggested the existence of mesoporous structure in ACs **[21]**. The hysteresis loop of AC-US was more obvious than that of AC-TH. Thus it is reasonable to imply that AC-US contains more mesoporosity than AC-TH.

The amount of nitrogen gas adsorbed at a relative pressure of 0.99, AC-US higher volume adsorbed than AC-TH.

4.1.3 Pore size distribution

Figure 4.2 shown micropore diameter size distribution of both ACs using by MP-plot method. Ranges of micropore diameter size distribution and modal micropore diameter for AC-US was made from coal based of 0.4-2.0 and 0.8 nm, respectively. In case AC-TH was made from coconut shell based, ranges of micropore diameter size distribution and modal micropore diameter size of 0.4-1.6 and 0.6 nm, respectively. The mesopore diameter size distribution of both commercial granular activated carbon shows in **Figure 4.3**. Mesopore size distribution using by BJH-plot method found mesopore volume of AC-US more than AC-TH.

ศูนย์วิทยทรัพยากร
จุฬาลงกรณ์มหาวิทยาลัย

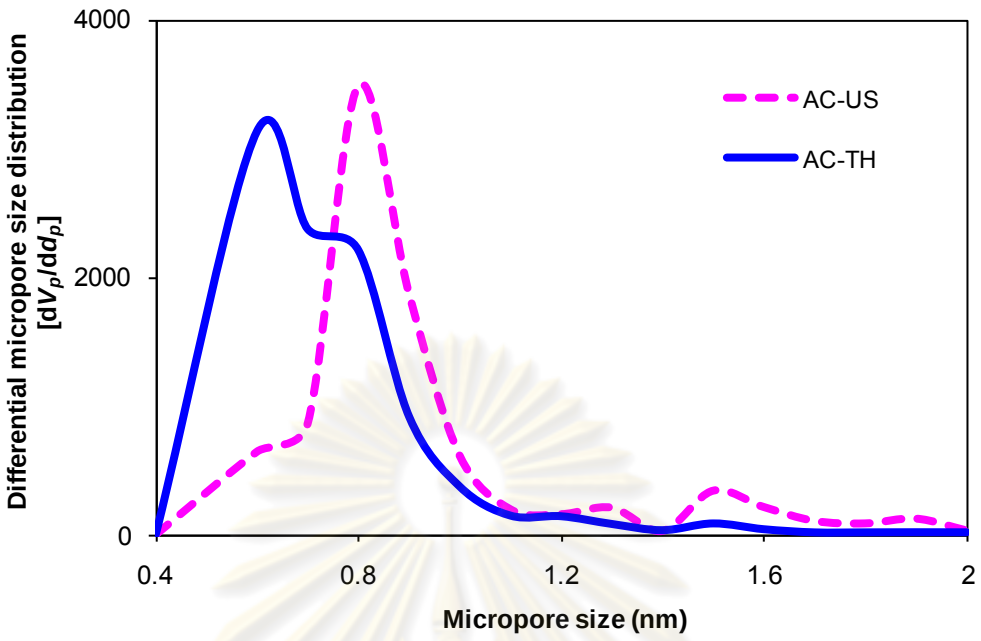

Figure 4.2 Micropore size distribution of AC-US and AC-TH

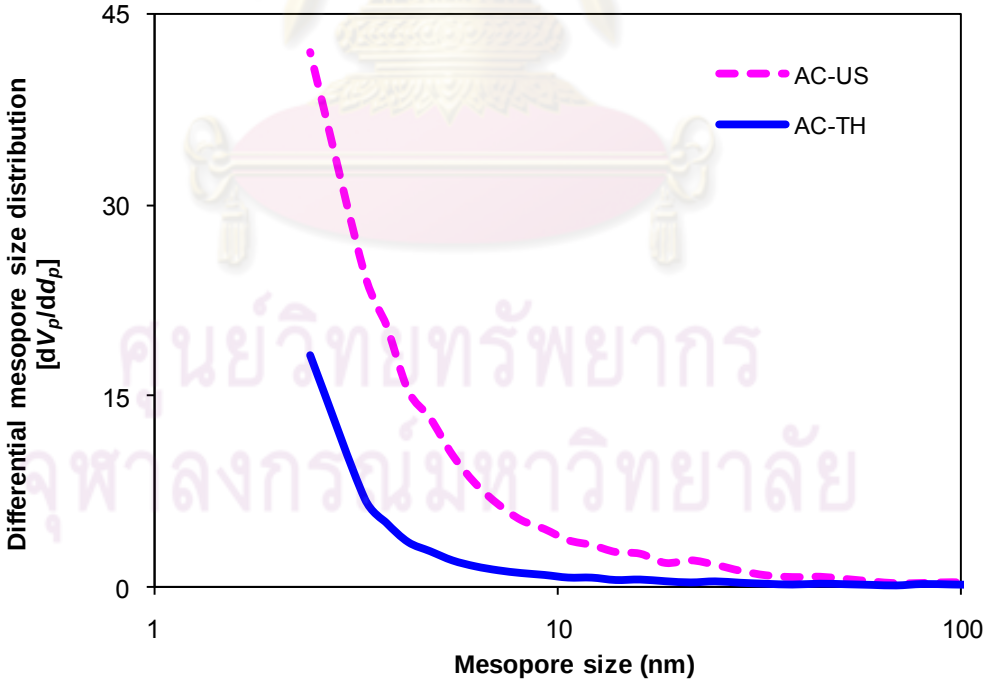

Figure 4.3 Mesopore size distribution of AC-US and AC-TH

4.1.4 Surface area of activated carbons

The porous characteristics of virgin AC supports were presented in **Table 4.2**. N_2 adsorption/desorption isotherms of AC-US and AC-TH exhibit meso-microporous and microporous structure, respectively. Total pore volume of AC-US and AC-US of 0.61 and 0.49 cm^3/g, respectively. The specific surface area was obtained by BET-plot. Average pore diameter size of AC-TH narrower than AC-US as 1.7 and 2.3 nm, respectively. Consequently, specific surface area of AC-TH larger than specific surface area of AC-US of 9% of 1,154 and 1,060 m^2/g, respectively. The microporous structure studied by using MP-plot method. The micropore volume of AC-US and AC-TH of 0.46 and 0.49 cm^3/g, respectively. Therefore, micropore volume of AC-TH higher than AC-US but total pore volume of AC-US higher than AC-TH. Comparison between total pore volume and micropore volume of both ACs, total pore volume of AC-TH consist by huge micropore volume but AC-US consist by huge micropore volume and slightly mesopore volume that found hysteresis loop in **Figure 4.1**.

Table 4.2 The porous characteristics of virgin AC

Sample	Porosity	BET surface area (m^2/g)	Total pore volume (cm^3/g)	Average pore diameter (nm)	Micropore volume (cm^3/g)	Modal micropore diameter (nm)
AC-US	meso-micropore	1,060	0.61	2.3	0.46	0.8
AC-TH	micropore	1,154	0.49	1.7	0.49	0.6

4.1.5 Attrition resistance of commercial activated carbon

Attrition resistance for solid particle is an important factor in use to three-phase fluidized bed reactor. Attrition can occur by loss of particles size smaller than 0.42 mm pieced due breakages by impact or collision of particles. Two types of commercial granular activated carbon which AC-US made from coal and AC-TH made from coconut shell. In this work, hardness number from the technical specification of granular activated carbons on **Table 3.1** exhibit the commercial granular activated coconut shell based carbon harder than the commercial granular activated carbon coal based. AC-TH made from abundant biomass in local country and AC-TH could be more available than AC-US.

Table 4.3 Properties of commercial activated carbon

Commercial activated carbon	Productive country	Hardness number (%)	Cost (Bath/kg)
AC-US	USA	MIN. 95	1,000
AC-TH	Thailand	MIN. 98	100

4.2 Effect of activated carbon

Ozone generated from air can used to decompose phenol by oxidation. The effect on the removal of phenol by activated carbon come from possess large surface areas for adsorption of hydrophobic compounds, including aqueous phenol **[22]**.

Investigation of a decomposition rate of 6 L of 10 ppm aqueous phenol by using three-phase fluidized bed with activated carbon and/or ozone was obtained in **Figure 4.4**. And investigation of TOC removal obtained in **Figure 4.5**. From result, Ozone could be decomposed phenol and some organic carbon intermediate to carbon dioxide **[23]**. Efficiency of activated carbon with air could be remove phenol and TOC better than only ozone. At first 10 minutes, the rate of reduction of phenol and TOC concentration were essentially the same. This implies that both of them were removed by adsorption of activated carbon. After that the rate of reduction of TOC becomes slower than that of phenol. This implies that a portion of the adsorbed phenol was decomposed to intermediate products **[22]**. Ozone combined with activated carbon gave the best result for removal phenol and TOC because activated carbon has adsorptive ability and enhanced surface area as active site for ozone and phenol reaction.

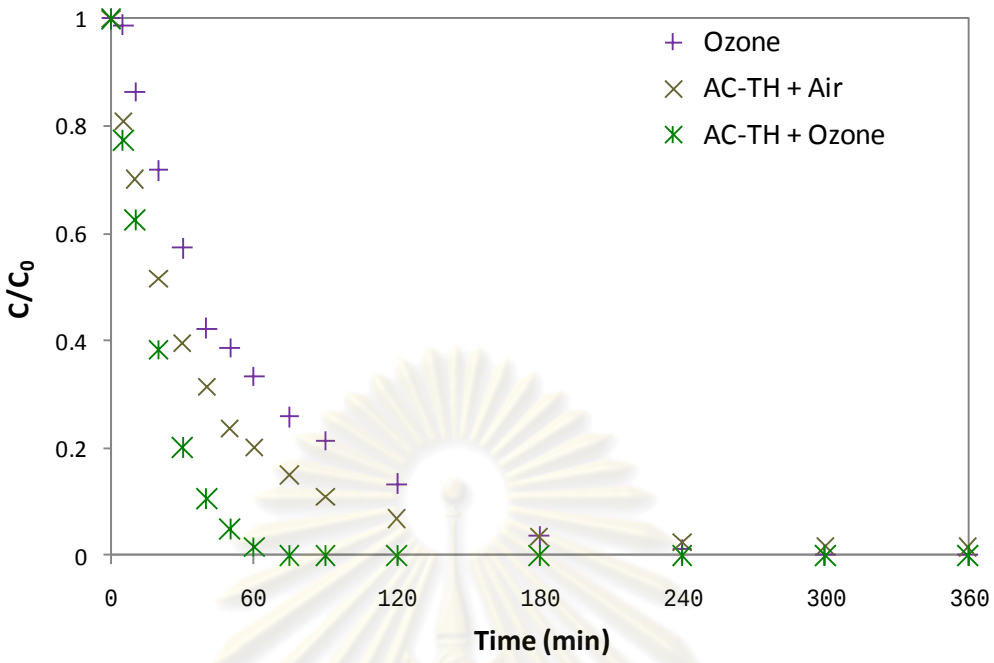

Figure 4.4 Phenol concentrations as a function of time for Ozone, AC-TH + Air and AC-TH + Ozone

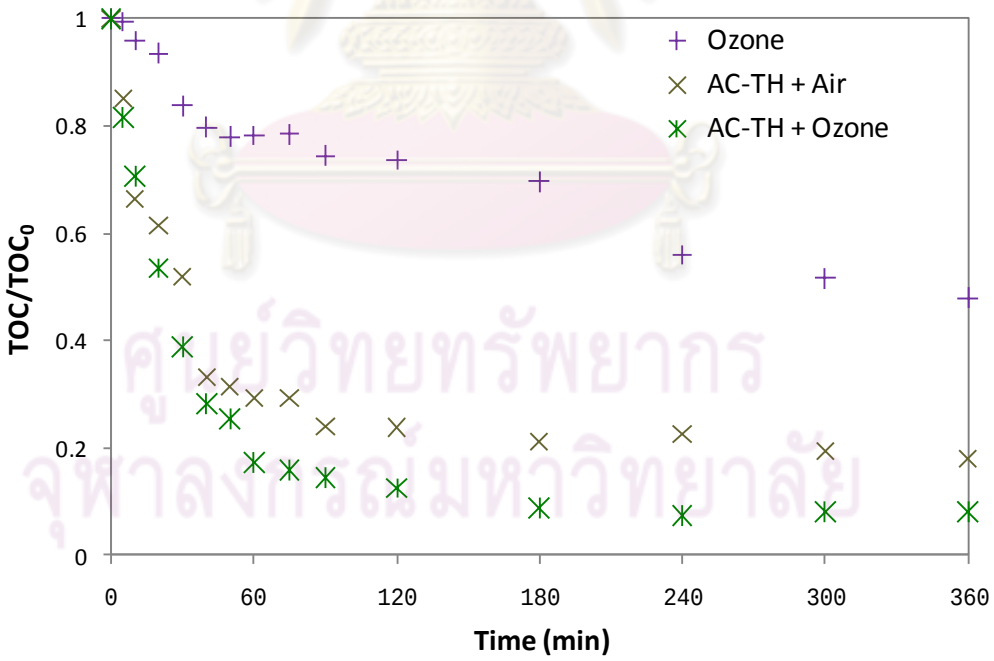

Figure 4.5 TOCs as a function of time for Ozone, AC-TH + Air and AC-TH + Ozone

4.3 Characteristics of activated carbon doped iron oxide

Activated carbon doped with iron oxide by two techniques of impregnation. After impregnation, activated carbons are calcined by two different conditions. **Table 4.4** shows code name of activated carbon doped with iron oxide prepared by different condition.

Table 4.4 Code name of Fe/AC particles

Fe/AC particles	Support	Weight percent of Fe	Impregnation technique	Calcination condition
5%CAT-TH-A-500	AC-TH	5%	IMA technique	500 °C nitrogen gas condition
5%CAT-TH-B-500	AC-TH	5%	IMB technique	500 °C nitrogen gas condition
5%CAT-TH-B-200	AC-TH	5%	IMB technique	200 °C ambient air condition
10%CAT-TH-B-500	AC-TH	10%	IMB technique	500 °C nitrogen gas condition

4.3.1 The thermal stability

The calcination condition was a necessary factor for effect of iron on activated carbon. The optimum condition simulated by TGA analysis. The thermal stability of the virgin activated carbon and activated carbon impregnated with metal oxide were studied under air or nitrogen gas atmosphere.

The TGA curves of different calcination conditions of virgin AC were shown in **Table 4.5 and 4.6**. From **Table 4.5**, it was found that the amount of weight loss at burning temperature (30-500 °C under nitrogen gas atmosphere) was around 6% and this occurred mainly due to the presence of impurity on surface and moisture in the activated carbon. **Table 4.6** was shows total weight loss at 200 °C under air atmosphere of 2%.

Table 4.5 Weight loss of activated carbon at 500 °C under N_2 flow

Temperature (°C)	Weight (%)
30.0	100.0
78.0	98.09
375.9	97.15
500.0	94.11

Table 4.6 Weight loss of activated carbon at 200 °C under air flow

Temperature (°C)	Weight (%)
30.0	100.0
35.0	99.92
105.2	97.95

Table 4.7 shows weight loss of 5% Fe on activated carbon for heat up from 30 °C to 500 °C under nitrogen gas flow, found that a significant weight loss was 11.07% at temperature changing from 30 °C to 89 °C, may at most to point at the presence of hygroscopic water in particle **[24]**. Next burning step was at around 125 °C shows decomposition of iron nitrate **[25]**. Weight loss of 6.74% at 89 °C to 492 °C was. Total weight loss of 17.81%.

Table 4.7 Weight loss of 5 wt.% Fe on activated carbon at 500 °C under N_2 flow

Temperature (°C)	Weight (%)
30.0	100.0
56.2	99.41
88.8	88.93
491.7	82.19

Table 4.8 Weight loss of 5 wt.% Fe on activated carbon at 500 °C under air flow

Temperature (°C)	Weight (%)
30.0	100.0
52.9	99.90
85.2	90.70
382.4	86.5
475.9	6.6

Weight loss curve of 5% Fe on activated carbon at 500 °C under air flow shown in **Table 4.8**. The amount of weight loss at temperature range from 30 °C to 382 °C of 13.5%, presence of loss of moisture and decomposition of iron nitrate. At high temperature around 400 °C under air flow condition, weight loss of 79.9% because activated carbon burned under heat and oxygen. Total thermal weight loss of 93.4%.

Table 4.9 Weight loss of 5% Fe on activated carbon at 200 °C under air flow

Temperature (°C)	Weight (%)
30.0	100.0
53.9	99.98
162.3	85.30

At mild condition, TGA analyzed at 30-200 °C under air flow that shown in **Table 4.9**. TGA curve around 30 °C to 162 °C presence for loss of moisture and decomposition of iron nitrate. Finally, total weight loss was 14.7% by complete decomposed iron nitrate to iron oxide **[24]**.

For activated carbon doped with iron oxide preparation, calcined at 500 °C under air flow shows huge weight loss of activated carbon. Activated carbon burning down by oxygen from air combined with highly temperature. The suitable calcination conditions at 500 °C under nitrogen gas flow and 200 °C under air flow, because that conditions shows completely decomposed iron nitrate and avoid burning down of activated carbons doped with iron.

ศูนย์วิทยทรัพยากร
จุฬาลงกรณ์มหาวิทยาลัย

4.3.2 Surface area of activated doped with iron oxide

The specific surface area of Fe/AC could be observed that virgin activated carbon support (AC-TH). AC support was gives larger surface area than Fe/AC form identical support. The code name of different Fe/AC elucidate in **Table 4.4**. And **Table 4.10** shows as the porous characteristics of virgin AC supports and Fe/AC particles.

Table 4.10 The porous characteristics of virgin AC supports and Fe/AC particles

Sample	Porosity	BET surface area (m^2/g)	Total pore volume (cm^3/g)	Average pore diameter (nm)	Micropore volume (cm^3/g)	Modal micropore diameter (nm)
AC-TH	micropore	1,154	0.49	1.7	0.49	0.6
5%CAT-TH-A-500	micropore	1,088	0.47	1.7	0.47	0.6
5%CAT-TH-B-500	micropore	1,081	0.46	1.7	0.46	0.7
5%CAT-TH-B-200	micropore	1,067	0.47	1.8	0.47	0.7
10%CAT-TH-B-500	micropore	1,000	0.45	1.8	0.44	0.8

In case of prepared by IMA technique (5%CAT-TH-A-500), BET surface area and total pore volume of 1,088 m^2/g and 0.47 cm^3/g (loss 6% and 4% of AC support), respectively. In case of prepared by IMB technique (5%CAT-TH-B-500), BET surface area and total pore volume of 1,081 m^2/g and 0.46 cm^3/g (loss 6% and 6% of AC support). Compared between two impregnation techniques, BET surface area of both case was approach. Total pore volume and modal micropore diameter show slightly difference, 5%CAT-TH-A-500 shows higher pore volume than 5%CAT-TH-B-500 but modal micropore diameter of 5%CAT-TH-A-500 narrower than 5%CAT-TH-B-500 as 0.6 and 0.7 nm, respectively.

In case of calcined by 200 °C ambient air condition (5%CAT-TH-B-200), BET surface area and total pore volume of 1,067 m^2/g and 0.46 cm^3/g (loss 8% and 4% of AC support). Compared between different calcination conditions (5%CAT-TH-B-500 and 5%CAT-TH-B-200), BET surface area, total pore volume and average pore diameter show slightly difference. BET surface area of 5%CAT-TH-B-500

larger than 5%CAT-TH-B-200. In contrast, 5%CAT-TH-B-500 shows narrower pore volume than 5%CAT-TH-B-200.

Compared between different Fe content on activated carbon (5%CAT-TH-B-500 and 10%CAT-TH-B-500), In case of 10 wt.% Fe (10%CAT-TH-B-500), BET surface area and total pore volume were 1,000 m^2/g and 0.45 cm^3/g (loss 13% and 8% of AC support). BET surface area of 5%CAT-TH-B-500 larger than 10%CAT-TH-B-500. In contrast, 5%CAT-TH-B-500 shows narrower pore volume than 10%CAT-TH-B-500.

Specific surface area of activated carbon doped with iron oxide after calcined was decrease from virgin activated carbon support, calculated to be 1,088-1,000 m^2/g. Loss surface area was about 6-13% of AC support. This indicates the plugging of the loaded metal on the activated carbon pore **[26]**.

4.3.3 Energy dispersive X-ray spectroscopy

Activated carbon and 5 wt.% Fe on activated carbon after calcined at different condition were investigated by SEM at 20 kV shows in **Figure 4.11**. EDS of samples revealed the presence of metal layers on surface of activated carbon, as can be observed in **Table 4.11**.

Table 4.11 Element compositions of different calcination condition of activated carbons doped with iron oxide

Sample	Atomic %		
	C	O	Fe
AC-TH	92.43	7.57	-
5%CAT-TH-B-200	76.98	19.50	3.52
5%CAT-TH-B-500	83.00	14.07	2.93

(a)

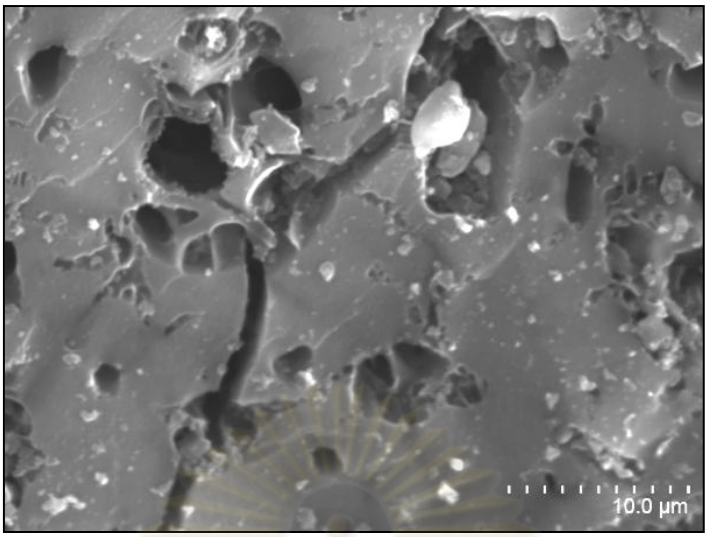

(b)

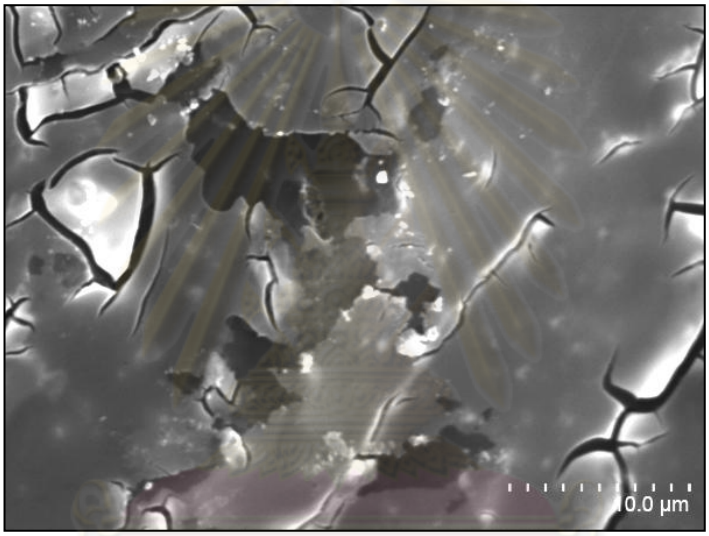

(c)

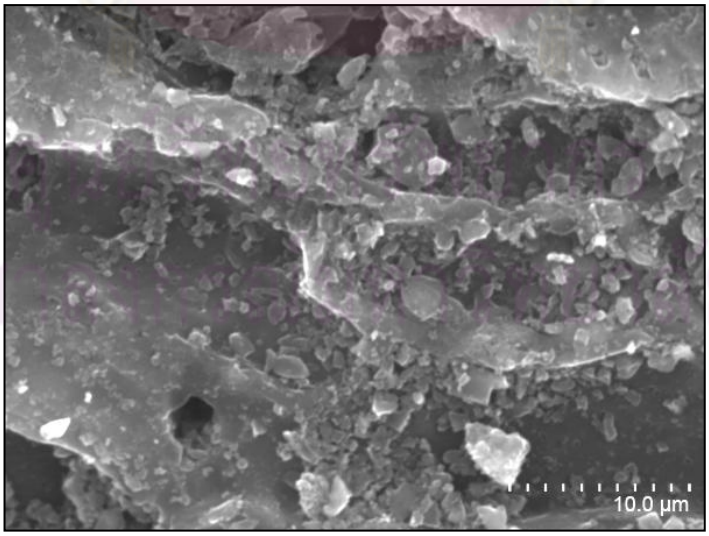

Figure 4.6 SEM of (a) AC-TH, (b) 5%CAT-TH-B-200 and (c) 5%CAT-TH-B-500

Figure 4.6(a) showed the surface of fresh activated carbon. It was very clear and no deposition was detected on the surface. The atomic percentage of carbon and oxygen element of fresh activated carbon was 92.43 and 7.57%, respectively.

From SEM image shows in **Figure 4.6(b)**, morphology of particle that by 5 wt.% Fe on AC-TH at calcined temperature of 200 °C under ambient air (5%CAT-TH-B-200) was quite different from AC-TH. Iron molecules were dispersedly coated on the surface of activated carbon. The atomic percentage of carbon, oxygen and Fe of 5%CAT-TH-B-200 were 76.98, 19.50 and 3.52, respectively. The Fe content on the surface of 3.52% that could be calculated approximately 70% of target.

From **Figure 4.6(c)**, morphology of particle that by 5 wt.% Fe on AC-TH at calcined temperature of 500 °C under flowing of N_2 (5%CAT-TH-B-500) was quite different from AC-TH. Iron molecules were dispersedly coated on the surface of activated carbon. The atomic percentage of carbon, oxygen and Fe of 5%CAT-TH-B-500 were 83.00, 14.07 and 2.93, respectively. The Fe content on the surface of 2.93% that could be calculated approximately 59% of target.

Fe content in catalysts analyzed by XRF was shows in **Table 4.12**. XRF could confirm Fe content in 5%CAT-TH-A-500, 5%CAT-TH-B-500, 5%CAT-TH-B-200 and 10%CAT-TH-B-500 were 3.25, 3.05, 3.11 and 6.16 wt. %, respectively. That could be calculated approximately 65, 61, 62 and 62% of target, respectively. All Fe/AC show stability of Fe loading on catalytic support around 62 % of target.

Table 4.12 Fe content in activated carbon

Sample	Fe content (wt. %)
5%CAT-TH-A-500	3.25
5%CAT-TH-B-500	3.05
5%CAT-TH-B-200	3.11
10%CAT-TH-B-500	6.16

4.3.4 Crystal structure on activated carbons

XRD patterns of Fe/AC calcined at different conditions shows in **Figure 4.7**. The calcination conditions studied was between 200 °C under ambient atmosphere and 500 °C under nitrogen gas flow.

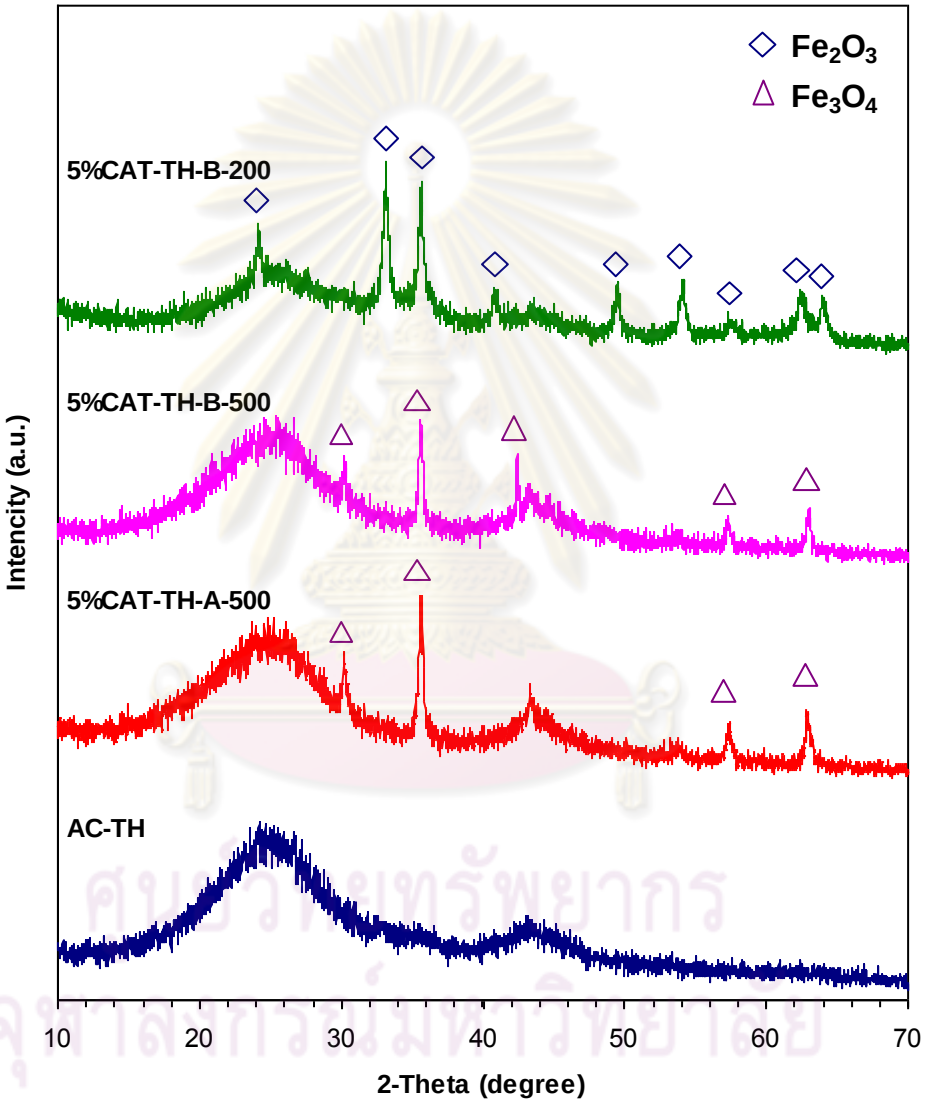

Figure 4.7 XRD of AC and Fe/AC

Virgin AC-TH found broad diffraction peaks at 2-Theta of 26.3° and 44.8° could be assigned to amorphous carbon from activated carbon **[27]**. 5%CAT-TH-A-500 and 5%CAT-TH-B-500 were calcinated at same condition, 500 °C under nitrogen gas flow for 5 hrs shown pattern peaks identify that Fe_3O_4 around 2-Theta of 30.2°, 35.5°, 43.4°, 57.2° and 62.8° **[28,29]**. A series of characteristic peaks of 5%CAT-TH-B-200 was catalyst calcination under ambient air at 200 °C for 5 hrs observe Fe_2O_3 around 2-Theta of 24.0°, 33.0°, 35.5°, 40.8°, 49.2°, 53.9°, 57.2°, 62.3° and 63.7° **[30]**.

4.3.5 Production data

a) Comparison for different preparation

Summarization of different preparation shows in **Table 4.13**. It should be noted that in view of ease of preparation and energy saving, the IMB technique showed higher application potential at the industrial scale.

Table 4.13 Information of Fe/AC prepared by different impregnation

Sample	Impregnation technique	Fe(NO3)3•9H2O solution		Preparative condition		Production rate (g/batch)
		Concentration in water (mol/L)	Volume (L/kg_{AC})	Temperature (°C)	Pressure (bar)	
5%CAT-TH-A-500	IMA	0.09	10	60	0.05	10
5%CAT-TH-B-500	IMB	1.79	0.5	80	1	100
10%CAT-TH-B-500	IMB	3.58	0.5	80	1	100

b) Comparison for two different calcination conditions

Table 4.14 is show summarization of Fe/AC calcined by two different calcinations. It should be noted that in view of large-scale for product and saving cost of calcination, 200°C under ambient air atmosphere is appropriate condition for the industrial scale.

Table 4.14 Information of Fe/AC calcined in two different conditions

Sample	Calcination condition		Iron oxide	Production rate (g/batch)
	Temperature (°C)	atmosphere		
5%CAT-TH-B-500	500	nitrogen gas	Fe_3O_4	30
5%CAT-TH-B-200	200	ambient air	Fe_2O_3	300

4.4 Effect of iron oxide on activated carbon for aqueous phenol removal

To compare the activity of solid particle combined with ozone, virgin activated carbon or activated carbon doped with iron oxide was removing aqueous phenol in three-phase fluidized bed under operating condition following as **Table 4.9**. The characteristic of virgin AC and Fe/AC shows in **Table 4.15**. AC was AC-US and Fe/AC prepared form AC-US by IMA techniques. After that Fe/AC calcined under nitrogen atmosphere at 500°C for 5 hours **[22]**.

Table 4.15 Experimental condition of a laboratory-scaled three-phase fluidized bed reactor

Parameter	Value
Initial concentration of phenol (ppm)	10
Aqueous phenol volume (L)	2
Liquid recirculation flow rate (L/min)	1
Gas flow rate (L/min)	1
Solid particle weight (g)	5
Temperature (°C)	17-25

Table 4.16 The characteristics of AC and Fe/AC particles **[22]**

Sample	BET surface area (m^2/g)	Total pore volume (cm^3/g)	Average pore diameter (nm)	Micropore volume (cm^3/g)	Modal micropore diameter (nm)
AC	1,060	0.61	2.3	0.49	0.6
Fe/AC	888	0.49	2.2	0.46	0.7

The removal of phenol by AC combined with ozone and Fe/AC combine with ozone present in **Figure 4.8**, two cases show that rapidly removing phenol. The combination of Fe/AC and ozone was more efficiency more than the combination of AC. In addition, the TOCs removal are expressed in **Figure 4.9**. The comparison between Fe/AC and AC combined with ozone show that AC was slightly more effective even thought the amount of Fe **[22]**.

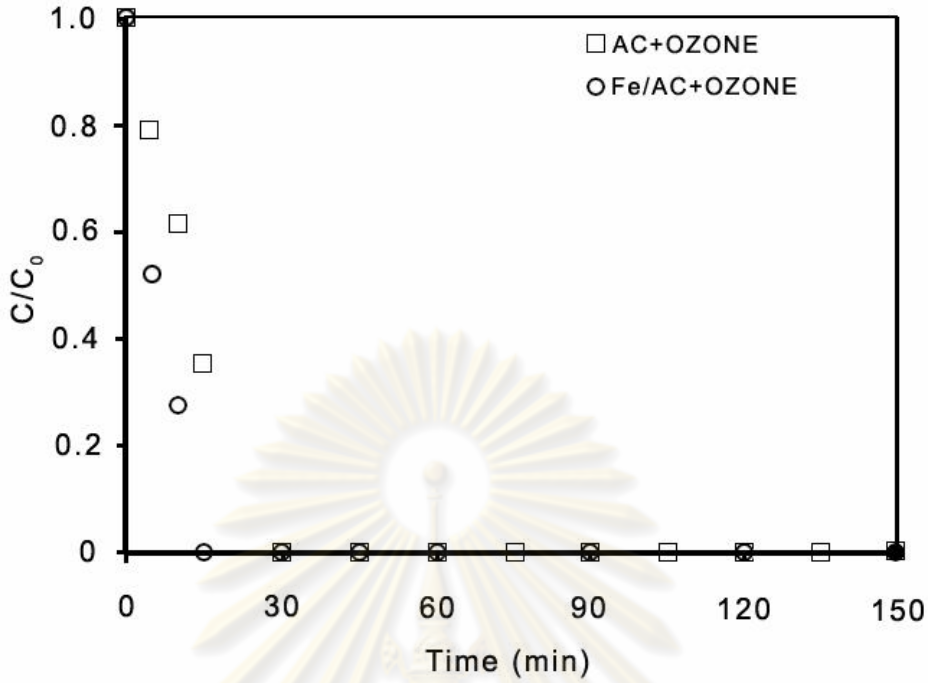

Figure 4.8 Phenol concentrations as a function of time for ozonation combined with AC-TH and Fe/AC

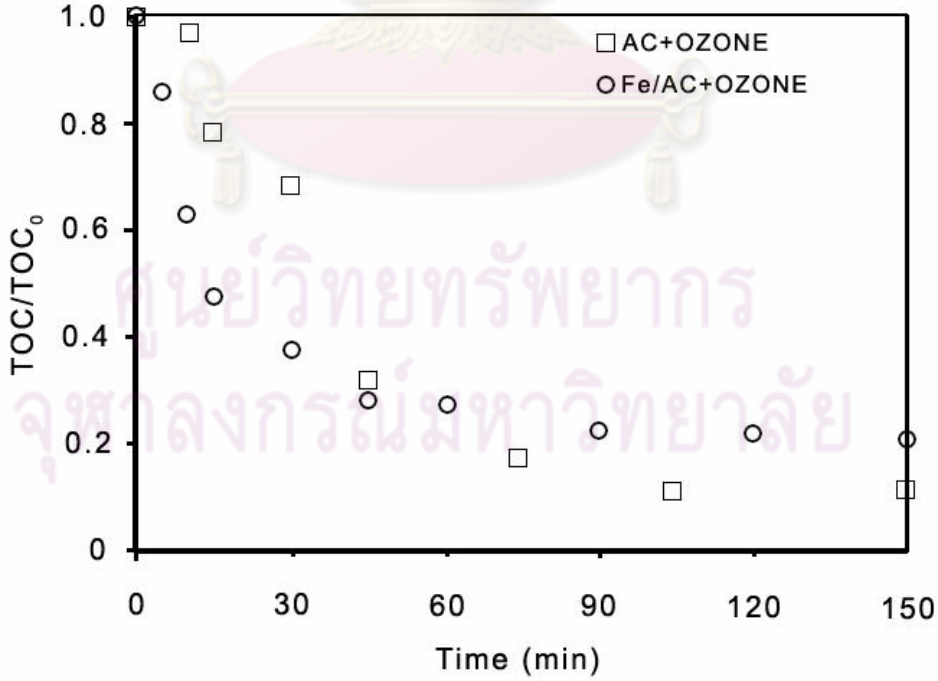

Figure 4.9 TOCs as a function of time for ozonation combined with AC and Fe/AC

4.5 Aqueous phenol removal in a laboratory-scaled fluidized bed reactor

Aqueous phenol (liquid phase) removal in a laboratory-scaled three-phase fluidized bed reactor using activated carbon doped with iron oxide (solid phase) as bed particle with ozone (gas phase) as oxidizing agent. A preliminary study of phenol and TOC removal efficiency and initial phenol removal rate constant was necessary for select optimum solid particle using in pilot-scaled three-phase fluidized bed reactor. The experimental condition of a laboratory-scaled three-phase fluidized bed reactor is shown in **Table 4.17**.

Table 4.17 Experimental condition of a laboratory-scaled three-phase fluidized bed reactor

Parameter	Value
Initial concentration of phenol (ppm)	10
Aqueous phenol volume (L)	6
Liquid recirculation flow rate (L/min)	1
Gas flow rate (L/min)	2
Solid particle weight (g)	5
Temperature (°C)	30

The principle calculation of phenol and TOC removal efficiency as given in equations 4-1 and 4-2.

Phenol removal efficiency:

$$X_{ph} = \frac{C_0 - C_t}{C_0} \times 100\% \qquad (4\text{-}1)$$

TOC removal efficiency:

$$X_{TOC} = \frac{TOC_0 - TOC_t}{TOC_0} \times 100\% \qquad (4\text{-}2)$$

4.5.1 Phenol removal by different impregnation techniques of activated carbons

The removal of 6 L of 10 ppm initial phenol concentration by laboratory-scaled three-phase fluidized bed reactor to study the activity of ozonation combined with virgin activated carbon or iron oxide on activated carbons from different impregnation techniques. Experimental condition was constant at temperature 30 °C, gas flow rate of 2 L/min and liquid flow rate of 1 L/min. 5%CAT-TH-A-500 and 5%CAT-TH-A-500 were Fe/AC from different impregnation techniques, prepared from AC-TH by IMA and IMB techniques, respectively.

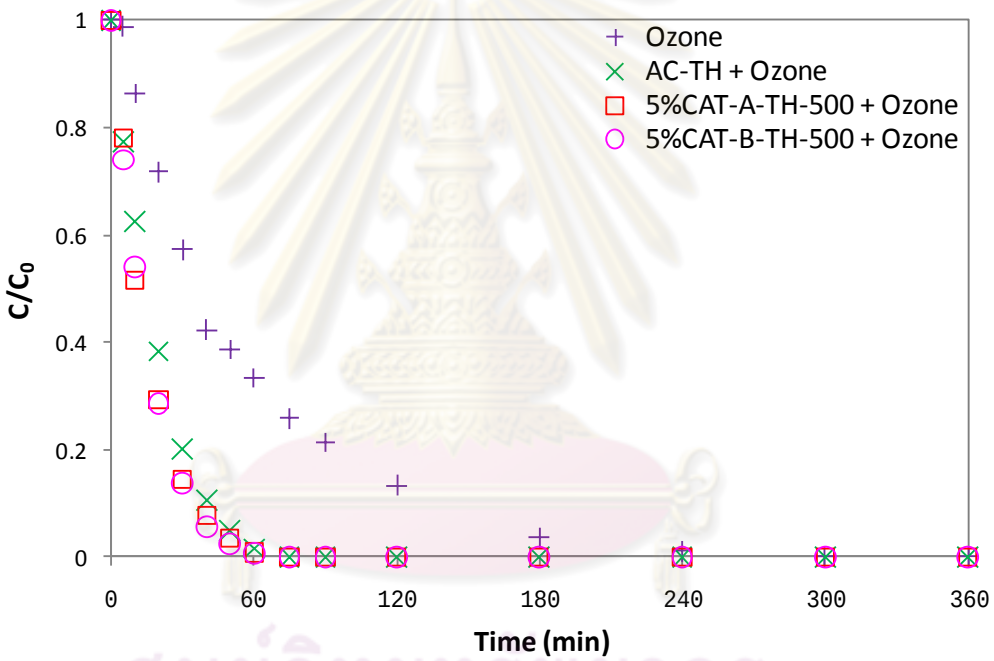

Figure 4.10 Phenol concentrations as a function of time for ozonation combined with AC-TH, 5%CAT-TH-A-500 or 5%CAT-TH-B-500

Figure 4.10 shows normalized phenol concentrations as function of time for removal in the three-phase fluidized bed reactor using ozone gas combined with three different types of activated carbon (AC-TH, 5%CAT-TH-A-500 or 5%CAT-TH-B-500). In cases of ozonation combined with three different types of activated carbon show phenol removal efficiency higher than only ozonation. In fact, activated carbon is highly adsorptive material because it extremely porous thus to has high pore volume and large surface area available for adsorption as shown in **Table 4.10 [6,31]**.

Removal of phenol could be occurred by adsorption and oxidation. For fresh AC and Fe/AC particles, the adsorptive ability was extremely high because the gradient of concentration between the pore sites and aqueous phenol was still high **[32]**.

Virgin AC combined with ozone compare with both Fe/AC combined with ozone reveals that the both Fe/AC was more phenol removal efficiency higher than that virgin AC in first 60 minutes, as reported by Limsuwan et al. **[22]**. However, it could be clearly observed that three different activated carbons can completely decompose phenol within 75 minutes. In Fe/AC case combined with ozone, 5%CAT-TH-A-500 compare with 5%CAT-TH-B-500 that show slightly phenol removal efficiency of 5%CAT-TH-B-500 higher than 5%CAT-TH-A-500. It should be noted that in view of ease of preparation and energy saving, the 5%CAT-TH-B-500 prepared by IMB technique showed higher application potential at the industrial scale.

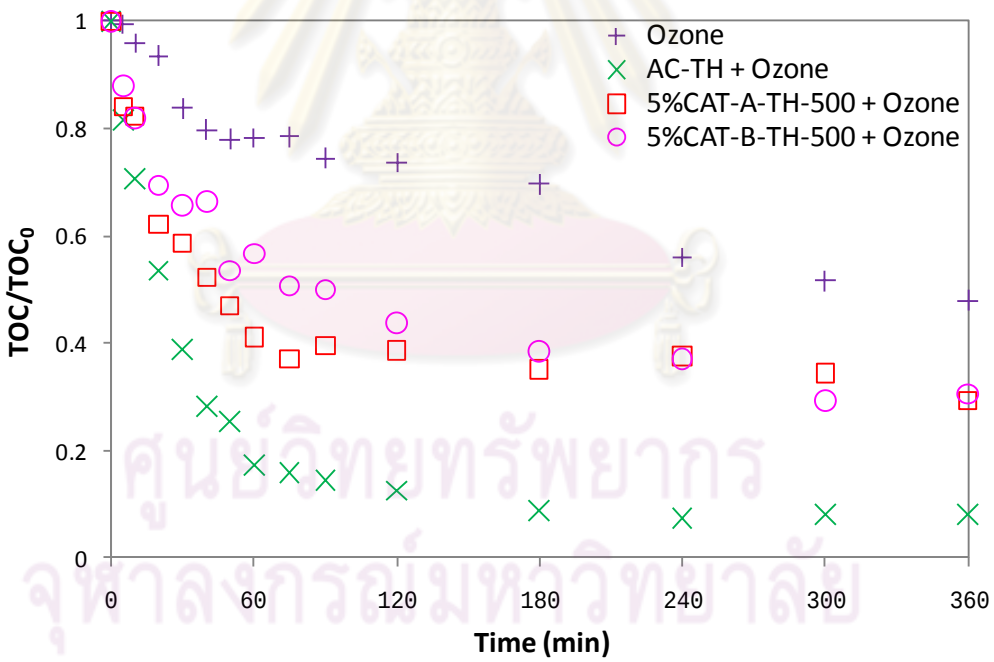

Figure 4.11 TOCs as a function of time for ozonation combined with AC-TH, 5%CAT-TH-A-500 and 5%CAT-TH-B-500

Table 4.18 Phenol decomposition efficiency and TOC removal efficiency for AC-TH, 5%CAT-TH-A-500 and 5%CAT-TH-B-500

Time (min)	Phenol decomposition (%)				TOC decomposition (%)			
	Ozone	AC-TH + Ozone	5%CAT-TH-A-500 + Ozone	5%CAT-TH-B-500 + Ozone	Ozone	AC-TH + Ozone	5%CAT-TH-A-500 + Ozone	5%CAT-TH-B-500 + Ozone
10	14	37	46	49	4	29	18	18
60	67	98	99	99	22	83	59	43
75	74	100	100	100	22	84	63	49
300	100	100	100	100	48	92	66	71
360	100	100	100	100	52	92	71	69

TOCs are total organic carbon of phenol and intermediate from phenol decomposition. AC-TH, 5%CAT-TH-A-500 and 5%CAT-TH-B-500 combined with ozone can decompose phenol in aqueous solution to some intermediate products. Time dependence of intermediate TOC which were derived from phenol is depicted in **Figure 4.11**. First, the removal of phenol using only ozonation gave the worst result when compared to other case which employed activated carbon, as report by Limsuwan P. et al. **[22]** and Turhan. K and Uzman S. **[23]**. Phenol could be decomposed by ozonation but intermediate products (catechol, hydroquinone, p-benzoquinone, maleic acid and oxalic acid) can occur at the end of process. Products intermediate can be oxidized completely with ozone to CO_2 and H_2O but destruction of some organic compounds requires a long ozonation time and high ozone dosages **[23]**.

Second, ozonation combined with three different types of activated carbons exhibit to enhance efficiency of TOC removal higher than only ozonation. In other word, AC and Fe/AC which high porosity and large surface area was enhance adsorption and oxidation organic compounds on surface of solid particle. At completely phenol removing by case of ozonation combined with three different types of activated carbons (75 min), TOC removal efficiency of AC-TH, 5%CAT-TH-A-500 and 5%CAT-TH-B-500 were 84%, 63% and 49%, respectively. Finally at 360

minutes, TOC removal efficiency of AC-TH, 5%CAT-TH-A-500 and 5%CAT-TH-B-500 were 92%, 71% and 69%, respectively. In all cases of oxidative decomposition, TOC still remain because some intermediate products were hard to decompose. Both Fe/ACs show TOC removal efficiency lower than AC. 5%CAT-TH-A-500 combined with ozone exhibited slightly higher TOC removal efficiency than 5%CAT-TH-B-500 combined with ozone. However, Fe on activated carbon could be enhance the mass transfer of ozone to disperse thorough the solution and enhance the decomposition of ozone. TOC removal efficiency by AC-TH combined with ozone gave the best result **[22]**. Our result following effects reported by Amin et al. to support on application of activated carbon and ozone to treat organic observed several effects: (1) activated carbon is a strong absorbent in the case of phenol, (2) ozone undergoes rapid decomposition to generate highly oxidative radicals when in contract with activated carbon and (3) organics adsorbed by activated carbon can be oxidized by ozone, restoring its porous for further adsorption. Therefore, activated carbon initialed the transformation of ozone to hydroxyl radicals, that are not bound to the surface of carbon but are free to react with organics in the aqueous solution **[22,33]**.

4.5.2 Phenol removal by different Fe content in activated carbon

On laboratory-scaled three-phase fluidized bed reactor, aqueous phenol was removing by ozone with three different Fe content in activated carbons. Data of the optimal Fe content in activated carbon is desirable for effective operation of oxidative systems. To find out the appropriate amount of Fe/AC by varying the Fe content in activated carbon, the experiment of 0, 5 and 10 wt.% of Fe were AC-TH, 5%CAT-TH-B-500 and 10%CAT-TH-B-500, respectively.

Figure 4.12 shows normalized phenol concentrations as function of time for removal in the three-phase fluidized bed reactor by ozone combined with three different Fe content in activated carbons. In three cases of solid particle combined with ozone, 5%CAT-TH-B-500 gave the best result. AC-TH, 5%CAT-TH-B-500 and 10%CAT-TH-B-500 can completely removing phenol in aqueous solution at 75, 75 and 90 minutes, respectively. Time dependence of intermediate TOC which were derived from phenol is depicted in **Figure 4.13**.

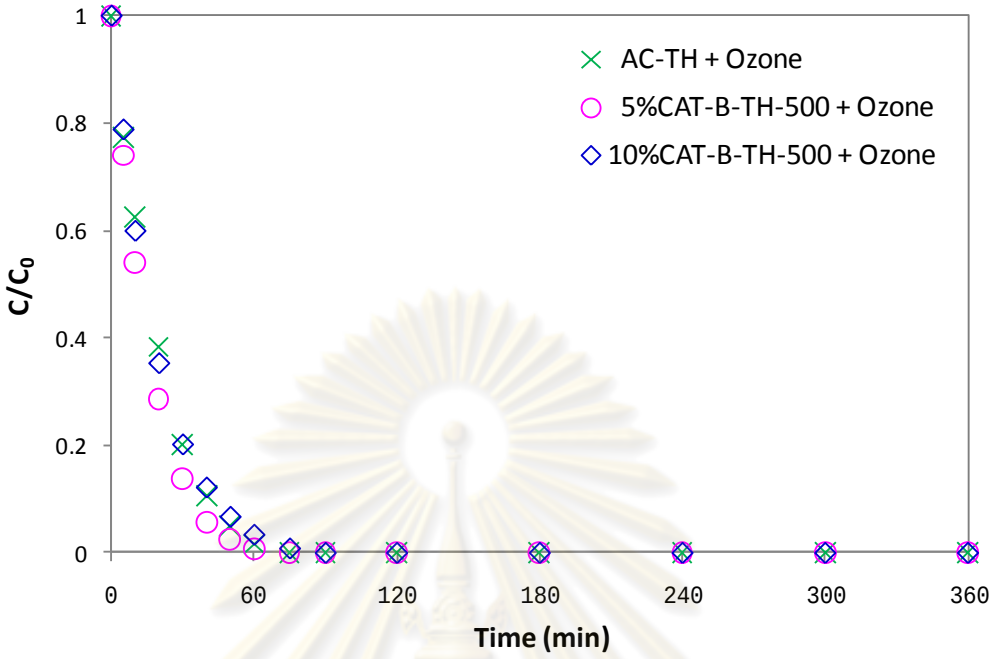

Figure 4.12 Phenol concentrations as a function of time for ozonation combined with AC-TH, 5%CAT-TH-B-500 and 10%CAT-TH-B-500

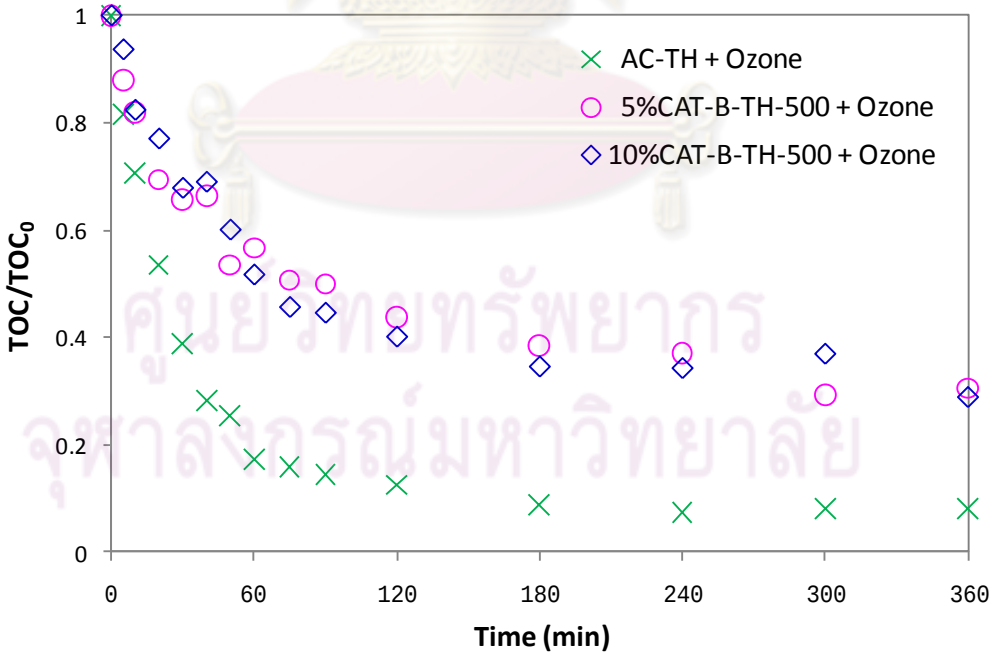

Figure 4.13 TOCs as a function of time for ozonation combined with AC-TH, 5%CAT-TH-B-500 and 10%CAT-TH-B-500

Table 4.19 Phenol decomposition efficiency and TOC removal efficiency for AC-TH, 5%CAT-TH-B-500 and 10%CAT-TH-B-500

Time (min)	Phenol decomposition (%)			TOC decomposition (%)		
	AC-TH	5%CAT-TH-B-500	10%CAT-TH-B-500	AC-TH	5%CAT-TH-B-500	10%CAT-TH-B-500
10	37	49	40	29	18	18
75	100	100	99	84	49	54
90	100	100	100	86	50	55
360	100	100	100	92	69	71

At 75 minutes, the TOC removal efficiency of AC-TH, 5%CAT-TH-A-500 and 5%CAT-TH-B-500 were 84%, 49% and 54%, respectively. Finally, 5%CAT-TH-A-500 and 5%CAT-TH-B-500 shows approachable removal efficiency at 360 minutes. The TOC removal efficiency of AC-TH, 5%CAT-TH-B-500 and 10%CAT-TH-B-500 were 92%, 69% and 71%, respectively. AC-TH combined with ozone gave the best result for TOC removal. From **Table 4.10** shows specific surface area of AC-TH of 1,154 m^2/g, 5%CAT-TH-B-500 of 1,081 m^2/g and 10% CAT-TH-B-500 of 1,000 m^2/g. AC-TH exhibit larger specific surface area than 5%CAT-TH-B-500 and 10%CAT-TH-B-500. The total surface area of catalyst has an important effect on the reaction rate. The rate of catalytic reaction was proportional to the surface area because catalytic reaction of heterogeneous catalyst will away occur on interface **[34]**.

However, an increase in the Fe content on activated carbon from 5 to 10 wt. % instead results in the approachable removal efficiency. The optimal amount of Fe content in activated carbon was found to be around 5 wt. % of support.

4.5.3 Phenol removal by different calcination condition of activated carbons

The efficiency of phenolic removal was investigated based on different calcinations temperature. In case of 5%CAT-TH-B-500, particle calcined by 500 °C under nitrogen gas flow. In case of 5%CAT-TH-B-200, particle calcined by 200 °C under ambient air. Both particles enhanced with ozone in three-phase fluidized bed reactor. **Figure 4.14 and 4.15** show change residual phenol and TOC concentrations as a function of time, respectively.

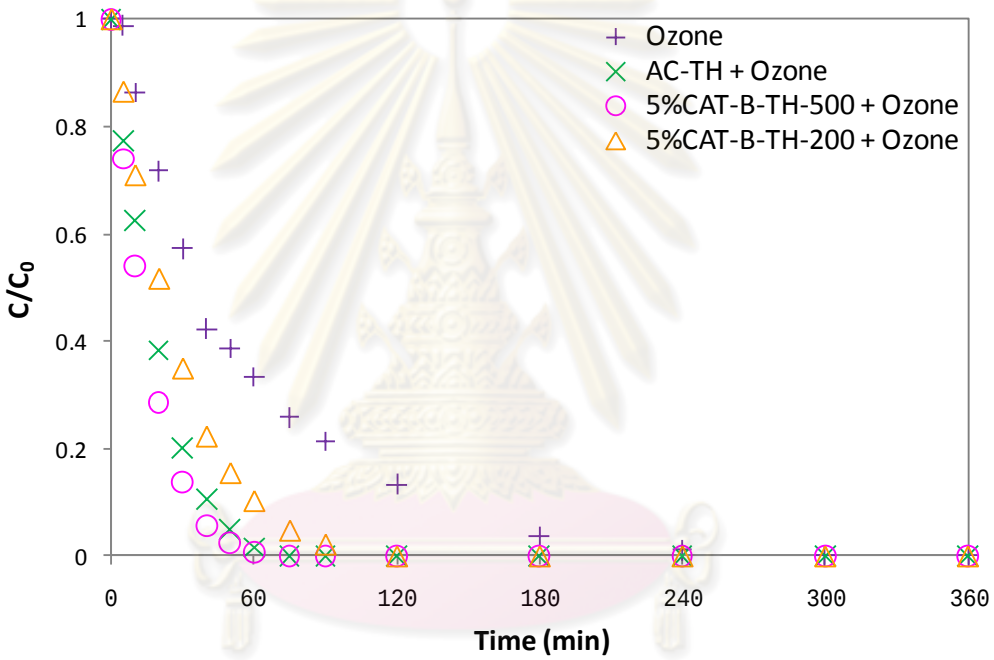

Figure 4.14 Phenol concentrations as a function of time for ozonation combined with AC-TH, 5%CAT-TH-B-500 and 5%CAT-TH-B-200

Investigation of a removal rate of aqueous phenol by using a laboratory-scaled fluidized bed reactor by only ozone or ozone combined with activated carbons. The removal efficiency of phenol from initial concentration of 10 ppm by treatment with ozone combined with AC-TH, ozone combined with 5%CAT-TH-B-500, ozone combined with 5%CAT-TH-B-200 and only ozone were present in **Figure 4.14**. The case of ozone combined with activated carbons doped iron oxide shows higher performance for removal of phenol than only ozone.

For comparison, 5%CAT-TH-B-200 sample was prepared on the AC-TH support by IMB method similar to 5%CAT-TH-B-500 but with different calcinations temperature. Based on the experimental results, the rates of reduction in phenol of 5%CAT-TH-B-500 was faster than when 5%CAT-TH-B-200 as employed. It could be clearly observed that 5%CAT-TH-B-500 and 5%CAT-TH-B-200 can completely removing phenol within 75 and 90 minutes, respectively.

As shown in **Table 4.10**, the possession of 5%CAT-TH-B-500 of larger specific surface area than 5%CAT-TH-B-200. Higher quantity of active site for surface reaction would be the main attribution of these adsorption and oxidation of phenol.

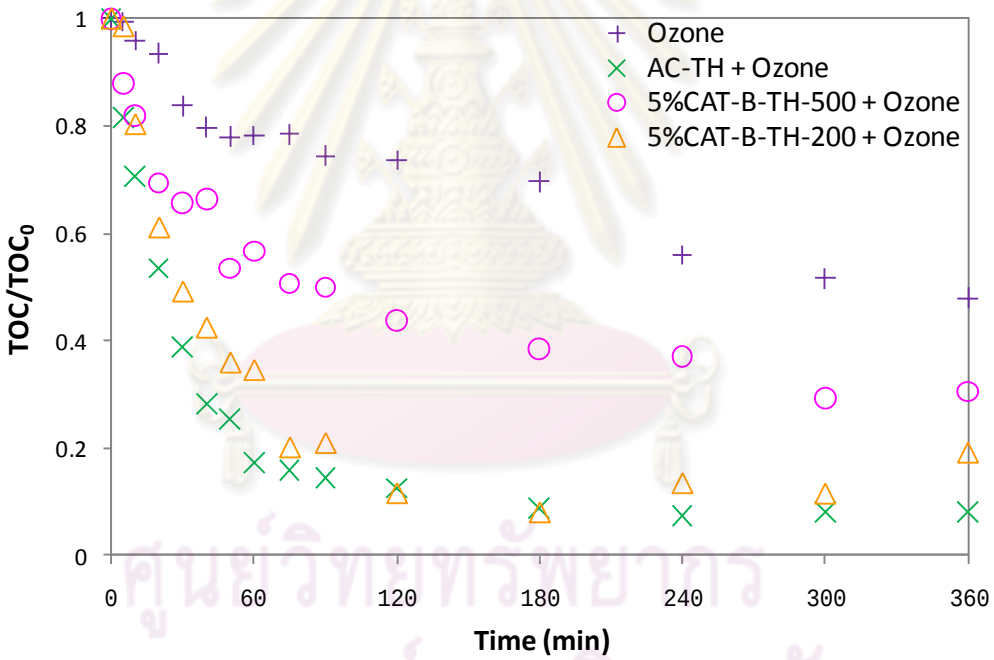

Figure 4.15 TOCs as a function of time for for ozonation combined with AC-TH, 5%CAT-TH-B-500 and 5%CAT-TH-B-200

Table 4.20 Phenol decomposition efficiency and TOC removal efficiency for AC-TH, 5%CAT-TH-B-500 and 5%CAT-TH-B-200

Time (min)	Phenol decomposition (%)				TOC decomposition (%)			
	Ozone	AC-TH + Ozone	5%CAT-TH-B-500 + Ozone	5%CAT-TH-B-200 + Ozone	Ozone	AC-TH + Ozone	5%CAT-TH-B-500 + Ozone	5%CAT-TH-B-200 + Ozone
10	14	37	46	29	4	29	18	20
75	74	100	100	95	22	84	49	80
120	87	100	100	100	26	87	56	88
300	100	100	100	100	48	92	71	89
360	100	100	100	100	52	92	69	81

In case of ozonation, bubble of ozone is injected into a liquid phase. The process is free radical chain and direct ozone molecule oxidation reactions: First, ozone transfers from gas phase to liquid phase. Then ozone self-decomposes in water to produce •OH radicals. High-activated hydroxyl radicals are consumed by organic compounds oxidation (4-5) and reactions between radicals. Meanwhile, direct ozonation decomposition of pollutants (4-6) occurs, but the reaction rate is respectively low compared to that between •OH radical and organic compounds **[23,35]**.

Indirect:

$$O_3 + OH^- \rightarrow HO_2^- + O_2 \quad (4\text{-}3)$$

$$O_3 + OH_2^- \rightarrow \bullet OH + O_2^- + O_2 \quad (4\text{-}4)$$

$$OH + C\ (\text{organic compounds}) \rightarrow P\ (\text{intermediate or final product}) \quad (4\text{-}5)$$

Direct:

$$O_3 + C\ (\text{organic compounds}) \rightarrow P'(\text{intermediate or final product}) \quad (4\text{-}6)$$

In case of ozone combined with activated carbon doped with iron oxide (5%CAT-TH-B-500 or 5%CAT-TH-B-200) could enhance remove organic compounds by react with both ozonation and oxidation of adsorbed organic. Fe on

activated carbon could enhance produces hydroxyl radicals form ozone decomposition. Furthermore, activated carbon doped with iron oxide could enhance interface for adsorbed on active site **[23,36]**. However, the higher TOC removal of 5%CAT-TH-B-500 in **Figure 4.15** may be attributed to types of iron oxide after calcination at different temperature. The iron oxide on the 5%CAT-TH-B-200 surface was found as Fe_2O_3 **[24]** but the 5%CAT-TH-B-500 was found Fe_3O_4. Therefore, Fe_2O_3 on the 5%CAT-TH-B-200 can remove other intermediate products better than Fe_3O_4 on the 5%CAT-TH-B-500. It should also be noted that the 5%CAT-TH-B-200 could be prepared at a cost lower than that of 5%CAT-TH-B-500. Therefore, it would be more promising for preparation of bed particle in bulk for actual application in industrial-scale. However, TOC removal by ozonation combined with AC-TH gave the best result because AC-TH is high ability of adsorption and decompose ozone to •OH.

ศูนย์วิทยทรัพยากร
จุฬาลงกรณ์มหาวิทยาลัย

4.6 Aqueous phenol removal in a pilot-scaled fluidized bed reactor

Based on laboratory-scaled experimental results, AC-TH and 5%CAT-TH-B-200 with ozone was selected to employ in the pilot-scaled three-phase fluidized bed reactor for remove aqueous phenol. The experimental condition for a pilot-scaled three-phase fluidized bed reactor is shown in **Table 4.21**. The performance of phenol and TOC removal efficiency in the pilot-scaled fluidized bed reactor shows in this section.

Table 4.21 Experimental condition of a pilot-scaled three-phase fluidized bed reactor

Parameter	Value
Initial concentration of phenol (ppm)	20
Aqueous phenol volume (L)	200
Liquid recirculation flow rate (L/min)	8
Gas flow rate (L/min)	5
Catalyst weight (g)	1,300
Temperature (°C)	30-35

4.6.1 Ozonation combined with activated carbons in pilot-scaled

The removal of phenol from the initial concentration of 20 ppm by treatment with pilot-scaled fluidized bed reactor were studied. The activities of ozonation and ozonation combined with activated carbons were presented in **Figure 4.16** and **4.17**.

From **Figure 4.21**, phenol was oxidized by ozone and its concentration decreased respect to time. At first 10 minnutes, the efficiency of phenol removal by only ozonation was 9%. In contrast, the corresponding decomposition efficiency of ozonation combined with AC-TH and 5%CAT-TH-B-200 were 73% and 63%, respectively. At 120 mintues, ozonation combined with AC-TH and 5%CAT-TH-B-200 were completely phenol removed. In contrast, removal efficiency of ozonation was 51%. Finally, removal efficiency of ozonation was 97% at 360 minutes.

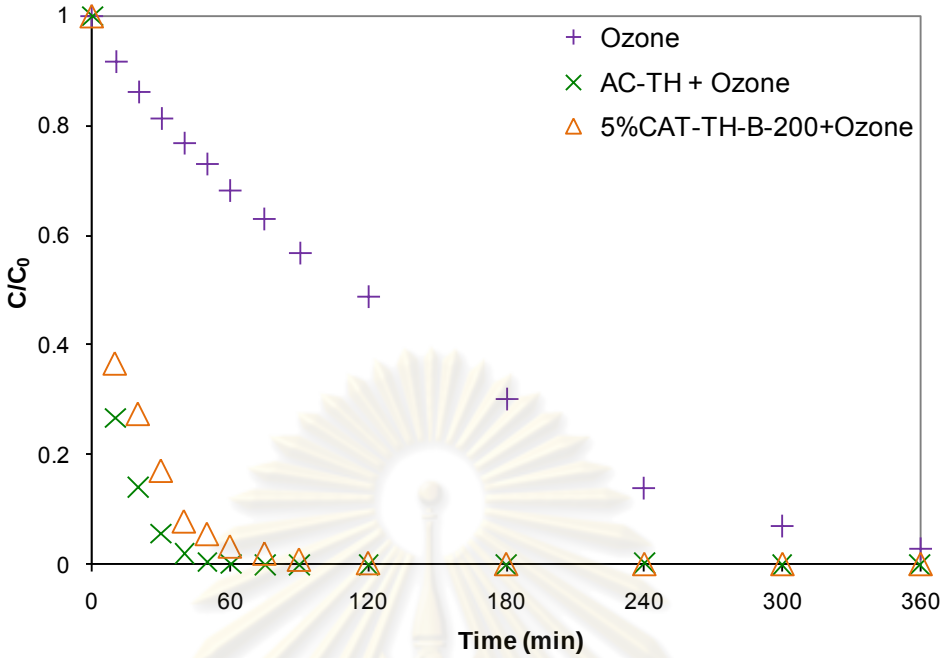

Figure 4.16 Phenol concentrations as a function of time for oxidation with only ozone and ozone combined with solid particle in pilot-scaled

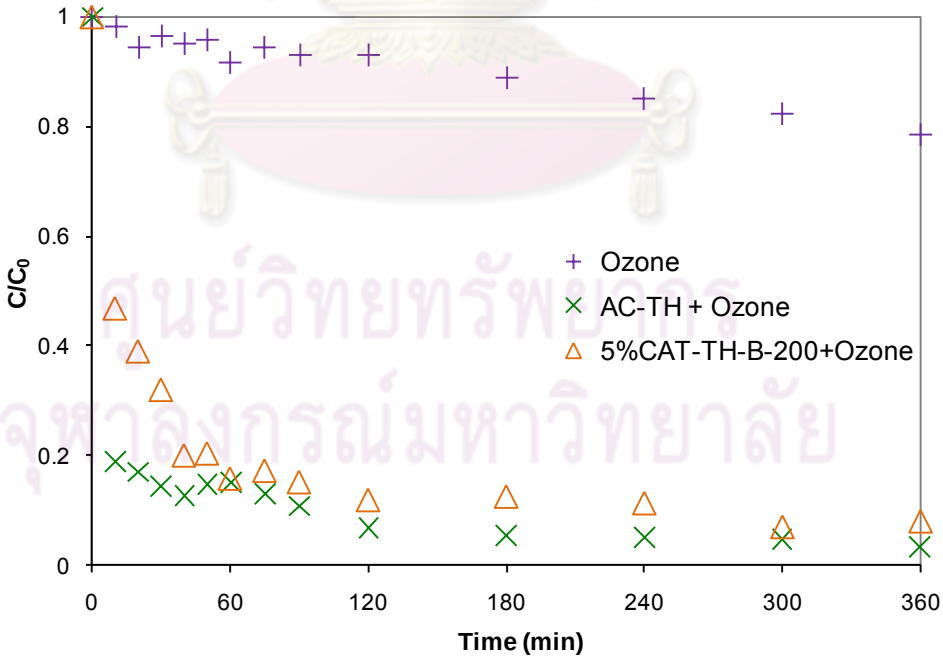

Figure 4.17 TOCs as a function of time for oxidation with only ozone and ozone combined with solid particle in pilot-scaled

Table 4.22 Phenol decomposition efficiency and TOC removal efficiency in pilot-scaled fluidized bed reactor

Time (min)	Phenol decomposition (%)			TOC decomposition (%)		
	Ozone	Ozone + AC-TH	Ozone + 5%CAT-TH-B-200	Ozone	Ozone + AC-TH	Ozone + 5%CAT-TH-B-200
10	9	73	63	2	81	53
50	27	100	95	4	85	80
120	51	100	100	8	93	88
360	97	100	100	22	97	92

TOC removal efficiency shows in **Figure 4.17**. At 10 min, case of ozonation and case of ozonation combined with AC-TH and 5%CAT-TH-B-200 exhibit efficiency of 2%, 81% and 53%, respectively. Finally at 360 min, decomposition efficiency of ozonation and ozonation combined with AC-TH and 5%CAT-TH-B-200 exhibit efficiency of 22%, 97% and 92%. Compare the TOC removal by using only ozone between **Figure 4.15** from laboratory-scaled and **Figure 4.17** from pilot-scaled it can be seen that the figure present the same results. Ozonation could decompose phenol to intermediate but long time for decompose intermediate to carbon dioxide. Virgin activated carbon and activated carbon doped with iron oxide could enhance oxidizing intermediate to carbon dioxide.

In case of ozonation combined with 5%CAT-TH-B-200 test remove aqueous phenol in pilot-scaled three-phase fluidized bed reactor; phenol could be removed from 20 ppm to complete and TOC removal efficiency over of 80% at 120 minutes. Since the total volume of recirculated solution around 200 L, that means this an once through system operated continuously under equivalent conditions should be able to treat the aqueous phenol wastewater satisfactory at 1.25 L/min. In corresponding, case of ozonation combined with AC-TH at 50 minutes this system could completely removed phenol and 93% of TOC removal efficiency that means this an once through system operated continuously under equivalent conditions should be able to treat the wastewater satisfactory at around 4 L/min.

4.6.2 Deactivation of activated carbon doped with iron oxide

The useful life of activated carbon doped with iron oxide is a critical criterion for the commercialization of the present fluidized bed reactor technology, as the cost of the activated carbon doped with iron oxide is an essential factor contributing to the operating costs of the system. The activated carbon doped with iron oxide which have been used until now undergo serious activity losses and deactivations due to the strong oxidation conditions of the processes used. 5%CAT-TH-B-200 was used and enhancing with ozone, the removal efficiency of phenol and TOC gradually decreased proportional to increase of iteration. The removal of phenol from the initial concentration of 20 ppm by treatment with pilot-scaled fluidized bed reactor were studied. The activities of fresh and reused 5%CAT-TH-B-200 enhancing with ozone were presented in **Figure 4.18** and **4.19**.

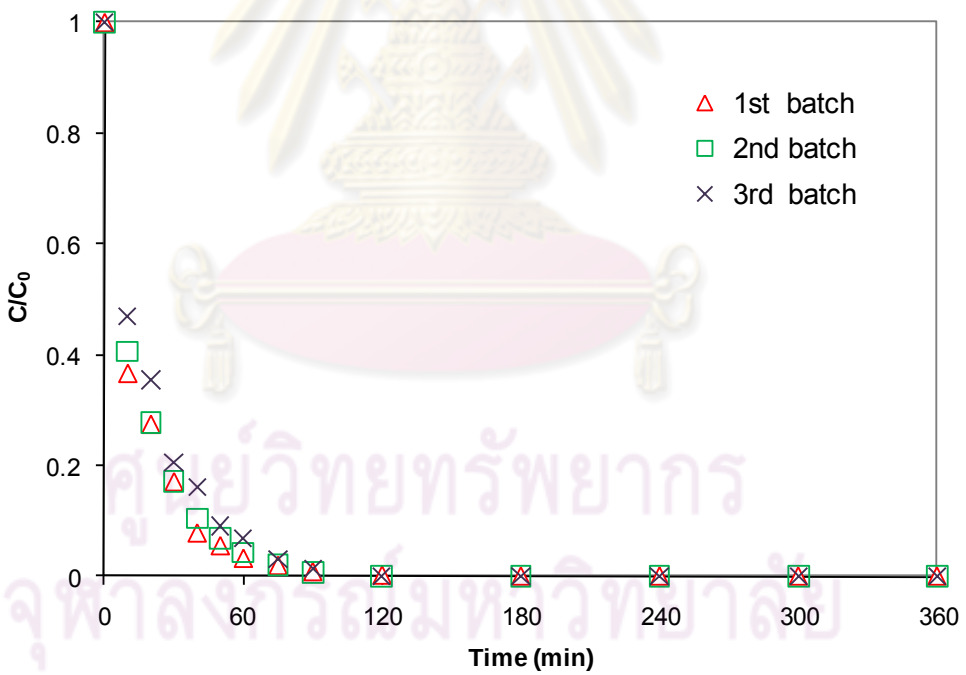

Figure 4.18 Phenol concentrations as a function of time for oxidation with 5%CAT-TH-B-200 after repeated use in three consecutive runs

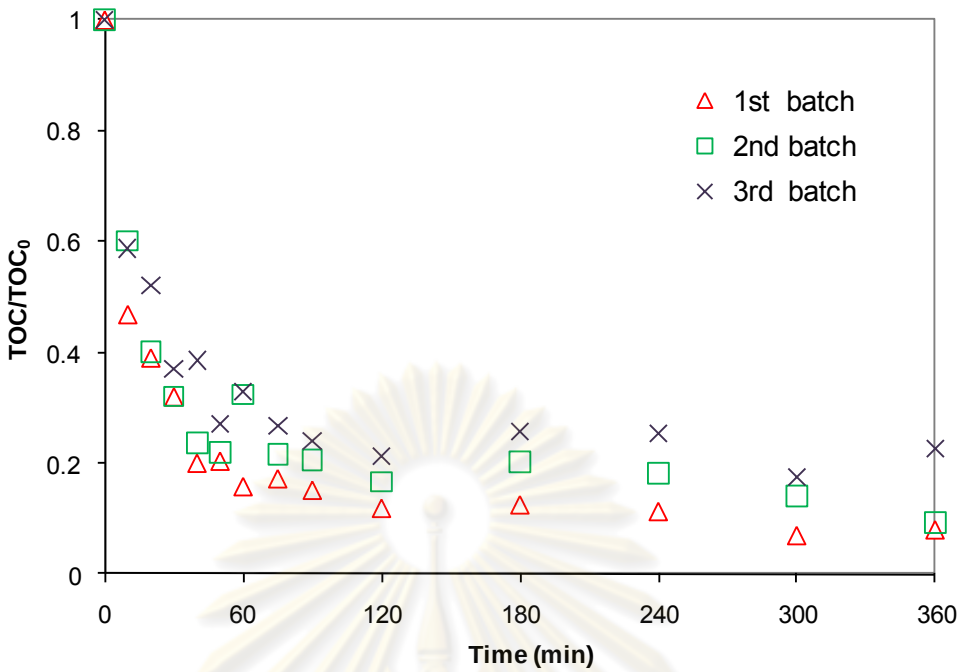

Figure 4.19 TOCs as a function of time for oxidation with 5%CAT-TH-B-200 after repeated use in three consecutive runs

Table 4.23 Phenol decomposition efficiency and TOC removal efficiency for 5%CAT-TH-B-200 after repeated use in three consecutive runs

Time (min)	Phenol decomposition (%)			TOC decomposition (%)		
	1st batch	2nd batch	3rd batch	1st batch	2nd batch	3rd batch
10	63	59	53	53	40	41
60	97	96	93	84	68	67
120	100	100	100	88	83	79
360	100	100	100	92	91	77

To investigate the deactivation of 5%CAT-TH-B-200, the experiments were performed using 5%CAT-TH-B-200 on pilot-scaled three-phase fluidized bed reactor for three consecutive batches (360 minutes per each batch). When the experiment was repeated for three batches without changing the bed particles, the efficiency tended to decrease as shown in **Figure 4.18** and **4.19**. In case of 1st batch, ozonation combined with fresh 5%CAT-TH-B-200, phenol and TOC were rapidly removed and

concentrations decreased respect to time. At 360 min, phenol completely removed and 92% of TOC removal efficiency. In case 2nd batch, ozonation combined with 1st reused of 5%CAT-TH-B-200, phenol and TOC were fairly removed. At 360 min, phenol completely removed and 91% of TOC removal efficiency. Finally in case 3rd batch, ozonation combined with 2nd reused of 5%CAT-TH-B-200, phenol and TOC were slowly removed. At 360 min, phenol completely removed and 77% of TOC removal efficiency. The results suggested that the 5%CAT-TH-B-200 suffered deactivation in three-phase fluidized bed reactor. The cause of 5%CAT-TH-B-200 suffer deactivation during the oxidation process is by the leaching of the metal cation. It has been proved that the dissolved metal from the catalyst produces an important reaction extension in the liquid phase changing the heterogeneous catalysis into homogeneous and increases significantly the toxicity of the reactor effluent **[37]**.

5%CAT-TH-B-200 shows stability after repeated use in three consecutive runs (1,080 minutes), phenol could be completely removed in first 120 minutes. 5%CAT-TH-B-200 shows high efficiency of the useful life of re-used for 18 hours.

ศูนย์วิทยทรัพยากร
จุฬาลงกรณ์มหาวิทยาลัย

CHAPTER V

CONCLUSIONS AND RECOMMENDATIONS

Based on all experimental data which were explained and discussion in previous chapter conclusions and recommendations for future study are presented in this chapter.

5.1 Conclusions

The conclusions of this research are could be arranged in four issues as follows,

a) Specific surface area of activated carbon doped with Fe by impregnation would be deceased when compared with of virgin activated carbon. Impregnation techniques show stability of Fe content on activated carbon. However, amount of Fe content on activated carbon also affected to the phenol removal performance. 5%CAT-TH-B-500 exhibited higher removal efficiency than 10%CAT-TH-B-500.

b) The calcination condition affected to the type of Fe on activated carbon. At 500 °C under nitrogen gas flow. Fe_3O_4 appeared on activated carbon surface. In contrast, at 200 °C under ambient atmosphere. Fe_2O_3 occurred on activated carbon surface. At 500 °C under nitrogen gas flow, organic nitrate was removed faster than at the condition of 200 °C under ambient atmosphere. Fe_2O_3 on activated carbon can remove other intermediate products better than Fe_3O_4.

c) Ozontion combined with activated carbons can remove phenol intermediate products better than using only ozonation. And ozontion combined with virgin activated carbons gave the best result for remove aqueous phenol and TOC.

d) The removal efficiency of phenol tended to decrease with an increase of using iteration. 5%CAT-TH-B-200 particle shows stability after repeated use in three consecutive runs (1,080 minutes) in pilot-scaled system. Activated carbon doped with iron oxide shows high efficiency of the useful life of particle for 18 hours.

5.2 Recommendations for future studies

From the previous conclusions, the following recommendations for future studies are proposed.

- There are some fine powders detaching from the activated carbon support after testing for a certain period of time, therefore the stability of these particle stability should be improved.

- For applying these particles to this wastewater treatment system, an effective regeneration method of the particles is an interesting issue that should be further investigated.

- The scaling up is necessary for actual application of this process. From the results conducted in laboratory and pilot-scale, the best performing particle and suitable condition for degrading phenol should be used in the future work.

- A detailed economic analysis of metallic catalysts should be considered carefully. It could be conducted based upon the cost of raw materials, cost of catalyst preparation, cost of the metallic catalysts life cycle and the cost of generated ozone.

REFERENCES

[1] ScienceLab.com. Phenol MSDS. Material Safety Data Sheet[Online]. 2008. Available from: http://www.sciencelab.com/msds.php?msdsId=9926463 [2008, May 23]

[2] Massa, P., et al. Catalytic wet air oxidation of phenol aqueous solutions by 1% Ru/CeO_2-Al_2O_3 catalysts prepared by different methods. Catalysis Communications 8 (2007): 424-428.

[3] Quintanilla, A., et al. Wet air oxidation of phenol at mild conditions with a Fe/activated carbon catalyst. Applied Catalysis B: Environmental 62 (2006): 115-120.

[4] Charinpanitkul, T., et al. Synergetic removal of aqueous phenol by ozone and activated carbon within three-phase fluidized-bed reactor. Journal of Industrial and Engineering Chemistry 16 (2010): 91-95.

[5] Mungmart, M., et. al. Investigation and Comparison of catalytic decomposition rates of aqueous phenol in three-phase fluidized bed reactor. In, Regional Symposium on Chemical Engineering, Singapore: Nanyang Technological University, 2006.

[6] Bach, A.,G. Zelmanov, and R. Semiat. Cold catalytic recovery of loaded activated carbon using iron oxide-based nanoparticles. Water Research 42 (2008): 163-168.

[7] Thongprachan, N. A novel rotary drum filtering reactor for photocatalytic decomposition of phenol in slurry containing titanium dioxide nanparticles. Master's Thesis, Department of Chemical Engineering, Faculty of Engineering, Chulalongkorn University, 2005.

[8] Sittipraneed, S., Hydrothermal preparation and characterization of activated carbon from anthracite powder. Master's Thesis, Department of Chemical Engineering, Faculty of Engineering, Chulalongkorn University, 2003.

[9] Regalbuto, J. Catalyst preparation: Science and Engineering. New York: CRC Press, 2007.

[10] Mungmart, M., Investigation and Comparison of catalytic decomposition rates of Aque phenol in three-phase fluidized bed reactor. Master's Thesis, Department of Chemical Engineering, Faculty of Engineering, Chulalongkorn University, 2006.

[11] Kanki, T., et al. Water purification in a fluidized bed photocatalytic reactor using TiO_2-coated ceramic particles. Chemical Engineering Journal 108 (2005): 155-160.

[12] McCabe, W.L.,J.C. Smith, and P. Harriott. Unit Operations of Chemical Engineering. 7th ed. Singapore: McGraw-Hill, 2005.

[13] Wu, J.,K. Rudy, and J. Spark. Oxidation of aqueous phenol by ozone and peroxidase. Advances in Environmental Research 4 (2000): 339-346.

[14] Santos, A., et al. Catalytic wet oxidation of phenol on active carbon: stability, phenol conversion and mineralization. Catalysis Today 102-103 (2005): 213-218.

[15] Dong, Y., et al. Catalytic activity and stability of Y zeolite for phenol degradation in the presence of ozone. Applied Catalysis B: Environmental 82 (2008): 163-168.

[16] Pintar, A.,G. Bercic, and J. Levec. Catalytic liquid-phase oxidation of aqueous phenol solutions in a trickle-bed reactor. Chemical Engineering Science 52 (1997): 4143-4153.

[17] Santos, A., et al. Route of the catalytic oxidation of phenol in aqueous phase. Applied Catalysis B: Environmental 39 (2002): 97-113.

[18] Esplugas, S., et al. Comparison of different advanced oxidation processes for phenol degradation. Water Research 36 (2002): 1034-1042.

[19] Quintanilla, A., et al. Phenol oxidation by a sequential CWPO-CWAO treatment with a Fe/AC catalyst. Journal of Hazardous Materials 146 (2007): 582-588.

[20] Allia, K., et al. Biological treatment of water contaminated by hydrocarbons in three-phase gas-liquid-solid fluidized bed. Global NEST Journal 8 (2006): 9-15.

[21] Klaysom, C., Preparation, Characterization and continuous process design of activated carbon from waste tires. Master's Thesis, Department of Chemical Engineering, Faculty of Engineering, Chulalongkorn University, 2004.

[22] Limsuwan, P., Preparation of Fe catalyst coated on activated carbon for decomposition of aqueous phenol in three-phase fluidized bed reactor. Master's Thesis, Department of Chemical Engineering, Faculty of Engineering, Chulalongkorn University, 2008.

[23] Turhan, K. and S. Uzman. Removal of phenol from water using ozone. Desalination 229 (2008): 257-263.

[24] Lemine, O.M. Microstructural characterisation of nanoparticles using, XRD line profiles analysis, FE-SEM and FT-IR. Superlattices and Microstructures 45 (2009): 576-582.

[25] ScienceLab.com. Ferric nitrate nonahydrate MSDS. Material Safety Data Sheet[Online]. 2008. Available from: http://www.sciencelab.com/msds.php ?msdsId=9924040 [2008, Jan 21]

[26] Yang, R.T. Adsorbents: Fundamentals and Applications. New York: John Wiley & Sons, 2003.

[27] Anuwetch, L.,S. Inkum, and S. Mopoung. Production of Activated Carbon from Sugarcane Leave. NU Science Journal 5 (2008): 210-220.

[28] Shimada, H., et al. Dehydrogenation of isobutane to isobutene with iron-loaded activated carbon catalyst. Applied Catalysis A: General 168 (1998): 243-250.

[29] Zhang, X., et al. Influence of precipitator agents NaOH and NH_4OH on the preparation of Fe_3O_4 nano-particles synthesized by electron beam irradiation. Journal of Radioanalytical and Nuclear Chemistry 270 (2006): 285-289.

[30] Quintanilla, A.,J.A. Casas, and J.J. Rodriguez. Catalytic wet air oxidation of phenol with modified activated carbons and Fe/activated carbon catalysts. Applied Catalysis B: Environmental 76 (2007): 135-145.

[31] Wikipedia.com. Activated carbon. Wikipedia, the free encyclopedia[Online]. 2008. Available from: http://en.wikipedia.org/wiki/Activated_carbon [2008, Jan 25]

[32] Tan, I.A.W.,A.L. Ahmad, and B.H. Hameed. Adsorption of basic dye on high-surface-area activated carbon prepared from coconut husk: Equilibrium, kinetic and thermodynamic studies. Journal of Hazardous Materials 154 (2008): 337-346.

[33] Amin, N.A.S.,H.K.M. Singh, and M. Rashid. Remove of phenol and COD via catalytic treatment using activated carbon and alumina with ozone. Journal of Industrial Technology. 14 (2005): 175-182.

[34] Hegedus, L.L. Catalyst design. New York: John Wiley & Sons, 1987.

[35] Zhong, L.,W. Ren, and W. Guo. A pilot scale test of ozonation treatment of ethene wastewater for reuse. Front. Chem. Eng China 2 (2008): 191-195.

[36] Legube, B. and N. Karpel Vel Leitner. Catalytic ozonation: a promising advanced oxidation technology for water treatment. Catalysis Today 53 (1999): 61-72.

[37] Arena, F., et al. Activity and resistance to leaching of Cu-based catalysts in the wet oxidation of phenol. Applied Catalysis B: Environmental 45 (2003): 51-62.

ศูนย์วิทยทรัพยากร
จุฬาลงกรณ์มหาวิทยาลัย

APPENDICES

ศูนย์วิทยทรัพยากร
จุฬาลงกรณ์มหาวิทยาลัย

APPENDIX A

Proceedings

1. S. Chaeysiri, T. Charinpanitkul, P. Limsuwan, A. Sootitantawat, P. Tongprem , P. Wongsarivej and W. Tanthapanichakoonl, "Preparation of Fe Catalyst supported on Activated Carbon for Phenol Decomposition", *1st biannual NanoThailand Symposium 2008 (NTS 2008)*, 6-8 November 2008, Queen Sirikit National Convention Center, Bangkok, Thailand.

2. P. Limsuwan, S. Chaeysiri, N. Sano, T. Yamamoto, P. Wongsarivej, P. Tongpram, A. Soottitantawat, W. Tanthapanichakoon, and T. Charinpanitkul, "Removal of Aqueous Phenol in a Three-phase Fluidized Bed Reactor using Activated Carbon and/or Ozone", *1st Asian Conference on Inovative Energy & Environmental Chemical Engineering - A New Paradigm Emerging form Fluidized-Bed and Three-Phase Reactors (ASCON-IEEChE)*, 31st August - 3rd September, 2008, Sapporo, Japan.

3. P. Tongprem, P. Wongsarivej, P. Limsuwan, S. Cheaysiri, A. Sootitantawat and T. Charinpanitkul, "Oxidation of Phenol by a Laboratory Scale Three-Phase Fluidized Bed Reactor with a Fe on Activated Carbon Catalyst and/or Ozone", *The 2nd Thailand Nanotechnology Conference 2008 (TNC)*, Nanomaterials for Health, Energy and Environment, August 13-15, 2008, Phuket, Thailand.

4. P. Wongsarivej, P. Tongprem, S. Cheaysiri, P. Limsuwan, A. Sootitantawat, T. Charinpanitkul and W. Tanthapanichakoon, "Investigation of Catalytic Decomposition of Phenol in Pilot Scale Three-phase Fluidized Bed Reactor using Fe on Activated Carbon Support", *1st Asian Conference on Inovative Energy & Environmental Chemical Engineering - A New Paradigm Emerging form Fluidized-Bed and Three-Phase Reactors (ASCON-IEEChE)*, 31st August - 3rd September, 2008, Sapporo, Japan.

NanoThailand Symposium 2008
International Conference & Exhibition
NTS 2008
Come Together for a Brighter Future
NanoThailand
Symposium 2008
November 6-8, 2008
Queen Sirikit National Convention Center
Bangkok, Thailand

PREPARATON OF Fe CATALYST SUPPORTED ON ACTIVATED CARBON FOR PHENOL DECOMPOSITION

S. Chaeysiri[1], T. Charinpanitkul[1]*, P. Limsuwan[1], A. Sootitantawat[1], P. Tongprem[2], P. Wongsarivej[2] and W. Tanthapanichakoonl[1]

[1]Center of Excellence in Particle Technology, Faculty of Engineering, Chulalongkorn University,Bangkok, THAILAND
[2]National Nanotechnology Center (NANOTEC), National Science and Technology Development Agency, Patumtani, THAILAND

**Corresponding author: Tel & Fax: +66-2218-6899,*
E-mail: ctawat@chula.ac.th

KEYWORDS: Phenol, Activated Carbon, Fe catalyst, Impregnation, Three-phase fluidized bed reactor

I. INTRODUCTION

Industrial wastewater becomes one of the greatest problems in various countries, because it has exerted environmental and health threats to the society. Phenol is one of the most harmful aromatic hydrocarbon compounds existing in wastewater emitted from various chemical industries. It is known or suspected to be carcinogens as well as its high toxicity and high stability [1]. It can damage the skin and other tissues of the human and animals. When digested, phenol-containing liquids could also lead to liver damages, dark urine, irregular heart beats, muscle tremors and loss of spatial coordination, among others. Therefore, the treatment of phenolic pollutants is an important issue in environmental protection.

Phenol can be decomposed by many methods, such as the conventional energy-intensive combustion. Though decomposition of phenolic compounds by wet air oxidation using metallic catalysts and oxidizing agents have been investigated [1-4], there are some insufficient issues for further improvement. A three-phase fluidized bed reactor is an effective system for phenol oxidation. It readily provides intimate contact between the gas, liquid and solid phases. It fluidizes the activated carbon particles to decompose aqueous phenol and exploits ozone gas as oxidizing agent for cost-effective wastewater treatment [4].

Activated carbon (AC) could be widely used as adsorptive material to remove numerous organic compounds from wastewater because of its large specific surface area, highly porous structure and low cost [5]. Catalyst supported on AC is a promising alternative because of the synergy of huge number of active sites and the concentration of the adsorbed species on the internal surface area. In this research, AC-supported with Fe is aimed to maximize the oxidation efficiency.

II. EXPERIMENTAL

CATALYST PREPARATION

Two different granulated activated carbons were supplied from two sources (USA (AC-US) and in Thailand (AC-TH)). The AC-US activated carbon was made from coal and the AC-TH was made from coconut shell. Both ACs were sieved for classifying a specific size range of 0.42-2.00 mm. The Fe catalyst supported on activated carbon was prepared following either the wet impregnation or the incipient wetness impregnation techniques.

The classified particles were heated and held at 473 K for 4 hrs to eliminate their impurities, then impregnated with a solution of $Fe(NO_3)_3 \bullet 9H_2O$ to yield 5 %w/w of Fe. The metal catalyst, Fe, was loaded by two methods: Wet Impregnation (IMA) and incipient wetness impregnation (IMB). For the IMA method, one gram of AC was mixed with 10 ml of metal solution in a vacuum evaporator at 333 K until the aqueous phase could no longer be observed. On the other hand, in the IMB method 0.5 ml metal solution per 1 g AC was stirred at 353 K. After impregnation, the samples were dried overnight at 353 K and subsequently calcined at 773 K under nitrogen atmosphere (N_2 gas flow rate of 0.8 LPM) for 5 hrs. The catalysts identified as CAT-TH-A-500 and CAT-TH-B-500 were prepared with AC-TH support by IMA and IMB method, respectively. The CAT-TH-B-200 samples were prepared on the

AC-TH support by IMB method to be similar to CAT-TH-B-500 but calcined at 473 K under ambient atmosphere for 5 hrs.

CHARACTERIZATION

Based on the Brunauer-Emmett-Teller (BET) adsorption method, the specific surface area and porosities of the catalytic supported and catalysts were detremined via N_2 adsorption-desorption isotherms measured at 77 K using an automated adsorption apparatus (BELSORP 28, BEL Japan Inc., Japan, or AUTOSORB-1-C, Quantachrome, USA). The MP method was employed for determining micropore volume and micropore size distribution from the t-plot. The morphological structures of the catalysts were further characterized by X-ray diffraction (XRD).

APPARATUS AND PROCEDURE

An experimental set-up for ozonation is developed and employed in this work. The experiment set-up consists of a lab-scaled three-phase fluidized bed reactor, hold-up tank, liquid pump, flow meter, ball valve, air pump and ozone generator. The schematic diagram is shown in Figure 1. The reactor with effective volume 272 ml is made from transparent acrylics that easily observe the phenomenon occurring inside. The outside diameter and height of reactor are 40 and 300 mm, respectively. An aqueous solution and gas were separately fed through a distributor into the fluidized catalyst bed at the bottom of reactor. Gas flow was exhausted from the top of reactor while an aqueous solution was totally circulated and intermittently sample via a hold-up tank. An aqueous phenol concentration 10 mg L^{-1} and volume 6 L in a hold-up tank was used as sample tested with Fe on activated carbon concentration 0.83 g_{cat} $L^{-1}{}_{phenol}$. Ozone gas was produce from air by passing through an ozone generator used as oxidizing agent. An aqueous phenol and ozone gas were continuously fed to the reactor with co-current and up-flow at constant flow rate 1 and 2 L min^{-1}, respectively. The solution temperature in a hold-up tank was constantly measured and controlled at 303 K by thermocouple and a cooler, respectively.

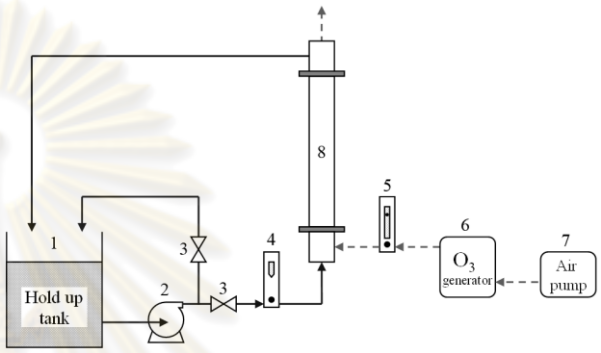

Fig. 1 Schematic diagram of experimental apparatus, 1. hold-up tank, 2. liquid pump, 3. ball valve, 4. liquid flow meter, 5. air flow meter, 6. ozone generator, 7. air pump, 8. three-phase fluidized bed reactor.

CHEMICAL ANALYSIS

The progress of the reaction was followed by taking periodically liquid samples from the reactor and immediately analyzed after filtration through 0.45 µm nylon filter. Phenol was identified and quantified by a high performance liquid chromatography (HPLC, Shimadzu, LC-20A Series) with a diode array detector at wavelengths of 210 and 254 nm. The 5 µm column of C18 column (Inertsil ODS-3, 25 cm long, 4.6 mm diameter) was used as stationary phase. The mixture of 4 mM aqueous sulfuric solution and 25% v/v aqueous acetonitrile solution was used as mobile phase at 1 mL min^{-1}. The total organic carbon (TOC) concentration was analyzed by a total organic carbon analyzer (Shimadzu, TOC-VCPH).

III. RESULTS AND DISCUSSION

Three cases to investigate for select appropriate catalyst on the efficiency of a novel element for wet air oxidation process, the experimental can classified as follows:

a. Comparison between AC-US and AC-TH for used as support.
b. Comparison between IMA and IMB technique for Fe on activated carbon preparation.
c. Comparison between two different calcination condition.

PERFORMANCE OF ACTIVATED CARBON

As illustrated in Figure 2, the N_2 adsorption-desorption isotherms of two different type of commercial granulated activated carbons were AC-US and AC-TH. Based on the shape of isotherm by International Union of Pure and Applied Chemistry (IUPAC) classification, both ACs exhibit Type I isotherm which indicated a huge quantity of microporsity. They had the little hysteresis loop which represents a small quantity of mesoporsity. The hysteresis loop of AC-US was more obvious than that

of AC-TH. Thus it is reasonable to imply that AC-US contains more mesopore than AC-TH. The micropore volume and micropore size distribution measured by MP-Plot method were also shown in Figure 3. The modal peak of micropore size of AC-US and AC-TH were 0.8 and 0.6 nm, respectively.

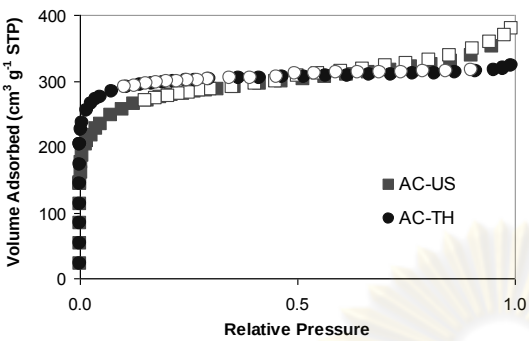

Fig. 2 N_2 adsorption-desorption isotherm on AC-US and AC-TH.

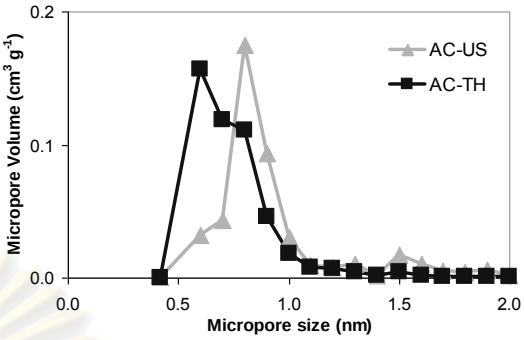

Fig. 3 Micropore size distribution of AC-US and AC-TH.

The specific surface area and porosity of the ACs were shown in Table 1. The surface area of AC with metallic catalyst was decreased after metal loading. However, it had slightly higher BET area than AC-US of 9 % but lower cost than AC-US. In comparison with the original AC, the decrease in surface area of 5 to 8 % loading is dependent upon the method for preparation catalyst from virgin AC-TH. It should be noted that the porosity of the obtained catalyst-loaded AC was insignificantly affected by the impregnation method.

Table 1 The porous characteristics of virgin AC supports and Fe catalyst

Sample	BET surface area (m^2 g^{-1})	Pore size	Total pore volume (cm^3 g^{-1})	Average pore diameter (nm)	Micropore volume (cm^3 g^{-1})	Modal micropore diameter (nm)
AC-US	1060	micropore	0.61	2.3	0.46	0.8
AC-TH	1154	micropore	0.49	1.7	0.49	0.6
CAT-TH-A-500	1088	micropore	0.47	1.7	0.47	0.6
CAT-TH-B-500	1081	micropore	0.46	1.7	0.46	0.7
CAT-TH-B-200	1067	micropore	0.47	1.8	0.47	0.7

PHENOL DECOMPOSITION BY DIFFERENT METHOD FOR CATALYST PEPARATION

Figure 4 shows normalized phenol concentrations as function of time for oxidative decomposition in the three-phase fluidized bed reactor with ozone and two different types of catalyst. In the both cases, CAT-TH-A-500 and CAT-TH-B-500 can decompose phenol in aqueous solution to some intermediate products. Time dependence of intermediate TOC which were derived from phenol is depicted in Figure 5. At 75 min, the phenol and TOC decomposition efficiencies of CAT-TH-A-500 were 100% and 63%, respectively. In contrast, the corresponding decomposition efficiencies of CAT-TH-B-500 were 100% and 49%, respectively. In both cases of oxidative decomposition, TOC still remain because some intermediate products were hard to decompose. CAT-TH-A-500 yield phenol and TOC decomposition with the same level of CAT-TH-B-500. It exhibited slightly higher efficiency than AC-TH-B-500. This would be attributed to the fact that CAT-TH-B-500 prepared by IMB method would provide lower loss of the Fe during the processing. It should be noted that in view of ease of preparation and energy saving, the IMB technique showed higher application potential at the industrial scale as well as less loss of the Fe metal during the processing.

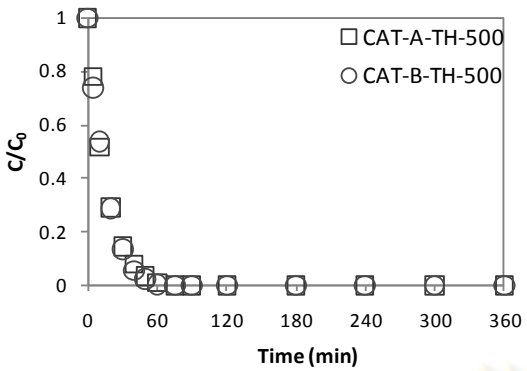

Fig. 4 Phenol concentrations as a function of time for oxidation with CAT-TH-A-500 and CAT-TH-B-500

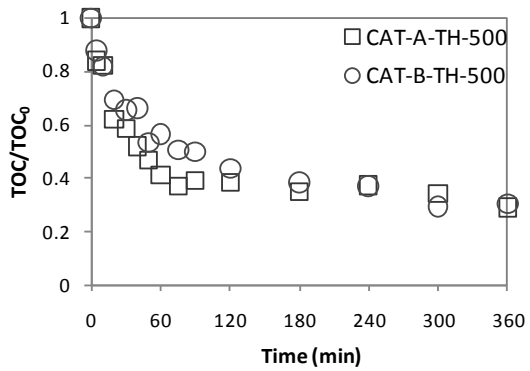

Fig. 5 TOCs as a function of time for oxidation with CAT-TH-A-500 and CAT-TH-B-500

PHENOL DECOMPOSITION BY DIFFERENT CALCINATION CONDITION TEMPERATURE

The efficiency of phenolic decomposition was investigated based on different calcinations temperature. Figures 6 and 7 show change residual phenol and TOC concentrations as a function of time, respectively.

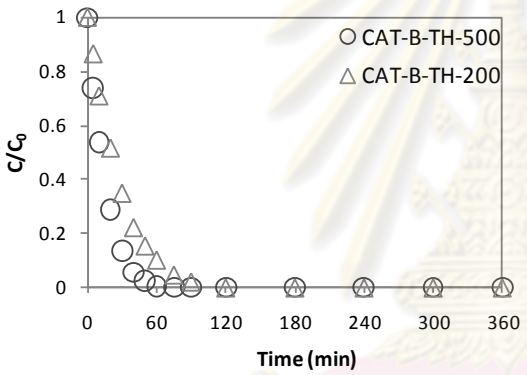

Fig. 6 Phenol concentrations as a function of time for oxidation with CAT-TH-B-500 and CAT-TH-B-200

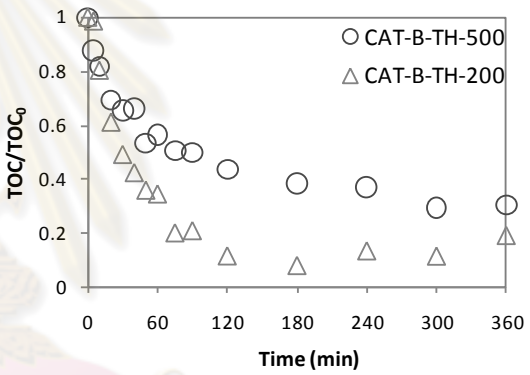

Fig. 7 TOCs as a function of time for oxidation with CAT-TH-B-500 and CAT-TH-B-200

For comparison, CAT-TH-B-200 samples were prepared on the AC-TH support by IMB method similar to CAT-TH-B-500 but with different calcinations temperature. Based on the experimental results, the rates of reduction in phenol concentrations of CAT-TH-B-500 were faster than CAT-TH-B-200. In contrast, the rates of reduction in TOC concentrations of CAT-TH-B-500 were slower than CAT-TH-B-200. It could be clearly observed that both CAT-TH-B can completely decompose phenol within 120 min. The phenol decomposition efficiencies of CAT-TH-B-200 were 100% and 88%, respectively. As shown in Table 1, the possession of CAT-TH-B-500 of larger specific surface area than CAT-TH-B-200. Higher quantity of active site for surface reaction would be the main attribution of these catalysts. However, the higher TOC decomposition of CAT-TH-B-200 in Figure 7 may be attributed to types of Fe catalyst after calcination at different temperature. The Fe catalyst on the CAT-TH-B-200 surface was found as Fe_2O_3 [2] but the CAT-TH-B-500 catalyst was found Fe_3O_4. Therefore, Fe_2O_3 on the CAT-TH-B-200 catalyst can remove other intermediate products better than Fe_3O_4 on the CAT-TH-B-500 catalyst. It should also be noted that the CAT-TH-B-200 catalyst could be prepared at a cost lower than that of CAT-TH-B-500 catalyst. Therefore, it would be more promising for preparation of catalyst in bulk for actual application in industrial scale.

IV. CONCLUSION

The oxidative decomposition of phenol in aqueous solution has been conducted in the three-phase fluidized bed reactor with ozone and activated carbon impregnated with Fe. The conclusions obtained from this investigation are as follows:

a. The commercial activated carbon prepared from coconut shell was more physically suitable as catalyst support which could provide better phenol removal.
b. It was also found that the impregnation method could provide insignificant difference in phenol decomposition. However, the incipient wetness impregnation method was more appropriate for preparing Fe/AC in bulk because of its simplicity.
c. Fe_2O_3 on commercial activated carbon after calcined at 473 K under ambient air atmosphere for 5 hrs was found to provide effective oxidative decomposition of intermediate from phenol.

ACKNOWLEDGEMENTS

This work has received financial support from NANOTEC, NSTDA. Commercial activated carbon was provided by Carbokarn Co.,Ltd. (Thailand). Partial support from Chulalongkorn University to Center of Excellence in Particle Technology is also acknowledged.

REFERENCES

[1] Zazo, J.A., Casas, J.A., Mohedano, A.F. and Rodríguez, J.J. 2006. Catalytic wet peroxide oxidation of phenol with a Fe/active carbon catalyst. Applied Catalysis B: Environmental, 65, 261-268.
[2] Quintanilla, A., Casas, J.A., Zazo, J.A., Mohedano, A.F., Rodríguez, J.J. 2006. Wet air oxidation of phenol at mild conditions with a Fe/activated carbon catalyst. Applied Catalysis B: Environmental, 62, 115-120.
[3] Massa, P., Ivorra, F., Haure, P., Cabello, M., F., Fenoglio. R. 2007. Catalytic wet air oxidation of phenol aqueous solutions by 1% $Ru/CeO_2–Al_2O_3$ catalysts prepared by different methods. Catalysis Communications, 8, 424-428.
[4] Mungmart, M., Charinpanitkul, T., Yamamoto, T., Tanthapanichakoon, W. 2006. Investigation and Comparison of catalytic decomposition rates of aqueous phenol in three-phase fluidized bed reactor. Regional Symposium on Chemical Engineering, Nanyang Technological University, Singapore, December 3-5, 2006
[5] Bach, A., Zelmanov, G., Semiat, R. 2008. Cold catalytic recovery of loaded activated carbon using iron oxide-based nanoparticles. Water Research, 42, 163-168.

ศูนย์วิทยทรัพยากร
จุฬาลงกรณ์มหาวิทยาลัย

APPENDIX B

CALCULATION OF HYDRODYNAMICS

In chapter II, hydrodynamic parameters of three-phase fluidized bed reactor was determined and summarized. According to the relations in chapter II, minimum fluidization velocity was preliminary calculated by using the physical properties of substances involving in this work. These properties and results from calculation are shown in below table.

Table B.1 Hydrodynamics data of lab-scaled experiment
Lab-scale

Properties	symbol	Value	SI unit	Remark
Density of liquid	ρ_L	1000	kg/m^3	
Viscousity of liquid	μ_L	0.001	kg/m.s	
Density of wet particle	ρ_S	1330	kg/m^3	
Diameter of particle	d_p	0.0012	m	
Density of ozone	ρ_G	2.14	kg/m^3	
Gravitional acceleration	g	9.81	m/s	
Flow rate of gas	F_G	0.000033	m^3/s	2 L/min
Flow rate of liquid	F_L	0.000017	m^3/s	1 L/min
Diameter of reactor	D_R	0.0316	m	
Cross section area of reactor	A_R	0.000785	m^2	

Calculation	symbol	Value	SI unit
Superficial gas velocity	U_G	0.021243	m/s
Superficial liquid velocity	U_L	0.042485	m/s
Archimedes number	Ar	5594	-
Minimum fluidization velocity of liquid	$U_{mf,LS}$	0.00269	m/s
Minimum fluidization velocity	U_{mf}	0.00115	m/s

Table B.2 Hydrodynamics data of pilot-scaled experiment
Pilot-scale

Properties	symbol	Value	SI unit	Remark
Density of liquid	r_L	1000	kg/m^3	
Viscousity of liquid	m_L	0.001	kg/m.s	
Density of wet particle	r_S	1330	kg/m^3	
Diameter of particle	d_p	0.0012	m	
Density of ozone	r_G	1.2	kg/m^3	
Gravitional acceleration	g	9.8	m/s	
Flow rate of gas	F_G	0.000067	m^3/s	5 L/min
Flow rate of liquid	F_L	0.000117	m^3/s	8 L/min
Diameter of reactor	D_R	0.2	m	
Cross section area of reactor	A_R	0.031400	m^2	

Calculation	symbol	Value	SI unit
Superficial gas velocity	U_G	0.00212	m/s
Superficial liquid velocity	U_L	0.00470	m/s
Archimedes number	Ar	5594	-
Minimum fluidization velocity of liquid	$U_{mf,LS}$	0.00269	m/s
Minimum fluidization velocity	U_{mf}	0.00205	m/s

APPENDIX C

RATE CONSTANT

In this appendix, the efficiency for decomposing of 6 L of 10 ppm phenol solution with activated carbon doped with iron oxide loading 5 g was revealed in term of $-ln(C/C_0)$ to express the rate constant (k). The disappearance of phenol followed pseudo first order kinetics. Initial rate constants were determined from the slope of $-ln(C/C_0)$ vs t (min) plots (**Figure C.1** and **Table C.1**.), where C_0 and C are the phenol concentration at zero time and time t, respectively.

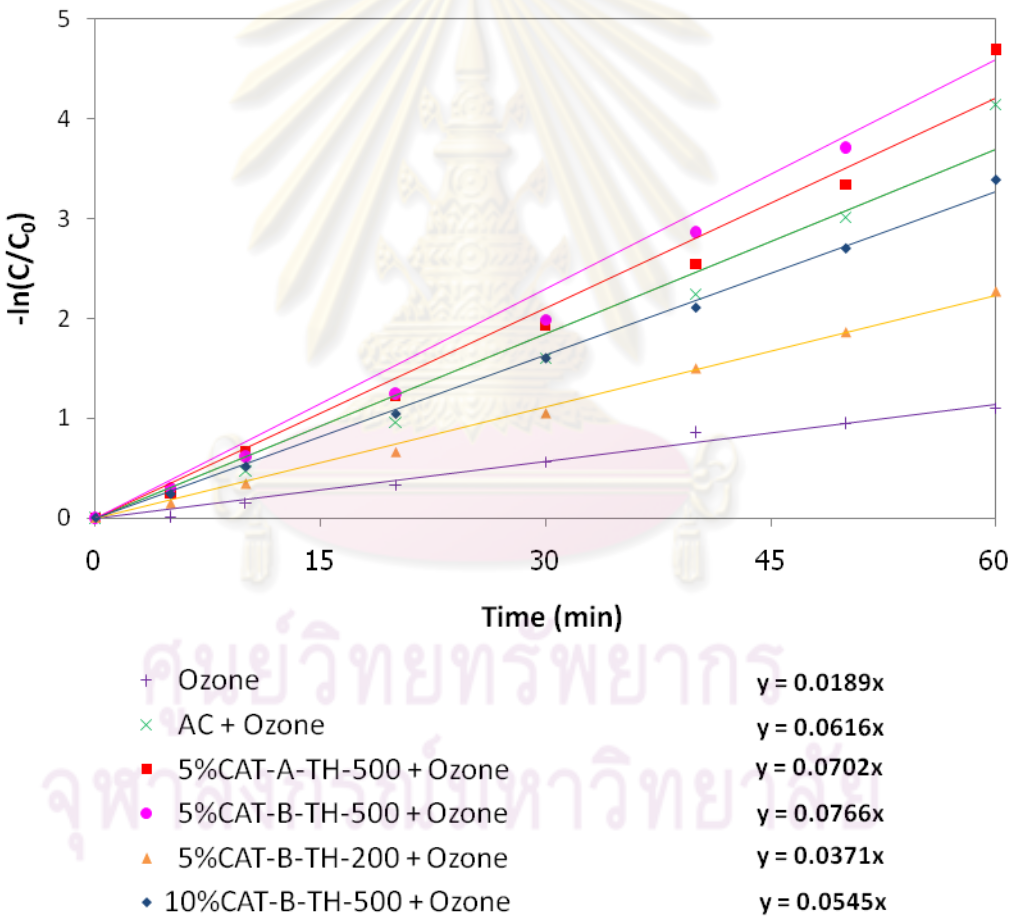

Figure C.1 Phenol removal rates.

Table C.1 Pseudo first order rate constant for removal of aqueous phenol

Condition	**R^{2a}**	**k (min^{-1})[b]**
Only Ozone	0.9829	0.0189
AC + Ozone	0.9724	0.0616
5%CAT-TH-A-500 + Ozone	0.9780	0.0702
5%CAT-TH-B-500 + Ozone	0.9771	0.0766
5%CAT-TH-B-500 + Ozone	0.9968	0.0371
10%CAT-TH-B-500 + Ozone	0.9975	0.0545

[a] Correlation coefficient of the straight line

[b] Pseudo first order rate constant determined for the 60 min of reaction

ศูนย์วิทยทรัพยากร
จุฬาลงกรณ์มหาวิทยาลัย

VITA

Mr. Sukhum Chaeysiri was born on Mar 28, 1984 in Chonburi, Thailand. He studied in primary and secondary educations at Chonradsadornumrung School. He received the Bachelor Degree of Chemical Engineering from Faculty of Engineering, Burapha University, in 2006. He continued his Master's study at Center of Excellence in Particle Technology (CEPT), Department of Chemical Engineering, Chulalongkorn University in November 2008.

ศูนย์วิทยทรัพยากร
จุฬาลงกรณ์มหาวิทยาลัย